WATER-SOLUBLE GRAPHENE IN AGAR GEL AS ELECTROLYTE FOR MAGNESIUM-AIR BATTERY

LIEW SIAW YING

INSTITUTE FOR ADVANCED STUDIES
UNIVERSITY OF MALAYA
KUALA LUMPUR

2020

WATER-SOLUBLE GRAPHENE IN AGAR GEL AS ELECTROLYTE FOR MAGNESIUM-AIR BATTERY

LIEW SIAW YING

DISSERTATION SUBMITTED IN FULFILMENT OF THE
REQUIREMENTS FOR THE DEGREE OF MASTER OF
PHILOSOPHY

INSTITUTE FOR ADVANCED STUDIES
UNIVERSITY OF MALAYA
KUALA LUMPUR

2020

UNIVERSITY OF MALAYA
ORIGINAL LITERARY WORK DECLARATION

Name of Candidate: Liew Siaw Ying

Matric No: HGA 150018

Name of Degree: Master of Philosophy

Title of Dissertation: Water-Soluble Graphene in Agar Gel as Electrolyte for Magnesium-Air Battery

Field of Study: Chemistry (Analytical Chemistry)

I do solemnly and sincerely declare that:

(1) I am the sole author/writer of this Work;
(2) This Work is original;
(3) Any use of any work in which copyright exists was done by way of fair dealing and for permitted purposes and any excerpt or extract from, or reference to or reproduction of any copyright work has been disclosed expressly and sufficiently and the title of the Work and its authorship have been acknowledged in this Work;
(4) I do not have any actual knowledge nor do I ought reasonably to know that the making of this work constitutes an infringement of any copyright work;
(5) I hereby assign all and every rights in the copyright to this Work to the University of Malaya ("UM"), who henceforth shall be owner of the copyright in this Work and that any reproduction or use in any form or by any means whatsoever is prohibited without the written consent of UM having been first had and obtained;
(6) I am fully aware that if in the course of making this Work I have infringed any copyright whether intentionally or otherwise, I may be subject to legal action or any other action as may be determined by UM.

Candidate's Signature Date:

Subscribed and solemnly declared before,

Witness's Signature Date:

Name:

Designation:

WATER-SOLUBLE GRAPHENE IN AGAR GEL AS ELECTROLYTE FOR MAGNESIUM-AIR BATTERY

ABSTRACT

Presently, ever-increasing demands on energy and the global environmental issues have given the impetus to investigate the new battery systems which are inexpensive, efficient, having high performance, and also green to the environment. Among all the battery technologies, magnesium-air (Mg-air) battery is an attractive battery to be developed owing to the interesting properties of the Mg anode. Mg has high specific energy (6.46 kWh kg^{-1}) and reactivity, apart from its high abundance, lower cost, low toxicity, and comparatively safe to handle in the atmosphere. Nevertheless, Mg-air battery is still not being widely investigated as compared to the other batteries. Electrolyte is one of the vital components in Mg-air battery. Mg corrodes readily in conventional aqueous electrolytes, resulting in battery self-discharge. Moreover, the aqueous electrolytes used may leak and evaporate through the open cell structure. Therefore, a gel polymer electrolyte with the corrosion inhibition property could be a new electrolyte material for Mg-air battery. Water-soluble graphene (WSG) was successfully synthesised through simplified Hummers' method followed by chemical reduction (with the addition of ammonia, NH_3). WSG was incorporated into agar (a natural polymer) as an environment-friendly gel polymer electrolyte for Mg-air battery. Continuous efforts have been focused on the improvement in electrochemical performance of Mg-air battery via the preparation of different WSG-AGAR gel electrolytes. Detailed investigations on different parameters, for instance, synthesis condition of WSG, agar concentration, WSG concentration, and types of electrolyte were conducted in order to produce the optimal WSG-AGAR gel electrolyte. It was found that the incorporation of 0.1% w/v WSG-7 in 3.5% w/v sodium chloride (NaCl), entrapped in 3% w/v agar gel exhibited the greatest electrochemical performance due to the optimisation between high ionic conductivity and sufficient anodic corrosion resistance. The optimal gel electrolyte had an ionic conductivity of 9.40×10^{-2} S cm^{-1}. The discharge capacity and energy density of assembled Mg-air battery with respect to the mass of Mg anode consumed during discharging can reach up to 1303.94 mAh g^{-1} and 1820.70 mWh g^{-1}, respectively, at the constant current density of 11.11 mA cm^{-2}. The incorporation of WSG-7 (optimal WSG) in agar gel electrolyte had demonstrated the improvement in ionic conductivity by 32.96% and discharge capacity by 58.34% as compared to that without electrolyte additive. The Mg-air battery with the optimal WSG-AGAR gel electrolyte was further discharged at different current densities. The peak discharge capacity and energy density with respect to the mass of Mg anode consumed during discharging were achieved at the current density of 1.11 mA cm^{-2}, with the value of 1632.74 mAh g^{-1} and 2432.78 mWh g^{-1}, respectively. The performance of the assembled Mg-air battery with this economical, inherently safe, and environmentally benign biopolymer electrolyte was notable.

Keywords: Mg-air battery, agar, water-soluble graphene, gel electrolyte, biopolymer

GRAPHENE LARUT AIR DALAM GEL AGAR-AGAR SEBAGAI ELEKTROLIT UNTUK BATERI MAGNESIUM-UDARA

ABSTRAK

Pada masa kini, peningkatan permintaan terhadap tenaga dan isu-isu alam sekitar telah mendorong pembangunan penyelidikan terhadap sistem bateri baru yang murah, cekap, berprestasi tinggi, dan juga mesra alam. Antara semua teknologi bateri, bateri magnesium-udara (Mg-udara) merupakan bateri yang menarik untuk dibangunkan disebabkan oleh ciri-ciri istimewa anod Mg. Mg mempunyai tenaga khusus (6.46 kWh kg^{-1}) dan kereaktifan yang tinggi, selain daripada kelimpahan yang tinggi, kos yang lebih rendah, ketoksikan yang rendah, dan agak selamat untuk dikendalikan di atmosfera. Walau bagaimanapun, kajian bateri Mg-udara masih tidak dijalankan secara meluas berbanding dengan bateri-bateri yang lain. Elektrolit adalah salah satu komponen yang penting dalam bateri Mg-udara. Mg mudah terkakis dalam elektrolit akueus yang konvensional dan mengakibatkan pelepasan diri bateri. Di samping itu, elektrolit akueus yang digunakan juga berkemungkinan bocor dan sejat disebabkan oleh struktur sel bateri yang terbuka. Justifikasinya, elektrolit gel polimer yang tidak mudah mengakis Mg diperlukan untuk bateri Mg-udara. Graphene larut air (WSG) telah disintesis melalui kaedah Hummers, diikuti dengan proses reduksi kimia (merangkumi penambahan ammonia, NH_3). WSG telah disisipkan ke dalam agar-agar (sejenis polimer semulajadi) sebagai elektrolit polimer gel yang mesra alam bagi bateri Mg-udara. Pelbagai parameter yang memberi kesan terhadap prestasi elektrokimia elektrolit seperti keadaan sintesis WSG, konsentrasi agar-agar, konsentrasi WSG, dan jenis elektrolit telah dikaji secara terperinci supaya menghasilkan elektrolit gel WSG-AGAR yang optimum. Melalui kajian yang telah dijalankan, telah didapati bahawa penyisipan 0.1% w/v WSG-7 dalam 3.5% w/v natrium klorida (NaCl) dan 3% w/v agar-agar menunjukkan prestasi elektrokimia yang tertinggi. Ini demikian kerana elektrolit gel WSG-AGAR yang optimum memberikan keseimbangan dari segi kekonduksian ionik yang tinggi serta rintangan kakisan anodik yang mencukupi. Elektrolit gel yang optimum mempunyai kekonduksian ionik setinggi 9.40×10^{-2} S cm^{-1}. Kapasiti nyahcas dan ketumpatan tenaga bateri Mg-udara (dengan mengambil kira pengurangan jisim Mg dalam proses nyahcas) mencapai sehingga 1303.94 mAh g^{-1} dan 1820.70 mWh g^{-1}, setiap satu pada ketumpatan arus sebanyak 11.11 mA cm^{-2}. Penyisipan WSG-7 (WSG yang optimum) dalam elektrolit gel agar-agar telah meningkatkan kekonduksian ionik sebanyak 32.96% dan kapasiti nyahcas sebanyak 58.34% berbanding dengan prestasi tanpa bahan tambahan elektrolit. Bateri Mg-udara yang dipasang dengan elektrolit gel WSG-AGAR yang optimum telah dinyahcas secara lebih lanjut pada ketumpatan arus yang berbeza. Kapasiti nyahcas dan ketumpatan tenaga (dengan mengambil kira pengurangan jisim Mg dalam proses nyahcas) yang tertinggi dicapai pada ketumpatan arus 1.11 mAh cm^{-2}, dengan nilai sebanyak 1632.74 mAh g^{-1} dan 2432.78 mWh g^{-1}. Prestasi bateri Mg-udara yang dihasilkan dengan mengaplikasikan elektrolit biopolimer yang ekonomikal, selamat, serta mesra alam ini adalah amat menonjolkan.

Kata kunci: Bateri Mg-udara, agar-agar, graphene larut air, elektrolit gel, biopolimer

ACKNOWLEDGEMENTS

This research work was conducted in Nanotechnology Catalysis and Research Centre (NANOCAT), University of Malaya. I would like to express my sincere appreciation to all those people who have assisted and encouraged me in the successful completion of my master study.

I would like to express my gratitude and appreciation to my main supervisor, Assoc. Prof. Dr. Juan Joon Ching and co-supervisor, Ir. Dr. Lai Chin Wei for their professional guidance, continuous encouragement, stimulating discussion, and constant support throughout the research. With their enormous help, I have gained a lot of precious research experience such as scientific thinking, knowledge in chemistry and materials, as well as the laboratory techniques. The supervision, support, and cooperation provided have truly helped the progression of my study. A special thanks goes to Emeritus Prof. Dr. Phang Siew Moi for supporting the seaweed for the initial research investigation.

Besides that, I am grateful to the academic and technical staffs of University of Malaya (especially the staffs from NANOCAT) for their advice, assistance, and cooperation in various aspects. A special thanks goes to my colleagues for all the help, discussion, and sharing throughout my master study. They always give their support during my laboratory works and thesis writing.

Last but not least, I would like to express my sincere thanks to my family members for their love, encouragement, and sacrifice. They have provided me with unfailing support and continuous encouragement throughout my years of study and through the process of researching and writing this thesis. This accomplishment would not have been possible without them. Thank you.

TABLE OF CONTENTS

LIST OF FIGURES

LIST OF TABLES

LIST OF SYMBOLS AND ABBREVIATIONS

[BMIM][TFSI]	:	[1-butyl-3-methylimidazolium][bis(trifluoromethanesulfonyl) imide]
[P6,6,6,14][Cl]	:	Trihexyl(tetradecyl)phosphonium chloride
0D	:	Zero dimensional
1D	:	One dimensional
2D	:	Two dimensional
3D	:	Three dimensional
AC	:	Alternating current
Ag/AgCl	:	Silver/Silver chloride
Al	:	Aluminium
ATR-FTIR	:	Attenuated total reflectance Fourier transform infrared
BMPTFSI	:	1-butyl-1-methylpyrrolidinium bis(trifluoromethylsulfonyl) imide
C	:	Carbon
Ca	:	Calcium
CAGR	:	Compound annual growth rate
Ce	:	Cerium
Cl^-	:	Chloride ion
CPE_{dl}	:	Constant phase element (double layer)
CPE_f	:	Constant phase element ($Mg(OH)_2$ film)
CS-[Ch][NO_3	:	Chitosan-choline nitrate
DMSO	:	Dimethylsulfoxide
DSSC	:	Dye-sensitized solar cell
EIS	:	Electrochemical impedance study
E_r	:	Rest potential

EtBr	:	Bromoethane
Fe	:	Iron
FESEM	:	Field emission scanning electron microscope
GO	:	Graphite oxide
GPE	:	Gel polymer electrolyte
H_2	:	Hydrogen
H_2O	:	Water
H_2O_2	:	Hydrogen peroxide
H_2SO_4	:	Sulphuric acid
HCl	:	Hydrochloric acid
HNO_3	:	Nitric acid
In	:	Indium
IR	:	Infrared
$KMnO_4$	:	Potassium permanganate
KOH	:	Potassium hydroxide
Li	:	Lithium
Li_2CrO_4	:	Lithium chromate
LIBs	:	Lithium-ion batteries
M	:	Molar
Mg	:	Magnesium
$Mg(OH)_2$	:	Magnesium hydroxide
$Mg(TFSI)_2$	:	Magnesium bis(trifluoromethanesulfonyl)imide
$MgCl_2•6H_2O$	:	Magnesium chloride hexahydrate
Mn	:	Manganese
MnO_2	:	Manganese dioxide
Mn_3O_4	:	Manganese tetroxide

MoS_2 : Molybdenum disulfide

N : Nitrogen

Na : Sodium

Na_2SO_4 : Sodium sulphate

Na_3PO_4 : Sodium phosphate

$Na_3PO_4 \cdot 12H_2O$: Sodium phosphate dodecahydrate

NaCl : Sodium chloride

NaOH : Sodium hydroxide

$NaVO_3$: Sodium metavanadate

NH_3 : Ammonia

NH_4Br : Ammonium bromide

NH_4NO_3 : Ammonium nitrate

NHE : Normal hydrogen electrode

Ni : Nickel

NMP : N-methylpyrrolidone

O_2 : Oxygen

OER : Oxygen evolution reaction

OH^- : Hydroxyl ions

ORR : Oxygen reduction reaction

PAN : Polyacrylonitrile

PBS : Phosphate buffered saline

PEO : Polyethylene oxide

PMMA : Polymethyl methacrylate

ppm : Parts per million

PSS : Poly (sodium 4-styrenesulfonate)

PVA : Polyvinyl alcohol

PVdF-HFP : Poly(vinylidene fluoride-co-hexafluoropropylene)

PVP : Polyvinylpyrrolidone

R_{ct} : Charge transfer resistance

R_f : $Mg(OH)_2$ film resistance

rGO : Reduced graphene oxide

R_s : Solution resistance

SDBS : Sodium dodecylbenzenesulfonate

SF-[Ch][NO_3] : Silk fibroin-choline nitrate

Si : Silicon

SiC : Silicon carbide

SPEs : Solid polymer electrolytes

THF : Tetrahydrofuran

WSG : Water-soluble graphene

WSG-AGAR : Water-soluble graphene-incorporated agar

XRD : X-ray diffraction

Y : Yttrium

Zn : Zinc

CHAPTER 1: INTRODUCTION

1.1 Research Background

The contemporary world is presently transitioning from a fossil fuel based economy to the green energy alternatives, as an essential step to reduce environmental impacts (Liu et al., 2017). Moreover, it is vital to look for a safe, reliable, inexpensive, high performance, and efficient energy storage technologies which are capable to supply energy for large-scale applications (An, Zhao, & Zeng, 2013; Lee et al., 2011; Rahman, Wang, & Wen, 2013; Richey, McCloskey, & Luntz, 2016). Among these devices, the battery is of great significance as the source of energy for many portable devices (such as laptops, smartphones, and remote controls) and also electric vehicles. The battery system is comprised of two different electrodes immersing in media such as liquids, gels, or solids that enables the transport of ions (Scherson & Palencsár, 2006). Reddy (2010) explained that the battery functions through an electrochemical oxidation-reduction (redox) reaction, in which the electrical energy is generated through the direct transformation of the chemical energy contained in its active materials.

As highlighted by Inkwood Research (2019), the global battery market is estimated to reach $135.43 billion by the year 2027, with the compound annual growth rate (CAGR) of 6.63% during the forecasting years of 2019-2027. The global battery market forecast for the year 2019-2027 is shown in Figure 1.1. The increased production of hybrid and electric vehicles (specifically in Western Europe and United States) will stimulate the market for high-cost batteries used to fuel such vehicles (DJDC Battery, 2015). In the developing countries, the growth in disposable income and consumers spending will sustain the sales of high-drain electronics, for instance, personal computers and mobile phones. This leads to a high demand for both primary and secondary batteries. Furthermore, income growth promotes a shift to the primary batteries with greater performance, in order to drive market advances in the developing world (DJDC Battery, 2015).

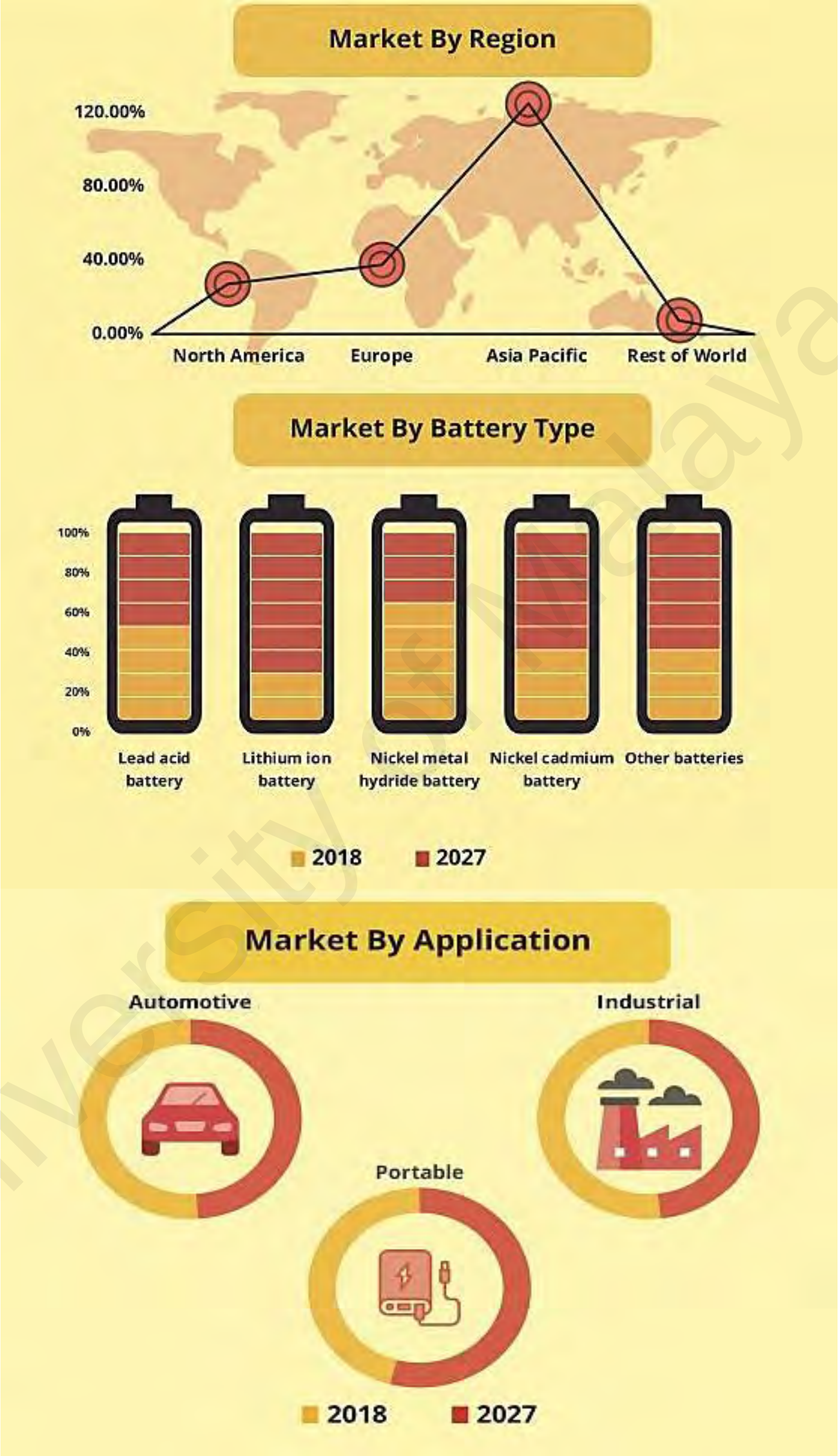

Figure 1.1: Global battery market forecast 2019-2027 (Inkwood Research, 2019).

Currently, lithium-ion batteries (LIBs) have predominated the market owing to their high capacity and also good energy efficiency (Bini, Capsoni, Ferrari, Quartarone, & Mustarelli, 2015; Liu et al., 2017). The energy density of the present LIBs is around 100 to 200 Wh kg^{-1}. Nevertheless, the future markets do demand for a greater energy density than LIBs could reasonably provide in the near future. As a result, this encourages the development of the interestingly new energy storage and conversion systems with high theoretical energy density necessary for future applications (Bini et al., 2015; Liu et al., 2017)

With the increase in interest towards new types of batteries, metal-air batteries have emerged as promising electrochemical energy storage and conversion device (Liu et al., 2017; T. Zhang, Tao, & Chen, 2014; Z. Zhang et al., 2014). The global market for advanced battery and fuel cell materials (which includes metal-air batteries) had achieved \$22.7 billion in 2016 (Saxman, 2017). It is forecasted that the market should reach \$32.8 billion by 2022, with a CAGR of 7.6% from 2017 to 2022 (Saxman, 2017). Metal-air batteries are the not widely known, but highly potential substituents to the common and also future power sources as primary batteries (Downing, 2016). Typically, metal-air batteries, for instance, magnesium-air (Mg-air) battery have an open cell structure, utilise oxygen from the ambient air, and high in energy density but low in power density. Great strides have been made and are continuously progressing in the metal-air technology. They have the possibility to substitute conventional batteries (such as zinc alkaline) and expensive hydrogen-based fuel cells owing to their high energy density, high capacity, relatively flat discharge voltage potential, long shelf life, and comparatively economical (Downing, 2016; T. Zhang et al., 2014; Z. Zhang et al., 2014).

Although a vast amount of works had been conducted in recent years on the metal-air batteries, there is less focus on the Mg-air battery. Magnesium (Mg) in fact is an ideal candidate in metal-air batteries application. It is highly abundant on the Earth, inexpensive, high in reactivity, low in toxicity, environmentally friendly, and also low in safety concern when handling in the air (Aurbach et al., 2000; Muldoon et al., 2012; Peng, Liang, Tao, & Chen, 2009; X. Wang, Hou, Zhu, Wu, & Holze, 2013; Yan, 2016; Yoo et al., 2013). A typical primary Mg-air battery is a battery which comprises of a Mg (or Mg alloy) anode, air cathode and saline electrolyte (T. Zhang et al., 2014).

Electrolyte has a significant role in Mg-air battery. It separates the anode and cathode, prevents the occurrence of the short circuit, and also affects the battery performance. In general, aqueous electrolytes are being employed in metal-air batteries, including Mg-air battery, owing to their high ionic conductivities (Z. Zhang et al., 2014). However, there are several drawbacks for the utilisation of aqueous electrolytes in Mg-air battery. These include Mg anode corrosion, electrolyte leakage and evaporation, obstruction in the permeability of the porous air electrode, and also the battery performance and safety issues concerning the drying and premature failure of the cell (An et al., 2013; Cheng & Chen, 2012; Mainar et al., 2018; Z. Zhang et al., 2014). All these issues have restricted the commercialisation of Mg-air battery in our daily life.

Therefore, the substitution of aqueous electrolytes with gel polymer electrolytes (GPE) for the metal-air batteries has gained much attention (Di Palma, Migliardini, Caputo, & Corbo, 2017; Z. Zhang et al., 2014). Apparently, it is an encouraging solution to solve the aforesaid issues of aqueous electrolytes in Mg-air battery. The preparation process of GPEs is uncomplicated and reliable (Di Palma et al., 2017). Among the GPEs, carbohydrate polymers, for instance, cellulose, starch, chitosan, agarose, carrageenan, xanthan, and alginic acid have been utilised for the preparation of hydrogels. GPEs prepared from the carbohydrate polymers have been widely explored for various electrochemical applications, for instance, fuel cells (Monisha et al., 2017; Purwanto et al., 2016), supercapacitors (Moon, Kim, Lee, Song, & Yi, 2015), batteries (Di Palma et al., 2017), solar cells (Aziz, Buraidah, Careem, & Arof, 2015), and sensors (Vaghela, Kulkarni, Haram, Karve, & Aiyer, 2016). The environmentally friendly, renewable, and inexpensive properties of biopolymers motivate the use of biopolymers as a source for preparing GPEs (Di Palma et al., 2017).

Among these natural type of GPEs, agar seems to be most potential because of the availability, high biocompatibility, high biodegradability, high hydrophilicity, and low cost (Boopathi et al., 2017; Cano, Crespo, Lafuente, & Barat, 2014). The liquid trapping, syneresis, and amorphous nature of agar gel aid in the water movement within the GPE, providing high conductivity and thus facilitating the battery operation (Barat & Cano, 2015; Sivadevi, Selvalakshmi, Umamaheswari, & Bhuvaneswari, 2016).

Agar is polysaccharides derived from the cell wall of Rhodophyta (red algae). Rhodophyta is among the oldest photosynthetic eukaryotes lineages. The commercial source of agar is the agarophytes genera *Gelidium* and *Gracilaria*. Agar is made up of agarobiose, a repeating disaccharide units with β-1,3-linked- D-galactopyranose and α-1,4-linked 3,6-anhydro-L-galactopyranose (Figure 1.2).

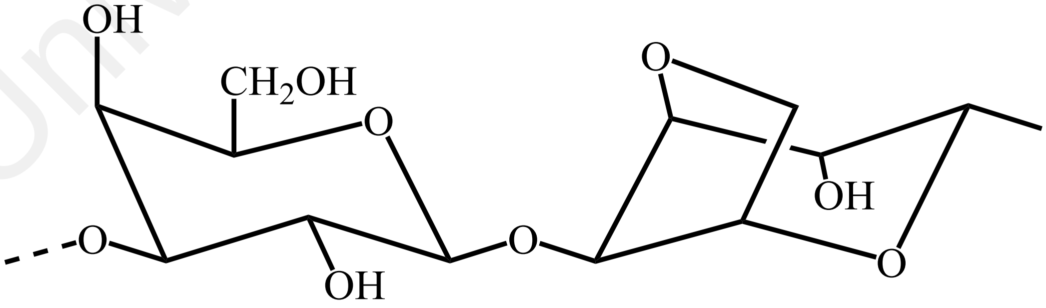

Figure 1.2: The basic repeating units of agarobiose.

Agar is principally comprised of agarose and agaropectin. Agarose is the neutral linear polysaccharides consisting of the repeating units of agarobiose, whereas agaropectin is the charged, acid polysaccharides with the attachment of sulphate groups, pyruvic acid, and D-glucoronic acid to agarobiose (Rhein-Knudsen, Ale, & Meyer, 2015; Venugopal, 2011). Agar has been extensively applied in industries including food, microbiological, pharmaceutical, and medical. The agar application in the electrochemistry field has also been explored for fuel cell, proton battery, and electrochromic cell (An et al., 2013; Raphael, Avellaneda, Manzolli, & Pawlicka, 2010; Selvalakshmi, Mathavan, Selvasekarapandian, & Premalatha, 2019). As a natural polymer, agar is more appealing in comparison to synthetic polymers as an electrolyte in the metal-air batteries.

Graphene is unsusceptible to corrosion effect (Lih, Ling, & Chong, 2012). This property is crucial for improving the corrosion resistance of Mg anode. Graphene is a monolayer sp^2 bonded carbon atoms with a two dimensional (2D) hexagonal honeycomb lattice structure (Selvam, Sakthipandi, Suriyaprabha, Saminathan, & Rajendran, 2013). It is demonstrated that graphene suppresses the Mg breakdown during the self-discharge and reduces the corrosion rate of Mg anode (Mayilvel Dinesh et al., 2015).

In this work, an environmentally friendly water-soluble graphene-incorporated agar (WSG-AGAR) as gel polymer electrolyte for Mg-air battery is fabricated. The electrochemical characteristics of the WSG-AGAR gel electrolyte prepared with different water-soluble graphene (WSG) synthesised, agar concentration, WSG concentration, and types of electrolyte are studied in order to obtain the optimal performance for Mg-air battery.

1.2 Problem Statement

Apart from the high performance and low cost properties, the fabrication of the new battery systems also needs to take the environmental impact into consideration in order to confront the current world environmental issues. A promising path to accomplish these goals is the development of Mg-air battery. Mg-air battery has a high theoretical energy density and also a low cost of production (due to high Mg abundance and the free and unlimited air from the ambient atmosphere) (Khoo, Howlett, Tsagouria, MacFarlane, & Forsyth, 2011; T. Zhang et al., 2014). It is also an environment-friendly and non-toxic battery (Deyab, 2016).

Despite the benefits of Mg-air battery, it still has limitations in practical uses. Cheng and Chen (2012) stated that Mg anode utilised in the Mg-air battery is very susceptible to corrosion. Mg anode dissolves severely in aqueous electrolytes and results in self-discharge, which leads to a decrease in operating life (Cheng & Chen, 2012). In addition, Mayilvel Dinesh et al. (2015) stipulated that the formation of hydrogen gas during the discharge cycle results in the reduction of battery life. Another limitation of Mg-air battery is the battery performance and safety concern regarding the use of aqueous electrolyte. Mg-air battery has an open cell structure in order to acquire oxygen from the ambient air. Consequently, the high fluidity of the aqueous electrolytes may cause the problems of electrolyte leakage and evaporation through the open cell structure (An et al., 2013; Mainar et al., 2018). The excessive water loss may increase the electrolyte concentration and negatively influence the discharge reaction, eventually causing the drying and premature failure of the cell. In addition, liquid accumulation at the air cathode due to electrolyte leakage (and also possibly through the ambient moisture uptake in a high relative humidity environment) may flood the air electrode, leading to obstruction in the permeability of the porous air electrode. This condition affects the transport of oxygen to the catalyst active sites and also reduces the electrochemical activity of the cathode, since oxygen cannot readily diffuse through water (An et al., 2013; Mainar et al., 2018).

One of the approaches to solve the aforementioned problems is to replace the aqueous electrolyte with gel polymer electrolyte (GPE). GPEs can solve the leakage and evaporation problem of aqueous electrolyte while providing greater ionic conductivity values (10^{-2} to 10^{-3} S cm^{-1}) than the solid electrolyte (Di Palma et al., 2017; Z. Zhang et al., 2014). The application of natural polymers as GPE is gaining much attention nowadays due to their attractive properties. Nevertheless, the use of agar gel to improve the battery performance of Mg-air battery is not yet investigated.

In order to increase the Mg-air battery performance, the addition of catalyst additives in the GPE can be conducted. Mayilvel Dinesh et al. (2015) revealed the use of reduced graphene oxide (rGO) as a catalyst additive in NaCl liquid electrolyte of Mg-air battery. The use of rGO has demonstrated the prevention of Mg anode breakdown during self-discharge, thus minimises the corrosion rate of Mg anode and results in the increase of maximum discharge capacity and battery life (Mayilvel Dinesh et al., 2015). rGO has long been recognised as an extraordinary material with good chemical and physical properties. It has received many interests owing to its notable properties, for instance, high surface area (> 2600 m^2 g^{-1}), high electrical conductivity (2000 S cm^{-1}), and good mechanical stability (Bhattacharya, 2016; Nasir, Hussein, Zainal, & Yusof, 2018). The prevention of aggregation is vital for rGO sheets in order to disperse well in the electrolyte and thus improve battery performance. Therefore, WSG was used as it is easily well dispersed in the agar gel electrolyte and will eventually improve the battery performance.

In the present study, considerable efforts have been given to the synthesis of desirable WSG, followed by incorporation into agar gel electrolyte in order to improve the Mg-air battery performance.

1.3 Research Objectives

The objectives of this research are listed as follows:

- To synthesise the WSG via chemical reduction method.
- To prepare, characterise and optimise the WSG-AGAR gel electrolyte for Mg-air battery via incorporation of different WSG synthesised, agar concentration, WSG concentration, and types of electrolyte in the agar gel electrolyte.
- To evaluate the electrochemical performance of the Mg-air battery based on the WSG-AGAR gel electrolyte.

1.4 Research Scope

Many studies highlighted the use of graphene in the battery application. However, most scholars focused on the role of graphene as an electrode, rather than the electrolyte additive. Agar has been widely used in the food and biotechnology industries. Nevertheless, it is considered as a comparatively new material for the gel polymer electrolyte in the battery application. To the best of my knowledge, there is no information regarding the incorporation of WSG in agar gel electrolyte for the Mg-air battery application. Therefore, a comprehensive study was conducted to optimise the preparation of WSG-AGAR gel electrolyte for the best primary Mg-air battery performance.

This study was focussed on the preparation and characterisation of the WSG powder and the development of WSG-AGAR gel electrolyte in primary Mg-air battery. WSGs were prepared at different condition (reduction of GO with the presence of a different amount of ammonia solution) and the different WSG synthesised were incorporated in the agar gel to form the electrolyte. Furthermore, various agar concentration, WSG concentration, and types of electrolyte were also used to produce the WSG-AGAR gel electrolyte in order to produce the optimal electrolyte for the primary Mg-air battery application.

X-ray diffraction (XRD) was used to determine the atomic structure, interlayer spacings, and crystallinity of the WSG samples. Moreover, the defects, disorders, and crystal structure of the graphene-based materials were characterised using Raman spectroscope. The vibrational information regarding the chemical bonds and symmetrical of molecules were obtained from ATR-FTIR spectroscope. In addition, the colloidal dispersion stability of the WSG samples was determined through the zeta potential measurement.

The electrochemical performance of the Mg-air battery system based on the different agar gel electrolytes prepared was tested. The ionic conductivity test was conducted to measure the ionic conductivity of the agar gel electrolyte. Furthermore, Mg corrosion was studied using a three-electrode system electrochemical impedance study (EIS) with Mg strip as the working electrode and the respective agar gel of different composition as the electrolyte. The performance of the Mg-air battery with the different agar gel electrolytes was also evaluated via the current discharge study. The optimal WSG-AGAR gel electrolyte was observed under FESEM in order to investigate its surface morphology, and the optimal Mg-air battery was further discharged under different current densities to better understand their discharge performance. The customised Mg-air battery in this study was constructed by applying Mg strip as the anode, commercial-based air electrode as the cathode, and the WSG-AGAR gel as the electrolyte.

1.5 Dissertation Outline

This thesis is well-structured into five chapters. The first chapter is associated with the research background, problem statements, research objectives, research scope, and the thesis outline. Chapter 2 introduces the basic concepts and working principles of batteries, metal-air batteries, and also Mg-air battery, including the electrolytes and electrolyte additives used in primary Mg-air battery in recent literature. In addition, the review on graphene, electrolyte variation, and agar are also included in Chapter 2. In Chapter 3, the specifications of the raw materials, experimental procedure, characterisation techniques, battery fabrication, and electrochemical measurements are presented in details. Chapter 4 presents the characterisation, results and electrochemical performances of the prepared samples along with the discussion. The performance evaluation of the WSG-AGAR gel electrolytes in Mg-air batteries is also critically discussed in this chapter. Lastly, Chapter 5 summarises the overall work and proposes several recommendations for future work.

CHAPTER 2: LITERATURE REVIEW

2.1 Introduction

The starting mark of battery history was the invention of the first “wet cell battery” in 1800 (Yan, 2016). Thereafter, the development of batteries has been continuously conducted over the past two centuries (Yan, 2016). A wide variety of technologies in the current world are supported by batteries. These technologies ranging from smaller scale portable consumer devices and medical devices to larger scale electric vehicles and electrical energy storage.

Energy is currently the centre of attention of the major world power and scientific community. The rising energy demand, depletion of the natural resource, and global environmental problems have created great interests in developing energy storage devices with higher efficiency and also environment-friendly property (An et al., 2013; Lee et al., 2011; Rahman et al., 2013; Richey et al., 2016). Metal-air batteries have emerged as one of the electrochemical energy storage and conversion devices with great potential. This is because the metal-air batteries have a high theoretical energy density, high capacity, and low cost (T. Zhang et al., 2014; Z. Zhang et al., 2014). Among them, Mg-air primary battery is a preferred source of power owing to its high energy density, high theoretical output, longer discharge time, low cost, and eco-friendly nature (Armand & Tarascon, 2008; Cheng & Chen, 2012; Linden & Reddy, 2002; T. Zhang et al., 2014).

Despite the advantages of Mg-air battery, it is still having limitations in practical uses. Mg anode is very susceptible to self-corrosion, and the use of aqueous electrolytes in Mg-air batteries also contributes to the problem of electrolyte leakage and evaporation (An et al., 2013; Cheng & Chen, 2012). Thus, the use of natural polymers to replace aqueous electrolytes is becoming a favourite research matter in the field of electrochemistry.

Lately, the addition of electrolyte additives such as graphene has gained much attention because it is capable of increasing the battery performance (K. K. Kumar et al., 2019; Mayilvel Dinesh et al., 2015). However, the relationship between electrolyte additive and natural polymer as well as their electrochemical performance in the Mg-air battery remain unclear. Therefore, the development of efficient Mg-air battery with the incorporation of graphene (electrolyte additive) and agar (natural polymer) remains to be determined.

This chapter mainly reviews the research progress on Mg-air battery, battery electrolyte materials, electrolyte additive materials, and natural polymers in recent decades. In addition, a brief introduction to some basic concepts and principles of batteries as well as metal-air batteries is also provided in this chapter.

2.2 Battery

2.2.1 Basic Concepts

As mentioned by Scherson and Palencsár (2006), the battery was invented by Alessandro Volta (1745-1827) of Como, Italy in 1800. Das (2016) defined batteries as the devices which generate electrical energy via electrochemical redox reactions, in which the energy in the chemical form stored in their active materials is converted into the electrical energy. A battery can be made up of one or more electrochemical cells. A typical battery comprises of an anode, a cathode, and an electrolyte. All the electrochemical cells are comprised of two electrodes (anode and cathode) which are separated by some distance. Anode (negative terminal) allows the flowing out of electrons whereas cathode (positive terminal) accepts the electrons. Electrolyte fills up the space between the anode and cathode, and acts as the medium for the transfer of charge (ions). Cells can be electrically connected in different series or parallel arrangement, producing different capacity, operating voltage, and current levels. Basically, batteries are classified into two major groups, which are the primary and secondary batteries. Primary batteries are non-rechargeable and they will be disposed of once they are being used up. On the other hand, secondary batteries are rechargeable and their electrochemical reactions are electrically reversible (Das, 2016).

2.2.2 Working Principles

Commonly, the anode (negative terminal) and cathode (positive terminal) material are electrochemically reactive and act as the dominant reactants (Yan, 2016). During the discharge process, the anode is being oxidised whereas the cathode is being reduced. When the anode material consists of a metal, the metal will lose electrons and produce cations (positive ions). The electrons flow from the anode to the cathode through an external circuit, as illustrated in Figure 2.1(a). The cathode material will be reduced and produce anions (negative ions) when it accepts the electrons. The electrolyte functions as the ionic conductor which maintains the charge balance by permitting the transfer of ions between the anode and cathode during the electrochemical reaction. The cations move from the anode towards the cathode whereas anions on the cathode move towards the anode (Yan, 2016). The charging process (for secondary batteries) is the reverse reaction of the discharging process. During the charging process, oxidation takes place at the positive terminal whereas reduction takes place at the negative terminal, as depicted in Figure 2.1(b). Since anode is defined as the electrode at which oxidation occurs whereas cathode is defined as the electrode at which reduction occurs, thus anode will be the positive terminal meanwhile cathode will be the negative terminal (Reddy, 2010).

Nevertheless, Yan (2016) stated that the anode and cathode materials are different from the active anodic and cathodic reactants for some batteries. For example, the electrode materials in fuel cells are not consumable or reactive during the reaction. In addition, they also act as the catalysts which improve the electrooxidation of hydrogen or electroreduction of oxygen (Yan, 2016).

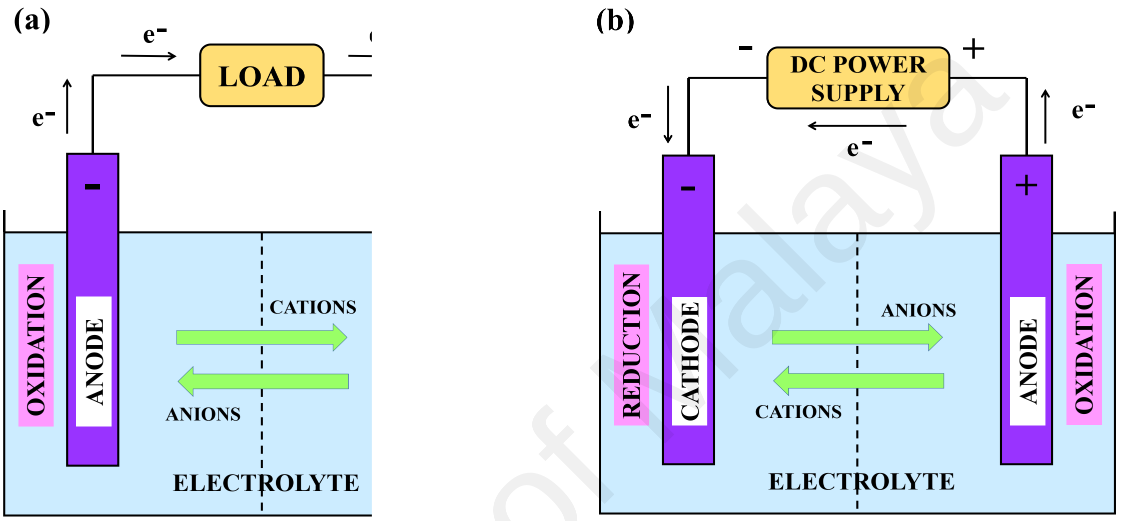

Figure 2.1: Electrochemical operation of a cell during (a) discharging process and (b) charging process.

2.3 Metal-air Batteries System

2.3.1 Basic Concepts

Yan (2016) explained metal-air or more particularly metal-oxygen battery as an open system which utilises an alkali or alkaline earth metal as the anode, besides having a porous, conductive material as the air cathode for the reduction of oxygen from the air during discharge. Metal-air batteries vary from the other batteries since the electro-active cathodic reactant is not a built-in electrode material, but the oxygen from the ambient air. Therefore, a potentially light battery can be produced since oxygen is not being kept in the batteries (Yan, 2016).

Metal-air batteries are comprised of primary and secondary batteries. For the primary metal-air batteries, the metal anode is oxidised and the electrons are released to the external circuit during the discharging process (Cheng & Chen, 2012). Simultaneously, oxygen diffuses from the air into the cathode, accepts the electrons from the anode and undergoes reduction to form oxygen-reduced species. The dissociated metal ions and oxygen-reduced species migrate across the electrolyte and react to produce metal oxides (Cheng & Chen, 2012).

The rechargeable metal-air batteries can be recharged through electrical recharging and mechanical recharging (Neburchilov, Wang, Martin, & Qu, 2010). For electrically rechargeable metal-air batteries, the charge/discharge process occurs within the battery configuration (H. Kim et al., 2013; Sen, Van Voorhees, & Ferrel, 1988). The charging process is the reverse of the discharging process, where the metal plating occurs at the anode whereas oxygen evolves at the cathode (Cheng & Chen, 2012). On the other hand, the mechanically rechargeable metal-air batteries involve external recharging (Cheng & Chen, 2012; H. Kim et al., 2013; Sen et al., 1988). The used anode and spent electrolyte are replaced periodically with fresh metal electrode and electrolyte. The anode discharged is replated from the spent electrolyte in a separate external system. Both the anode and the electrolyte regenerated are reused in the battery. As a result, these batteries are indirectly rechargeable (Cheng & Chen, 2012; H. Kim et al., 2013; Sen et al., 1988). At present, the electrically rechargeable metal-air batteries remain at research and development stage (Cheng & Chen, 2012).

Theoretically, metal-air batteries are expected to produce high energy densities as a result of excess oxygen intake from the ambient atmosphere at the cathode (Othman & Saputra, 2013). As mentioned by Yan (2016), the anode material is the crucial element which influences the energy capacity of the battery. Apart from the high battery capacity, metal-air batteries are also the low cost battery since oxygen from the atmosphere is free and unlimited (Yan, 2016). In addition, Mayilvel Dinesh et al. (2015) stated that the charging time of the batteries can be reduced since the anode in the metal-air batteries can be recharged mechanically. Metal-air batteries also have the other benefits, for instance, the capacity is not affected by the temperature within the operating range, flat discharge voltage, long dry storage, low cost for the metal used, and environmentally friendly (Hamlen, 1995).

Although metal-air batteries have many desirable properties as batteries, they also have a number of significant limitation. Generally, the performance of metal-air batteries is dependent on the surroundings of the environment, for example, temperature and humidity in the atmosphere which restricts the operating condition of the metal-air batteries (Othman & Saputra, 2013; Yan, 2016). Furthermore, owing to the open cell structure, the battery performance of metal-air batteries can be considerably affected by the water flooding into the electrolyte from the air or evaporation of water from the electrolyte due to atmospheric change. Metal-air batteries with aqueous electrolytes also have a problem with the leakage phenomenon, which restricts their applications (Roche & Scott, 2010). Moreover, anode corrosion, limited power output, and carbonation of alkali electrolytes are the other obstacles that need to be overcome in order to fabricate a greatly performed metal-air batteries with aqueous electrolyte (Othman & Saputra, 2013; Yan, 2016). As stipulated by Yan (2016), another crucial problem for metal-air batteries is the sluggish oxygen reduction reaction at the cathode. Hence, the reduction of oxygen requires the presence of a catalyst in order to accelerate the cathodic reaction. For the reversible metal-air battery, both the oxygen reduction reaction (ORR) and oxygen evolution reaction (OER) catalysts are needed to achieve high performance (Yan, 2016). The advantages and disadvantages of metal-air batteries are summarised in Table 2.1.

Table 2.1: Advantages and disadvantages of metal-air batteries (Hamlen, 1995; Mayilvel Dinesh et al., 2015; Othman & Saputra, 2013; Roche & Scott, 2010; Yan, 2016).

Advantages	Disadvantages
❖ Light weight battery ❖ High energy capacity ❖ High specific energy ❖ Low cost battery ❖ Mechanically rechargeable ❖ Capacity is not related to the temperature within the operating range ❖ Flat discharge voltage ❖ Long dry storage ❖ Environment-friendly	❖ Limited operating condition ❖ Air cathode flooding ❖ Drying of electrolyte ❖ Leakage of electrolyte ❖ Anode corrosion ❖ Limited power output ❖ Carbonation of alkali electrolyte ❖ Slow reduction of oxygen at cathode

To sum up, the development of metal-air batteries needs to be conducted continuously in order to produce advanced metal-air batteries. As highlighted by Yan (2016), the design of novel electrolyte systems, modification of the metal anodes (especially anti-corrosion properties), modification of air cathode matrix structure, and enhancement of the electro-activity of air catalysts are the leading areas of development that need to be focused when developing the metal-air batteries.

2.3.2 Classification of Metal-air Batteries

As stated by Gelman, Shvartsev, and Ein-Eli (2014), metal-air batteries are categorised according to the type of anode metal utilised in the battery system, as oxygen (from the air) is the common element. Lithium (Li) and zinc (Zn) are currently the most intensively investigated materials as the anodes in metal-air batteries. The examples of other anode materials for metal-air batteries are magnesium (Mg), aluminium (Al), iron (Fe), sodium (Na), and calcium (Ca). The electrochemical properties of selected metal anodes are summarised in Table 2.2.

Table 2.2: Electrochemical properties of selected metal anodes (Cohn, Starosvetsky, Hagiwara, Macdonald, & Ein-Eli, 2009; Linden & Reddy, 2002; J.-G. Zhang, Bruce, & Zhang, 2011).

Metal Anode	Specific Charge Capacity (Ah kg^{-1})	Standard Electrode Potential (V vs. SHE)	Specific Energy (kWh kg^{-1})
Li	3862	-3.01	11.60
Mg	2205	-2.37	6.46
Al	2980	-1.66	5.20
Fe	960	-0.88	0.96
Zn	820	-1.25	0.90

Theoretically, Li anode is the most attractive material in metal-air batteries due to its most negative standard potential, besides the greatest charge capacity and energy capacity (Yan, 2016). Nevertheless, the low natural abundance of lithium and the high cost of production restricts the use of Li-air battery to high-end products. In addition, Li reacts vigorously in the atmosphere, which leads to the safety issues of Li-air battery in an open system. Therefore, Mg was chosen because it has the second highest specific energy of 6.46 kWh kg^{-1}. Besides, Mg is more abundant, lower cost and greater safety under ambient conditions as compared to that of Li. Mg is also biocompatible and environment-friendly (Yan, 2016).

Electrolyte chemistry can also be used to classify the metal-air batteries. There are two major categories of electrolyte, which are the aqueous and non-aqueous electrolytes. The aqueous electrolytes can be divided into three types based on their acidity, which are the alkaline, neutral, and acidic electrolyte. Yan (2016) asserted that most of the primary metal-air battery systems utilised an alkaline electrolyte, for example, KOH or NaOH, owing to the high activity, high ionic conductivity, and low cost. Nevertheless, the highly concentrated alkaline electrolyte may reduce the reactivity of some anodes like Li.

Furthermore, aqueous electrolyte would face the problems of water evaporation, flooding, and carbonation of alkaline components which could affect the power output and life span of the batteries, apart from the difficulties to obtain reversibility of some metal-air batteries, like Mg-air battery, when applying these electrolytes (Yan, 2016). Therefore, non-aqueous electrolytes have been investigated as a solution to the problems related to the aqueous electrolyte. The investigation of non-aqueous electrolyte systems began from recent decades which includes organic solvents, ionic liquids, and all-solid-state electrolytes.

2.4 Magnesium-air (Mg-air) Battery System

2.4.1 Magnesium (Mg)

Magnesium is ranked as the fifth most abundant element in the earth crust and the third highest solubility in the seawater (Muldoon et al., 2012; Yan, 2016; Yoo et al., 2013). Mg is an alkaline earth metal which has comparable physical characteristics as the other elements in Group 2 of the Periodic Table. It is highly flammable and will give a strong white flash while burning, thus suitable for the applications in fireworks and marine flares (Yan, 2016). In addition, Mg and Mg alloys are commonly applied for structural purposes in the aerospace industry, electronics, and automotive applications since Mg is the lightest engineering metal with a high strength to weight ratio. A trace amount of Mg is vital to ensure human health, therefore it is general to find salts containing Mg in dietary and health products. In recent years, magnesium is also being applied in energy storage, primarily being utilised as the anode material owing to its strong activity (Yan, 2016).

The high natural abundance may contribute to the minimisation of the battery cost (Muldoon et al., 2012; Yoo et al., 2013). In addition, magnesium is an element which has high reactivity, low mass, low toxicity, environment-friendly, and comparatively safe to handle in the air than the other elements (Aurbach et al., 2000; Peng et al., 2009; X. Wang et al., 2013; Yan, 2016). The standard electrode potential of Mg is comparatively negative with a value of -2.37 V versus standard hydrogen electrode (SHE). Besides that, Mg has a high discharge capacity of 2205 Ah kg^{-1} and high specific energy of 6462 Wh kg^{-1} (Aurbach et al., 2000; Peng et al., 2009; X. Wang et al., 2013; Yan, 2016). All of these properties make Mg a suitable anode material in batteries.

2.4.2 Mg-air Battery System

The development of Mg-air battery has a long history. It has emerged as early as the 1960s, where a neutral NaCl solution Mg-air battery was produced by General Electric, an American company (Downing, 2016; T. Zhang et al., 2014). Nevertheless, there is no major advancement in Mg-air battery which makes it towards commercialisation due to the technological barriers, for instance, anode corrosion, electrolyte leakage, precipitation control, electrolyte composition, anode material and cathode material (Cheng & Chen, 2012; Downing, 2016; Mayilvel Dinesh et al., 2015; Yan, 2016; T. Zhang et al., 2014). Among them, the critical issue to be solved is the usage of aqueous electrolyte needs to be replaced with non-aqueous electrolyte, particularly gel polymer electrolyte, in order to avoid leakage and Mg anode corrosion while enhancing the Mg-air battery performance.

Currently, Mg-air battery remains as a primary battery (T. Zhang et al., 2014). Although it can be mechanically rechargeable by replacing the spent Mg anode and electrolyte with the fresh Mg anode and electrolyte, the fully electrically rechargeable Mg-air battery with reversible oxygen reduction and evolution reactions are facing great challenges (T. Zhang et al., 2014). Therefore, the focus of this study is directed towards the primary Mg-air battery.

T. Zhang et al. (2014) mentioned that the fundamental structure of Mg-air battery consists of a Mg (or Mg alloy) anode, an air cathode, and a saline electrolyte. The chemical reactions in Mg-air battery system are shown in Equation 2.1 to Equation 2.3:

$$\text{Anode: } Mg \rightarrow Mg^{2+} + 2e^{-} \qquad \text{(Equation 2.1)}$$

$$\text{Cathode: } O_2 + 2H_2O + 4e^{-} \rightarrow 4OH^{-} \qquad \text{(Equation 2.2)}$$

$$\text{Overall: } 2Mg + O_2 + 2H_2O \rightarrow 2Mg(OH)_2 \qquad \text{(Equation 2.3)}$$

W. Q. Yang, Yang, Sun, and Xin (2005) explained that when a Mg-air battery discharges, the Mg anode undergoes oxidation and forms Mg^{2+} ions, producing two electrons. At the air cathode, the reaction of oxygen (O_2), water (H_2O), and electrons reduces O_2 to OH^{-} (W. Q. Yang et al., 2005). The common structure and working principle of an Mg-air battery are shown in Figure 2.2.

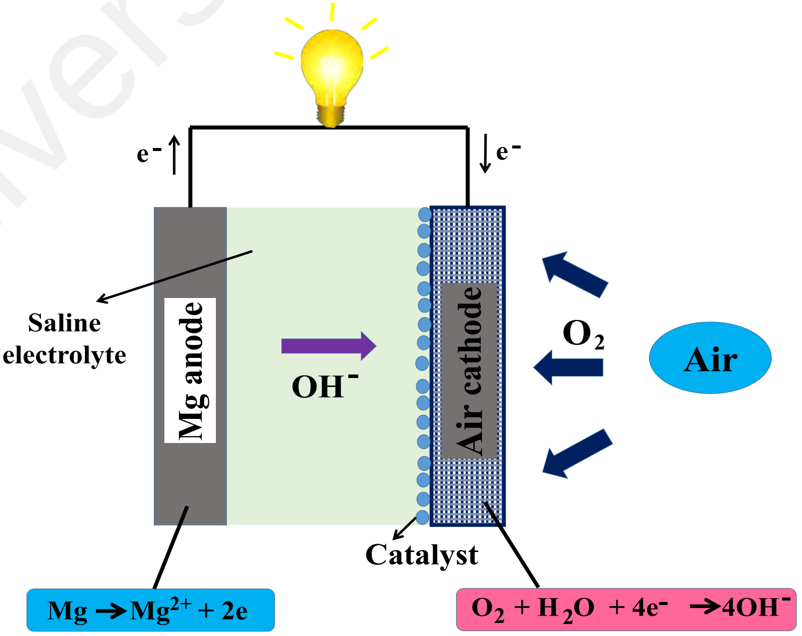

Figure 2.2: The common structure and working principle of a Mg-air battery system.

However, the corrosion of Mg anode may occur as a side reaction. The chemical reactions involved during the anode corrosion are presented by Equation 2.4 to Equation 2.7:

Anode: $Mg \rightarrow Mg^{2+} + 2e^-$ (Equation 2.4)

Cathode: $2H_2O + 2e^- \rightarrow H_2 + 2OH^-$ (Equation 2.5)

Product formation: $Mg^{2+} + 2OH^- \rightarrow Mg(OH)_2$ (Equation 2.6)

Overall corrosion reaction: $Mg + 2H_2O \rightarrow Mg(OH)_2 + H_2$ (Equation 2.7)

Mg-air battery has a theoretical voltage of 3.1 V and a high specific energy density (6462 Wh kg^{-1} excluding cathode) (Yan, 2016; T. Zhang et al., 2014). Moreover, it has longer discharge time, requires lower cost, and is environment-friendly (Armand & Tarascon, 2008; Cheng & Chen, 2012; Linden & Reddy, 2002). All of these properties enable Mg-air battery to function as a promising electrochemical energy storage and conversion device with high operating safety and also cost-effective.

The main electrolytes utilised in Mg-air battery are the neutral saline electrolytes, especially sodium chloride (NaCl) aqueous solution. As mentioned by Mayilvel Dinesh et al. (2015), 3.5% NaCl is recognised as the most suitable electrolyte for Mg electrode to produce a maximum discharge current.

2.4.3 Electrolytes in Mg-air Battery System

The electrolyte of an Mg-air battery is commonly a neutral saline aqueous solution. Both polarisation and coulombic efficiency of the Mg-air battery are dependence on the electrodes and electrolytes. Therefore, it is important to select a suitable electrolyte in order to improve the performance of the Mg-air batteries. Electrolyte plays a great influence on Mg anode corrosion. The corrosion potential of Mg in different aqueous solutions is listed in Table 2.3.

Table 2.3: Rest potential (E_r) of Mg with different aqueous solutions (Godard, Jepson, Bothwell, & Lane, 1967).

Electrolyte	E_r (V vs. NHE)
NaCl	-1.72
Na_2SO_4	-1.75
HCl	-1.68
HNO_3	-1.49
NaOH	-1.47
NH_3	-1.43

It can be observed that the resistance of Mg towards corrosion is greater in alkaline solution, as compared to the neutral or acidic solution. This is associated with the partial formation of magnesium hydroxide ($Mg(OH)_2$) film on the Mg surface which could protect the Mg anode from corrosion. Nevertheless, excess $Mg(OH)_2$ film on the Mg anode obstructs further reaction of the electrode, leading to a delayed response to a higher load. Therefore, a neutral electrolyte is generally utilised in Mg-air battery. Furthermore, the salt concentration in the electrolyte also affects the Mg corrosion. Mg tends to corrode easily in a solution with high salt concentration. As an example, the corrosion of pure Mg in seawater is approximately 0.25 mm per year whereas in 3 M $MgCl_2$ is increased by 1200 times. Hence, a low salt concentration is commonly required. Table 2.4 shows the types of electrolyte used in primary Mg-air batteries in recent literature. Since the theoretical voltage of 3.1 V and the theoretical specific energy (excluding cathode) of 6462 Wh kg^{-1} is yet to be achieved, there is still a room for improvement to achieve higher Mg-air battery performance through the influence of electrolyte.

Table 2.4: The electrolytes used in primary Mg-air batteries in recent years.

Electrolyte	Type of Electrolyte	Anode	Performance	Reference
1 M NaCl	Aqueous solution	Mg foil	Discharges for 300 min at 1 mA cm^{-2} at the operating voltage of 1.2 V.	Yifei Li et al. (2016)
3.5 wt% NaCl	Aqueous solution	Mg-Al-Pb-Ce-Y alloy	Average voltage of Mg-Al-Pb-Ce-Y anodes at 10 mA cm^{-2} reaches 1.276 V.	Feng, Xiong, Zhang, Wang, and Wang (2016)
3.5 wt% NaCl	Aqueous solution	Mg ribbon	The assembled Mg-air battery has a specific discharge capacity of 1030.71 mAh g^{-1}.	Mayilvel Dinesh et al. (2015)
3.5 wt% NaCl	Aqueous solution	Mg-Al-Pb-In alloy	The maximum power density is 94.5 mW cm^{-2}.	N. Wang et al. (2014)
Silk fibroin-choline nitrate (SF-[Ch][NO_3])	Natural polymer-ionic liquid film	Thin-film AZ31	Mg-air battery has a specific capacity of 0.06 mAh cm^{-2} at a current density of 10 µA cm^{-2}.	Jia et al. (2017)
Chitosan-choline nitrate (CS-[Ch][NO_3])	Natural polymer-ionic liquid film	Mg alloy	The electrolyte has a high ionic conductivity of 8.9×10^{-3} S cm^{-1}. The assembled battery gives a maximum volumetric power density of 3.9 W L^{-1}.	Jia et al. (2014)
Phosphate buffered saline (PBS) electrolyte	Aqueous solution	Mg alloy	The assembled battery provides a discharge capacity up to 3.79 mAh cm^{-2} at a current of 10 µA cm^{-2}, and a specific energy density of approximately 4.70 mWh cm^{-2}.	Jia, Wang, Zhao, Ge, and Wallace (2016)

Table 2.4, continued: The electrolytes used in primary Mg-air batteries in recent years.

Electrolyte	Type of Electrolyte	Anode	Performance	Reference
BMPTFSI + THF + EtBr	Ionic-liquid-based non-aqueous electrolyte	Pure Mg coin electrode	A mechanism of EtMgBr is reported for Mg-air battery. The assembled cells have a discharge capacity of approximately 340 mAh g^{-1} at the current density of 0.1 mA cm^{-2}.	Luder and Ein-Eli (2014)
Butyl butyrate-[BMIM][TFSI]-$Mg(TFSI)_2$	Double liquid electrolyte (Aqueous and organic phases)	Mg foil	The assembled Mg-air battery has a discharge capacity of 2020 mAh g^{-1} at the discharge current of 4.5 mA, with the average operating voltage at approximately 0.75 V. Anodic efficiency of pure Mg achieved is 91.6%.	Du, Wang, Niu, Duan, and Wu (2014)
Trihexyl(tetradecyl)phosphonium chloride ionic liquid,[P6,6,6,14][Cl]	Ionic liquid	Mg ribbon	The electrolyte gives a high Mg potential (−1.6 V vs Ag|AgCl) and a stable high current density.	Khoo et al. (2011); Yan et al. (2014)

2.4.4 Electrolyte Additives in Mg-air Battery System

In common, there are two approaches to reduce the Mg electrode corrosion in the Mg-air battery. The first method is alloying Mg with elements such as Zn, Mn, and Al. The second approach is the influence of electrolyte. The addition of electrolyte additives to the battery is one of the methods in order to decrease the Mg corrosion and enhance the battery performance. Table 2.5 illustrates the electrolyte additives recently used in the study of primary Mg-air battery.

Among these electrolyte additives, rGO (graphene synthesised through the reduction of graphene oxide) seems to give a promising result. As asserted by Mayilvel Dinesh et al. (2015), graphene is an encouraging catalyst additive in the NaCl electrolyte of Mg-air battery. Graphene is not susceptible to corrosion effects (Lih et al., 2012). Apart from this corrosion inhibition effect, graphene also has many other interesting properties which make it stands out as the electrolyte additive. It has excellent electrical conductivity (Selvam et al., 2013). In addition, Jörissen (2006) and Zhu et al. (2010) mentioned that the large surface area of the graphene materials which serve as electrocatalyst results in high thermal stability and high mechanical stability. Zhu et al. (2010) stated that graphene is chemically inert and stable at temperature up to 400°C. The tensile modulus and ultimate strength values of graphene sheets are resembling those of the single-walled carbon nanotubes (Zhu et al., 2010). Nevertheless, it is widely known that rGO has low solubility and dispersibility in water or solvents, and tends to agglomerate. Therefore, there is a potential that when the solubility of rGO is improved (such as the formation of WSG), it can then be well dispersed in the gel electrolyte and lead to the enhancement of the Mg-air battery performance.

Table 2.5: Electrolyte additives in primary Mg-air battery.

Electrolyte Additive	Remark	Reference
MoS_2	MoS_2 restricts the Mg breakdown during self-discharge and also the rate of Mg anode corrosion. MoS_2-based Mg-air battery achieves maximum discharge capacity of 1170 mAh g^{-1}, which is 18.18% of Mg-air battery without MoS_2.	Shyma, Palanisamy, Rajendhran, and Venkatachalam (2019)
$NaVO_3$, $Na_3PO_4 \cdot 12H_2O$	The phosphate has a greater corrosion inhibition effect than vanadate. The anodic efficiencies of the Mg-air batteries with blank, phosphate-containing, and vanadate-containing electrolyte are 59.7%, 72.5%, and 68.8%, respectively, under constant-current continuous discharging.	Y. Zhao, Huang, Zhang, Peng, and Pan (2018)
Na_3PO_4 + SDBS	In the 3.5 wt% NaCl electrolyte containing both of the additives, the self-corrosion of AZ91 alloy anode is low and the inhibition efficiency reaches 95.2%.	Yaqiong Li et al. (2018)
Decyl glucoside	The maximum inhibition efficiency (>94%) is achieved at the additive concentration of 2.5 mM. It increases the operating voltage, anodic utilisation, and discharge capacity of Mg-air battery.	Deyab (2016)
Li_2CrO_4	Addition of Li_2CrO_4 in electrolyte reduces the anode self-corrosion rate, thus improve the efficiency of Mg-air battery by 28.4%.	Y.-C. Zhao et al. (2016)
rGO	The assembled Mg-air battery with rGO has a specific discharge capacity of 1030.71 mAh g^{-1}, which is 25.26% greater than that of the conventional type. The battery life is increased by 30.95%.	Mayilvel Dinesh et al. (2015)

2.5 Graphene

2.5.1 Structure

Lately, carbon nanomaterials have gained much attention in the fields of energy, catalysis, and environmental technologies (Qiu & Zou, 2012). Graphene, which is one of the carbon allotropes, was first experimentally found in 2004 (Novoselov et al., 2004). Graphene is a two dimensional (2D) carbon material. It is the monolayer sp^2 bonded carbon atoms, arranged in a hexagonal honey comb lattice structure (Selvam et al., 2013). Graphene is the fundamental building block of the carbon allotropes, for instance, graphite (3D), carbon nanotube (1D) and fullerene (0D), as shown in Figure 2.3.

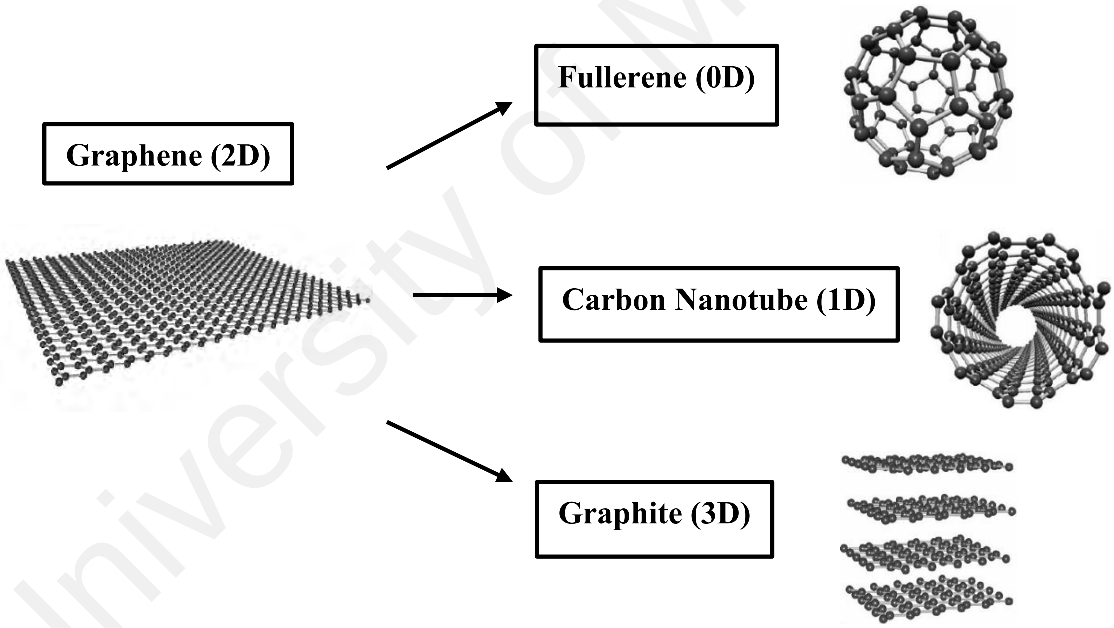

Figure 2.3: Graphene is the fundamental building block of the entire “graphitic” materials.

2.5.2 Synthesis

Graphene can be produced through different synthesis method, namely the chemical exfoliation, micromechanical exfoliation, colloidal suspension, chemical vapour deposition, and epitaxial growth. Each synthesis method results in graphene with differed quality. The last four synthesis methods can produce graphene with relatively high quality and perfect structure. However, chemical exfoliation tends to be the most popular route to prepare graphene (Pei & Cheng, 2012). Chemical exfoliation from bulk, inexpensive graphite can produce a high yield of graphene in a simple and economical way (Pei & Cheng, 2012).

2.5.2.1 Chemical Exfoliation (Reduction of Graphene Oxide)

Hernandez et al. (2008) and Parvez et al. (2014) stated that chemical exfoliation is the general method used by the researchers for synthesising graphene. Commonly, Hummers' method has been used for the production of graphene oxide (Hummers Jr & Offeman, 1958; Parvez et al., 2014). It utilises the mixture of sulphuric acid and potassium permanganate for the reaction to occur (Hummers Jr & Offeman, 1958; Parvez et al., 2014). Lai et al. (2015) stipulated that the mixture of sulphuric acid and potassium permanganate acts as the oxidising agent, which will oxidise the graphite to weaken the interlayer bonding. Consequently, thermal reduction or chemical reduction will be utilised to reduce the graphene oxide. Among the reducing agent, hydrazine is generally being used in research to reduce graphene oxide and forms highly exfoliated reduced graphene oxide (rGO) sheets. This method has a low cost of production and requires less operation time. In addition, it also obtains a high yield of graphene. Nonetheless, the graphene sheets produced may have structural defects (Lai et al., 2015).

2.5.2.2 Micromechanical Exfoliation (Scotch-Tape Method)

According to Huc et al. (2008), layers of graphene are peeled off from a graphite crystal by utilising the adhesive tape. Lai et al. (2015) mentioned that the flakes formed through this technique vary significantly in terms of their thickness and size. The sizes of the flakes for single-layer graphene lie between nanometers to several tens of micrometres. The cost of production for this technique is low since it only requires adhesive tapes and graphite powder. Besides, the prepared graphene has high quality with nearly no defects. Nevertheless, this technique has a problem with the low production of graphene and also the low reproducibility (Lai et al., 2015).

2.5.2.3 Colloidal Suspension

Graphene can be synthesised in liquid-phase in order to produce high production of graphene. Lotya, King, Khan, De, and Coleman (2010) mentioned that the simplest way would be the dispersion of graphite in an organic solvent, for example, ethanol, N-methylpyrrolidone (NMP), tetrahydrofuran (THF), and dimethylsulfoxide (DMSO) which have the surface energy similar to graphite.

After that, the solution is sonicated for a long duration or applied with a voltage (Su et al., 2011). Lai et al. (2015) stated that the solution is centrifuged after the dispersion to get rid of the thicker flakes. The graphene flakes produced via this method have similar quality with the graphene flakes obtained from micromechanical exfoliation. The cost of production of the colloidal suspension method is low and the yield of graphene is high. However, the production of graphene requires a long period of time (Lai et al., 2015).

2.5.2.4 Chemical Vapour Deposition

As mentioned by Lai et al. (2015), the formation of graphene via chemical vapour deposition method is conducted through the exposure of a substrate to gaseous compounds at high temperature. A thin film is grown when the gaseous compounds decompose on the surface of the substrate (Lai et al., 2015). At the temperature of 1000 °C, graphene can be grown when Ni film is exposed to a mixture of methane, hydrogen, and argon gases (K. S. Kim et al., 2009; Strudwick et al., 2014). The diffusion of carbon into Ni occurs after the methane decomposes on the Ni surface. After that, the Ni surface is cooled in an argon atmosphere and the graphene layer will develop on the surface (K. S. Kim et al., 2009; Strudwick et al., 2014). According to Lai et al. (2015), graphene synthesised from this method has very high quality with nearly no defects. However, the cost of graphene production is very high as compared to the other methods (Lai et al., 2015).

2.5.2.5 Epitaxial Growth

The heating and cooling down of SiC crystals can produce single- or bi-layer graphene on the Si face of the crystal, while the few-layer graphene is formed on the C face (Cambaz, Yushin, Osswald, Mochalin, & Gogotsi, 2008; W. Yang et al., 2013). The processing parameters like pressure, temperature, and rate of heating will give a significant influence on the results. For example, nanotubes will be produced instead of graphene, if the pressure and temperature are too high (Cambaz et al., 2008; W. Yang et al., 2013). Enderlein (2010) mentioned that the evaporation of a thin Ni layer onto a SiC crystal is the common epitaxial growth method. Depending on the heating rate, graphene or graphite oxide will be grown on the surface as the carbon diffuses through the Ni layer.

With the presence of Ni, the graphene produced is easily detached from the SiC crystal surface (Enderlein, 2010). According to Lai et al. (2015), graphene begins to grow at various locations on the crystal, and these graphene islands gradually grow together. Consequently, the graphene produced may have defects or grain boundaries, which causes it to be imperfectly homogeneous. Therefore, the graphene produced has a lower quality as compared to that of micromechanically exfoliated graphene, unless the graphene is grown on a perfect single crystal. Although this method is unable to form a large amount of graphene as compared to the liquid-phase exfoliation method, the results obtained are reproducible (Lai et al., 2015).

2.5.3 Water-Soluble Graphene (WSG)

Technological applications of graphene sheets normally require graphene solutions (or dispersions) either in water or in a solvent (G. Wang, Shen, Wang, Yao, & Park, 2009). Nonetheless, many of the as-prepared graphene itself is not soluble, thus cannot be dispersed in water or solvents (G. Wang et al., 2009). This makes aggregation a crucial obstacle in synthesising and processing bulk quantities of graphene sheets (D. Li, Müller, Gilje, Kaner, & Wallace, 2008). Graphene sheets that are not well separated from each other might produce irreversible agglomerates or even restack to form graphite in aqueous solution, via van der Waals interactions. This problem has been an issue in the large scale production of graphene via chemical or thermal reduction. Therefore, the prevention of aggregation is vital for rGO sheets in order to maintain their distinctive properties, which are mostly associated with individual sheets (D. Li et al., 2008). This motivates the production of WSG, which are the isolated graphitic sheets with greater water solubility (or dispersibility), as well as the prevention of aggregation in the aqueous solution (Si & Samulski, 2008). As an electrolyte additive in Mg-air battery, the full utilisation of WSG will inevitably depend on the ability to achieve good dispersion in the gel electrolyte, thus improving the battery performance. Table 2.6 shows the various synthesis methods for obtaining WSG in the past literature.

Table 2.6: Various synthesis methods for the production of WSG.

Synthesis Method	**Reference**
Formation of aminoclay-rGO composites via *in situ* condensation of aminoclay over graphite oxide prior to chemical reduction.	Achari, Datta, De, Dravid, and Eswaramoorthy (2013)
Coating the graphite oxide with polyacrylate (3-sulfopropyl methacrylate and its combination with polyethyleneglycol methacylate and N-(3-aminopropyl) methacrylamide), followed by chemical reduction into water-soluble polyacrylate-coated graphene.	Saha, Basiruddin, Ray, Roy, and Jana (2010)
Non-covalent functionalisation of rGO with lignin and cellulose derivatives (sodium lignosulfonate, sodium carboxymethyl cellulose, and pyrene-containing hydroxypropyl cellulose).	Q. Yang, Pan, Huang, and Li (2010)
Functionalisation of rGO with sulphonated polyaniline by chemically reducing the graphite oxide in the presence of sulphonated polyaniline.	Bai, Xu, Zhao, Li, and Shi (2009)
rGO sheets covalently functionalised with poly-L-lysine during chemical reduction.	Shan et al. (2009)
Covalent grafting of polystyrene-polyacrylamide copolymer on rGO sheets via *in situ* living free-radical polymerisation during chemical reduction.	Shen, Hu, Li, Qin, and Ye (2009)
rGO nanoplatelets were coated with the amphiphilic polymer, poly(sodium 4-styrenesulfonate) by chemically reducing the exfoliated graphite oxide in the presence of poly(sodium 4-styrenesulfonate).	Stankovich et al. (2006); G. Wang et al. (2009)
Sulphonation of the partially reduced graphene oxide by using aryl diazonium salt of sulfanilic acid prior to the final reduction stage.	Si and Samulski (2008)
Formation of stable aqueous rGO colloid through electrostatic stabilisation with NH_3 during chemical reduction.	D. Li et al. (2008)

As shown in Table 2.6, most of the synthesis methods for obtaining WSG (except the last synthesis method) consist of the functionalisation of rGO sheets with other molecules or polymers, in order to minimise the aggregation of the sheets. Nevertheless, the existence of these foreign stabilisers can influence the other favourable properties of rGO sheets, which is undesirable for most application (D. Li et al., 2008). Therefore, the synthesis of WSG through the electrostatic stabilisation during the chemical reduction process appears to be a suitable approach that can improve the solubility of WSG while minimising the influence on the other properties.

2.6 Electrolytes

An electrolyte is a substance comprising of free ions which enables it to be electrically conductive. Commonly, the electrolyte is formed when a solute dissolved in a solvent. Electrolyte has a significant role in the electrochemical performance of batteries, regarding the capacity, energy density, and power density. Electrolytes can be categorised into two groups based on their physical states, which are the liquid and solid electrolytes. Liquid electrolytes are electrolytes in the liquid state, which have high conductivities. On the other hand, solid electrolytes are electrolytes in the solid state. The ionic conductivity of solid electrolyte differs from 10^{-2} to 10^{-6} S cm^{-1}, which is lower than the liquid electrolytes.

2.6.1 Liquid Electrolytes

Liquid electrolytes have been extensively investigated in the electrochemical devices. Although liquid electrolytes have high ionic conductivity, they have several drawbacks in their application. The electrolytes in the liquid state could possess the leakage problem, evaporation of the electrolyte, electrolytic degradation of the electrolyte, poor long term stability, and also safety concern regarding the use of the flammable organic solvent (Ramesh, Liew, & Ramesh, 2011; Y. Yang et al., 2008). Moreover, the bulky size of the liquid requires a larger space, which in turn lowers the energy and power density. Other disadvantages of liquid electrolytes include the narrow range of operating temperature, handling and manufacturing problem due to the liquid phase present in the electrolyte, and also the risk of internal short circuit (Gray, 1997; Stephan, 2006). As a solution to the aforementioned problems, solid electrolytes have emerged to replace the conventional liquid electrolytes.

2.6.2 Solid Electrolytes

Classification of solid electrolytes is shown in Figure 2.4. Solid electrolytes are mainly classified into four categories, which are the crystalline solid electrolytes, glass electrolytes, molten electrolytes, and polymer electrolyte according to their microstructure and physical properties.

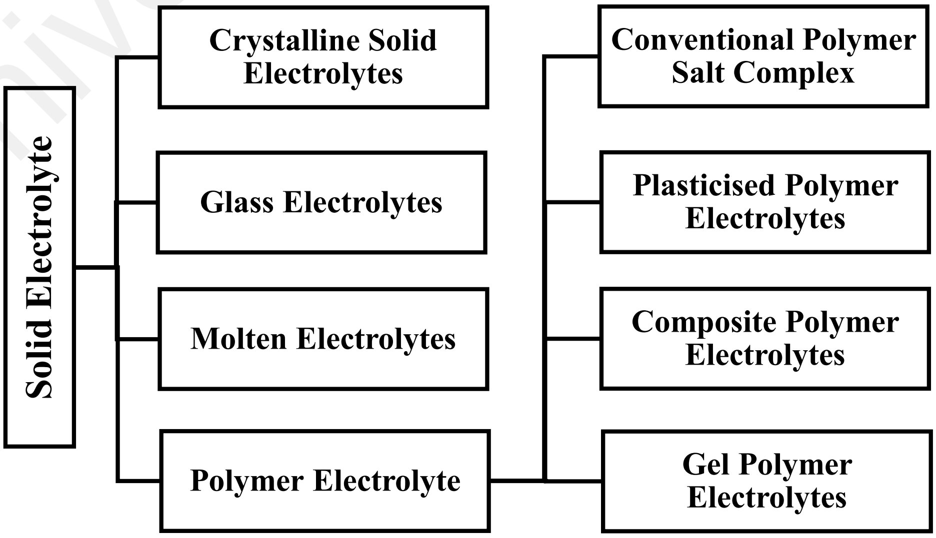

Figure 2.4: Classification of solid electrolytes.

The polymer electrolyte was first studied in 1973. However, the technology applications of the polymer electrolytes in diverse solid state electrochemical devices were started in late 1970. Polymer electrolytes are more preferable as compared to crystalline and glassy electrolytes (Gray, 1991; Kuo et al., 2013; Q. Zhang, Liu, Ding, & Liu, 2017). This is because polymer electrolytes are true solids which are able to offer liquid-like degree of freedom at the atomic level, whereas the crystalline solid and glassy electrolytes are hard and brittle materials. Polymer electrolytes are intermediate between liquid electrolytes and solvent-free molten electrolytes. They possess various advantages over the other three types of solid electrolyte such as simple processing procedures, leakage-free, excellent flexibility, light weight, good interfacial contact with electrodes, superior mechanical properties, low electronic conductivity, and high chemical stability (Gray, 1991; Kuo et al., 2013; Q. Zhang et al., 2017).

Polymer electrolytes can be further categorised into conventional polymer salt complex, plasticised polymer electrolytes, composite polymer electrolytes, and gel polymer electrolytes based on their preparation method. Conventional polymer salt complex (Dry SPEs) are polymer-salt complexes which are formed by complexation of salt in a polar polymer host (Gray, 1991; Kuo et al., 2013; Q. Zhang et al., 2017). Plasticised polymer electrolytes are prepared from the addition of a plasticiser (low molecular weight and high dielectric constant material) to dry SPEs. Composite polymer electrolytes are produced by inserting a small proportion of micro/nano size organic or inorganic filler particle into the conventional SPE host. However, for gel polymer electrolytes (GPEs), they are produced through the addition of non-conducting polymer to a liquid electrolyte at an optimum ratio in order to produce a gel by polymerisation. The polymer added provides mechanical support to the system (Gray, 1991; Kuo et al., 2013; Q. Zhang et al., 2017). GPEs is an electrolyte with a solid-liquid like properties (Scrosati & Vincent, 2011).

2.6.3 Gel Polymer Electrolytes (GPEs)

Gels are defined as the 3D network structure of the polymer and their swollen mattes which are insoluble in any solvent. They integrate both the diffusive transport properties of liquid and the cohesive properties of solids (Sekhon, 2003). Depending on their chemical composition, their properties may differ from viscous liquid to hard solid, based on the polymer network structure and also the interaction between the network and the solvent. Gels commonly have high mobility due to the large amount of trapped solvent in the polymer network. The salt, solvent, and polymer play different roles in GPEs. The salt mainly dissociates to give mobile ions which participate in the conduction process. Solvent aids in solvating the salt besides acting as a conducting medium. For the polymer, it gives mechanical stability by increasing the viscosity of electrolyte (Sekhon, 2003).

Di Noto, Lavina, Giffin, Negro, and Scrosati (2011) defined GPEs as the electrolyte material in which a supramolecular system is doped with ions, and has a significant conductivity. Masri, Nazeri, and Mohamad (2010) mentioned that GPEs consist of a dopant-solvent-polymer hybrid system. GPEs can prevent the electrolyte leakage problem of aqueous electrolytes while solving the low ionic conductivity problem of solid polymer electrolyte. GPEs have the benefits of both the liquid and solid electrolytes. They have gained much attention since they act as both electrolytes and separators (Arya & Sharma, 2017; Osada, de Vries, Scrosati, & Passerini, 2016; Jinqiang Zhang, Sun, Huang, Chen, & Wang, 2014). In addition, the workability of GPEs allows the production of energy storage devices with great flexibility and adjustable size (Cui et al., 2017; Weng et al., 2015; Y. Zhang et al., 2015). Subsequently, GPEs become one of the most appealing electrolytes for the electrochemical energy storage devices.

2.6.4 Synthetic and Natural Polymers

Polymers are mainly categorised into two classes, which are the synthetic polymers and natural polymers. Synthetic polymers are man-made polymers using chemicals. The most generally studied synthetic polymer electrolytes are polyethylene oxide (PEO). However, the PEO-based SPEs normally has low ionic conductivity (10^{-7} S cm $^{-1}$) at the room temperature, which restricts their practical applications. There are also a wide variety of the other synthetic polymers, for example, polymethyl methacrylate (PMMA), polyacrylonitrile (PAN), polyvinyl alcohol (PVA), polyvinylpyrrolidone (PVP), and poly(vinylidene fluoride-co-hexafluoropropylene) (PVdF-HFP) which have been explored for the electrolyte applications. Most of the synthetic polymers are non-biodegradable, which makes them difficult to decompose. During the combustion of plastic materials, toxic gases are emitted. This results in the depletion of the ozone layer, which in turn causes environmental pollution.

In recent years, a growing interest has been devoted to the development of electrochemical devices which are light, safe, and also with a low production cost. Consequently, new electrolytes to substitute the current synthetic polymer electrolyte are continuously investigated. Natural polymers have become the target of the new materials research tendencies as a result of the increasing alerts regarding the environmental destruction caused by synthetic polymers. They have the advantages in term of their biodegradability, excellent physical and chemical properties, safety, economical, environmental friendliness, and good performance as SPEs (Avellaneda et al., 2007; Pawlicka, Danczuk, Wieczorek, & Zygadło-Monikowska, 2008). Among the natural polymers, the high abundance of polysaccharides and proteins in the environment makes them the great candidates to replace the synthetic polymers. These natural polymers are broadly applied in the food, pharmaceutical, and cosmetic, before the discovery of their electrochemical applications. The few types of natural polymer used for the preparation of SPEs are shown in Table 2.7. From the literature, it is worth noting that biopolymers are good candidates for the invention of a new form of electrolytes.

Among these natural polymers, agar seems to be a good candidate as a gel polymer electrolyte. Agar is a highly available, low cost, and chemically stable natural polymer (Boopathi et al., 2017). It is made up of the soluble dietary fibres which have a high solubility in water or electrolyte, thereby having the ability to form gel with a variety of aqueous electrolytes (Barat & Cano, 2015). It also has the syneresis property (the expelsion of liquid from the gel) which helps to wet the surface and enhances the electrode/electrolyte contact (Barat & Cano, 2015). The liquid trapping and syneresis properties of agar gel enable the storing, transporting and releasing of water in the GPE produced, thereby facilitating the battery operation (Barat & Cano, 2015). In addition, the liquid trapping and amorphous nature of agar gel may contribute to the high conductivity of GPE produced (Sivadevi et al., 2016), which is a favourable property required as the electrolyte. Cano et al. (2014) mentioned that the utilisation of agar gel as the electrolyte can produce an electrolyte which is generally simple to prepare, biodegradable, and also innocuous to both human beings and environment. Nevertheless, there is lacking of study to apply agar gel as GPE of Mg-air battery.

Table 2.7: Natural polymers used for the preparation of SPEs.

Natural Polymers	Description	Sources	Application
Cellulose	• Polysaccharides comprising of a linear chain of β-1,4 linked d-glucose units with a polymerisation degree of several hundred to more than ten thousand. • The most abundant organic polymer.	Plants, bacteria	• Fuel cells (Bayer et al., 2016) • Dye-sensitized solar cells (DSSCs) (Chiappone et al., 2014)
Starch	• Polysaccharides with a stable helix structure, which are formed from the repeating glucose monomers linked by glycosidic bonds. • The largest percentage of carbohydrate in human diets.	Staple food such as wheat, corn, and potatoes	• DSSCs (Nagaraj, Sasidharan, David, & Sambandam, 2017) • Lithium sulphur battery (Lin et al., 2016)
Chitosan	• A derivative of chitin. • The most abundant natural amino polysaccharide.	Crab and shrimp shells	• Lithium micro batteries (Begum, Pandian, Aswal, & Ramasamy, 2014) • Mg-air battery (Jia et al., 2014)
Agar	• Comprised of agarose and agaropectin. • Basic repeating unit of β-1,3-linked- D-galactopyranose and α-1,4-linked 3,6-anhydro-L-galactopyranose	Agarophyte red seaweed	• Proton battery, fuel cell (Selvalakshmi et al., 2019) • Fuel cell (Boopathi et al., 2017)

Table 2.7, continued: Natural polymers used for the preparation of SPEs.

Natural Polymers	Description	Sources	Application
Agarose	• Linear polymer hydrocolloid consisting of alternating D-galactose and 3,6-anhydro-L-galactose units, which is isolated from agar.	Agarophyte red seaweed	• Supercapacitors (Moon et al., 2015) • DSSCs (Y. Yang et al., 2014)
Pectin	• Polysaccharides consisting of a linear chain of 1,4-linked galacturonic acids esterified with methacrylatecrylatenol.	Plants	• Proton battery (Muthukrishnan et al., 2018) • Primary lithium-ion battery (Perumal, Selvin, & Selvasekarapandian, 2018)
Gelatin	• A high molecular weight polypeptides derived from collagen (primary protein component of animal connective tissues)	Bone, skin, and tendon of animals	• Electrochromic devices (Vieira & Pawlicka, 2010) • Electrochromic devices (Al-Kahlout et al., 2010)
Carrageenan	• Polysaccharides consisting of hydrophilic sulphated linear galactans that primarily made up of D-galactopyranose units.	Carrageenophyte red seaweed	• Fuel cells (Selvin et al., 2018) • DSSCs (Bella, Mobarak, Jumaah, & Ahmad, 2015)

2.7 Agar Gel

2.7.1 Sources of Agar

Barat and Cano (2015) asserted that agar is a natural polysaccharide obtained from the cell matrix of some but not all species of red seaweeds. Biologically, agar provides the seaweeds with a flexible structure, which enables them to tolerate the different stresses of currents and wave motion (Hernandez-Carmona, 2013). According to Mantri, Reddy, and Jha (2010), red algae are eukaryotic autotrophs. They are mostly reported from the marine environment, with a few that are found in freshwater. The microscopic red algae which live in a marine environment is generally referred as red seaweeds (Mantri et al., 2010).

Among the various genus of red seaweeds, the genus *Gracilaria* and *Gelidium* are the major sources for agar production, which comprise of 53% and 44% respectively, of the total amount of agar produced (McHugh, 1991). The other types of agarophytes such as *Pterocladia* and *Gelidiella* only contribute a small quantity of agar (3%). The agar obtained from the genus *Gelidium* has the highest quality among the agarophytes. However, the agar extracted from the treated *Gracilaria* is becoming an outstanding substituent for *Gelidium* agar owing to the lower cost and greater wild stock abundance (McHugh, 1991).

2.7.2 Agar Extraction

The agar production process is shown in Figure 2.5. According to Hernandez-Carmona (2013), although the agar extraction procedure is different for each seaweed species, it commonly consists of an alkali treatment prior to the hot-water extraction. The main stages of the agar production process are the pretreatment, extraction, filtration, concentration, and dehydration.

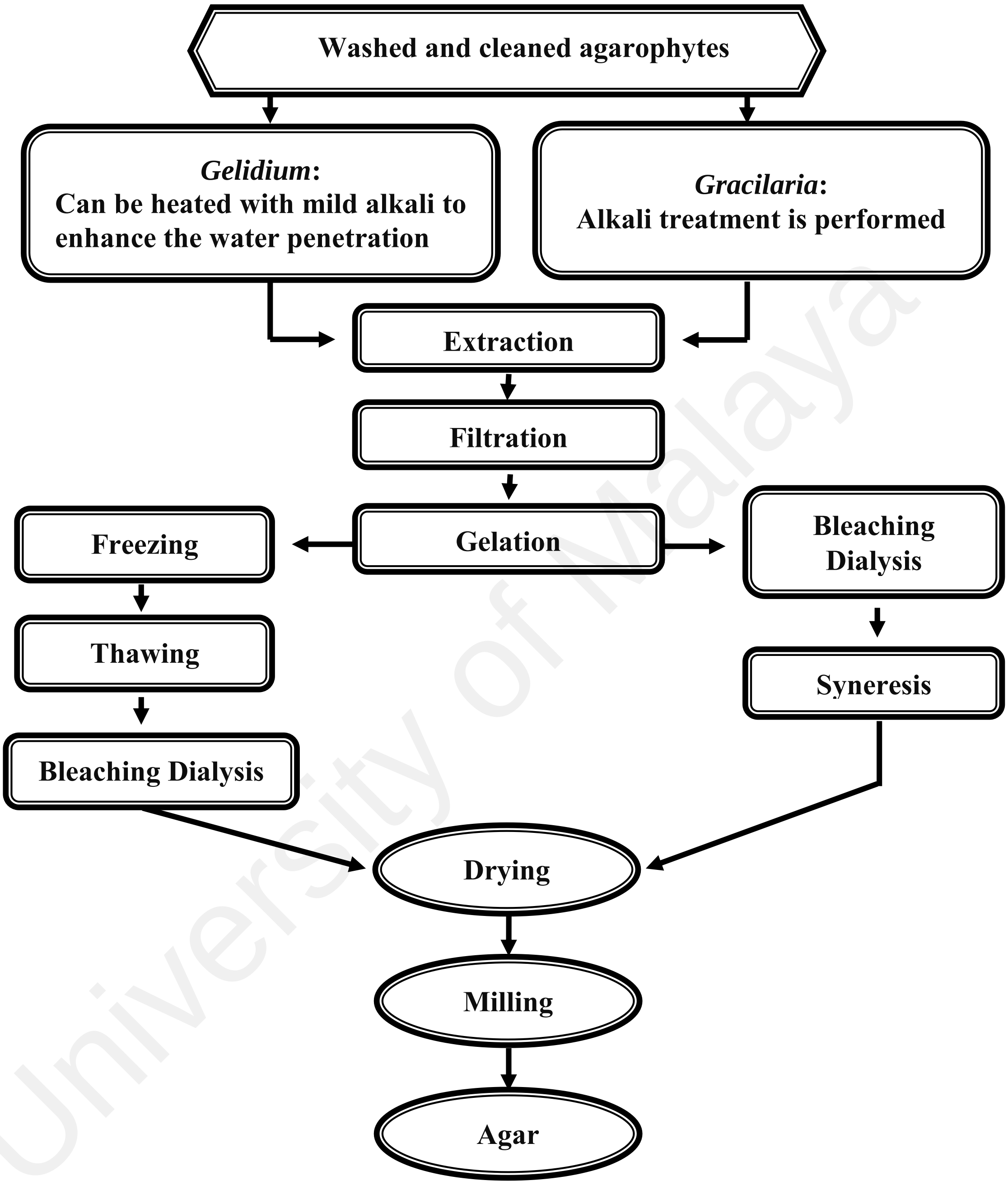

Figure 2.5: Agar production processes.

First of all, the seaweeds obtained from the seashore are washed and cleaned in order to discard the salts, sand, and other impurities. The type of pretreatment varies according to the genus of seaweed used. Pretreatment is not a compulsory step for *Gelidium* since it can produce high quality agar even without pretreatment. However, corrective treatment with a mild alkaline solution (commonly sodium carbonate) can be applied to remove the pigment phycoerythrin, apart from softening and preparing the seaweed for better extraction (Hernandez-Carmona, 2013). For *Gracilaria*, alkali treatment is performed prior to the extraction in order to improve solution (concentration range of 0.5% to 7%). The time, temperature, and concentration of the alkali are varied for each species of *Gracilaria* in order to promote desulphation while reducing yield loss. The seaweeds are heated for 1-2 hours at 85-90 °C in sodium hydroxide.

After that, the seaweeds are cleaned with water and dilute acid to neutralise the residual alkali. The agar extraction is done by using hot water extraction (cooking in an excess of water at boiling point), which can be further aided by the addition of acid to pH 6.3 - 6.5 or cooking the seaweeds under pressure). However, optimum conditions need to be established for different kind of seaweeds to avoid the potential destruction of these two conditions to the extracted agar. At the end of the extraction, the residual seaweed is removed by filtration, and the hot filtrate containing the dissolved agar is cooled to produce a gel. The gel may be treated with bleach (commonly sodium hypochlorite) for decolourisation, followed by washing to eliminate the bleach, forming a gel with about 1% agar. The remaining 99% is comprised of water and soluble impurities (oligomers, proteins, organic and inorganic salts) which is necessary to be removed. This removal is done by either the freeze-thaw process or syneresis (Hernandez-Carmona, 2013).

2.7.3 Structure and Properties of Agar

Matsuhashi (1990) explained that agar is a highly gelling seaweed hydrocolloid which consists of polysaccharides. The basic repeating units of agar would be agarobiose (galactose) with β-1,3-linked- D-galactopyranose and α-1,4-linked 3,6-anhydro-L-galactopyranose. Agar is primarily consisting of agarose and agaropectin. Agarose is a neutral (non-ionic) polysaccharides with linear arrangement which functions as a gelling component (Matsuhashi, 1990). As mentioned by Venugopal (2011), agarose is enzymatically polymerised and desulphated. It has a double helix structure which aggregates into a 3-dimensional network and holds the water molecules within the interstices of the network, thus producing the gels (Venugopal, 2011). On the other hand, agaropectin is an acid (ionic) polysaccharides which is the non-gelling component (Matsuhashi, 1990). Venugopal (2011) asserted that agaropectin contains sulphate group, pyruvic acid, D-glucuronic acid, and agarobiose. The presence of sulphate group is the main difference between the agarose and agaropectin (Venugopal, 2011). The composition of agarose and agaropectin in the agar are different for different commercial agar.

Koyikkal (2013) mentioned that the gelling power of agar in aqueous solutions is very high. Under the same concentrations, agar gel has a higher gel strength than the gel produced from the other gel-forming agents. The presence of additives is not required for the gelation process. It can be operated from pH 5 to pH 8, which is a wide range of pH values. In addition, it is able to resist the heat treatment even at a temperature above 100 °C. The gelling temperature of a 1.5% aqueous solution of agar is around 32 °C to 43 °C, whereas the melting point is 85 °C. The gelation of agar is a reversible process, which enables the repeat gelling and melting of agar gel without any loss of its properties. Agar gel is a stable compound and hence no precipitates will be formed in the presence of cations (Koyikkal, 2013). Agar has been widely applied in the food, microbiology, pharmaceutical, medical and the other industries.

2.7.4 Application of Agar Gel in Electrochemistry

Kasem (2005) had conducted a study to investigate the propriety of agar gel as an alternative immobilised electrolyte media and also as a polymer electrolyte for electrochemical studies. The results obtained revealed that agar gel is a vital representation of the new type of electrolyte, which has an intermediate state between liquid- and solid-state electrolytes (Kasem, 2005). In addition, Leones et al. (2012) and Lima et al. (2012) had studied the use of agar-ionic liquid-based and agar-europium-based electrolytes in electrochemical devices. Cano et al. (2014) had also found the use of agar gel electrolyte for in-situ application of corrosion electrochemical testing. Selvalakshmi et al. (2019) had investigated the use of NH_4Br-doped agar polymer electrolyte in battery and fuel cell. The best NH_4Br-doped agar polymer electrolyte had the ionic conductivity of 1.33×10^{-4} S cm^{-1}. The battery constructed by using the NH_4Br-doped agar polymer electrolyte had the output voltage of 1.80 V whereas the fuel cell had the output voltage of 500 mV (Selvalakshmi et al., 2019). Furthermore, Boopathi et al. (2017) had prepared a proton-conducting polymer electrolyte based on agar and NH_4NO_3. The prepared polymer electrolyte had the highest ionic conductivity of 6.57×10^{-4} S cm^{-1}, and the open circuit voltage of the fuel cell constructed by using the polymer electrolyte was 558 mV (Boopathi et al., 2017). All these results encourage the use of agar as the attractive gel polymer electrolyte for electrochemical device applications, including Mg-air battery.

CHAPTER 3: METHODOLOGY

3.1 Introduction

In this chapter, five important sections are explained and discussed (Figure 3.1). Firstly, the experimental procedures to synthesis GO and WSG are described. Then the preparation and optimisation of WSG-AGAR gel electrolyte performance are elucidated. The third section emphasises on the characterisation of the sample such as XRD, Raman, ATR-FTIR, zeta potential, and FESEM. The fourth section elaborates on the fabrication of the Mg-air battery with the agar gel electrolyte. The last section covers the electrochemical measurements of the samples which are investigated through the ionic conductivity, EIS, and discharge performances.

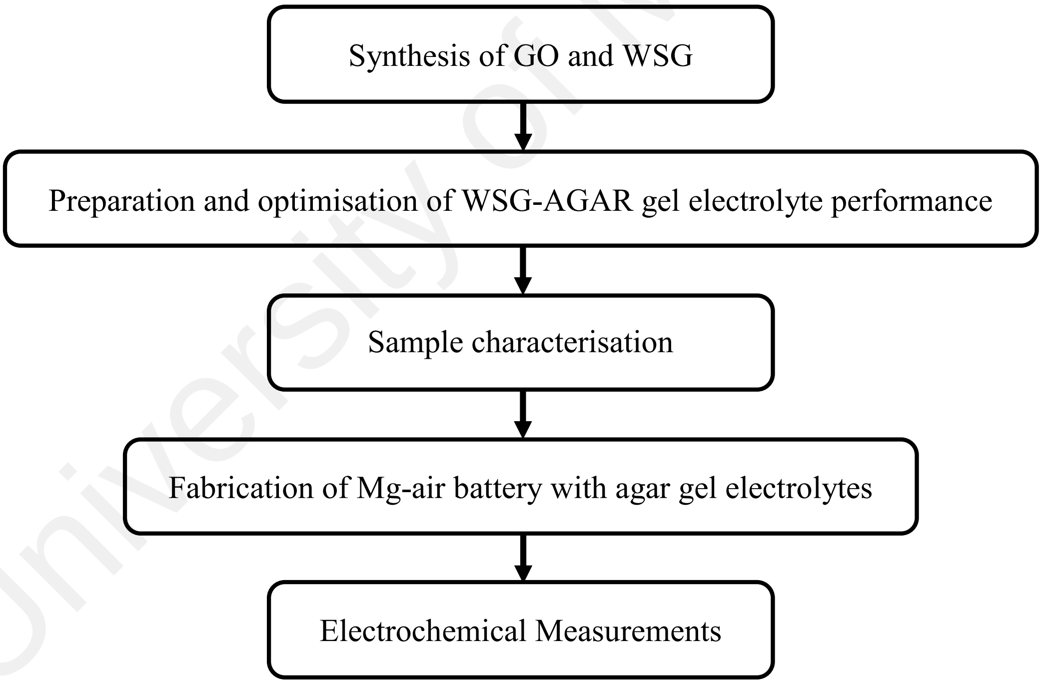

Figure 3.1: The research flow chart.

3.2 Raw Materials and Chemicals Selection

The raw materials and chemicals along with their roles and properties used in this study are shown in Table 3.1. All materials used were of analytical grade and no further treatment was required prior to their utilisation. Throughout the study, deionised water (18.2 MΩ) was utilised.

Table 3.1: The list of raw materials and chemicals used in the study.

Raw Materials/ Chemicals	Purity (%)	Molar Mass (g mol^{-1})	Roles	Manufacturer
Agar powder	-	-	Biopolymer material of the gel electrolyte	Sigma Aldrich (Steinheim, Germany)
Ammonia (NH_3)	25 wt% in H_2O	35.0	Create a basic reaction condition; Electrolyte	Merck (Darmstadt, Germany)
Carbon-based electrode	-	-	Cathode of the Mg-air battery	Magna Value (Sungai Petani, Malaysia)
Graphite powder	99	12.0	Precursor of WSG	Sigma Aldrich (Steinheim, Germany)
Hydrazine hydrate	80 wt% in H_2O	32.1	Reducing agent of WSG synthesis	Merck (Darmstadt, Germany)
Hydrochloric acid (HCl)	37	36.5	Remove the manganese salts in GO; Electrolyte	Friendemann Schmidt Chemical (Woodpark, Australia)

Table 3.1, continued: The list of raw materials and chemicals used in the study.

Raw Materials/ Chemicals	**Purity (%)**	**Molar Mass ($g\ mol^{-1}$)**	**Roles**	**Manufacturer**
Hydrogen peroxide (H_2O_2)	30	34.0	Terminate the oxidation reaction and eliminate the residual manganese dioxide and permanganate	Merck (Darmstadt, Germany)
Magnesium chloride hexahydrate ($MgCl_2•6H_2O$)	≥ 99.0	203.3	Electrolyte	Merck (Darmstadt, Germany)
Magnesium ribbon	≥ 99.5	24.3	Anode of the Mg-air battery	Merck (Darmstadt, Germany)
Potassium hydroxide (KOH)	≥ 85	56.1	Electrolyte	Merck (Darmstadt, Germany)
Potassium permanganate ($KMnO_4$)	99	158.0	Oxidising agent of GO synthesis	Friendemann Schmidt Chemical (Woodpark, Australia)
Sodium chloride (NaCl)	≥ 99.5	58.4	Electrolyte	Merck (Darmstadt, Germany)
Sodium sulphate (Na_2SO_4)	≥ 99	142.0	Electrolyte	Merck (Darmstadt, Germany)
Sulphuric acid (H_2SO_4)	95-97	98.1	Create an acidic reaction condition	Friendemann Schmidt Chemical (Woodpark, Australia)

3.3 Experimental Procedure

3.3.1 Synthesis of Graphite Oxide (GO)

GO was first produced through the simplified Hummers' method by Chong, Lai, and Abd Hamid (2015). 3 g of graphite powder was added to 70 mL of concentrated H_2SO_4 under ice bath condition. 9 g of $KMnO_4$ powder was gradually added into the mixture and stirred at a constant speed. The reaction temperature was cautiously kept at below 20 °C in order to prevent the explosion due to the heat generated from the exothermic reaction during the addition of $KMnO_4$. After the complete addition of $KMnO_4$, the temperature was increased to 35 °C and stirred for 24 hours to ensure the complete oxidation of the graphite powder. At the end of the oxidation, 150 mL of deionised water was added to the mixture, and the temperature was increased to 95 °C. Subsequently, 500 mL of deionised water and 15 mL of 30% H_2O_2 were added to the suspension for terminating the oxidation reaction. The colour of the solution turned from dark brown to yellow, illustrating the complete oxidation reaction. The product was centrifuged and washed with dilute HCl, followed by deionised water in order to remove the metal ions and acid residue (Chong et al., 2015). Finally, it was dried in the oven at 80 °C, producing GO.

3.3.2 Synthesis of Water-Soluble Graphene (WSG)

2 g of GO powder was added to 200 ml deionised water and the mixture was sonicated prior to the reduction. Different amount of NH_3 solution was added to the GO solutions to adjust the pH of the reactant solutions to pH 4, 7, 10, and 11, respectively. Subsequently, each reactant solution was poured into the round bottom flask, preparing for the reduction in a reflux setup. The reactant solution was first heated to 80 °C. After 15 minutes, 2 ml of N_2H_2OH was added to the reactant solution drop by drop, and the resulting solution was maintained at 80 °C for 6 hours. The experimental setup of the reduction process was

shown in Figure 3.2. The suspension was washed and finally dried in the oven at 80 °C, forming WSG. By controlling the amount of NH_3 solution added to the GO solutions, WSG-4, WSG-7, WSG-10, and WSG-11 were synthesised under similar experimental conditions. Reduced graphene oxide (rGO) was also produced without the addition of NH_3 prior to the reduction.

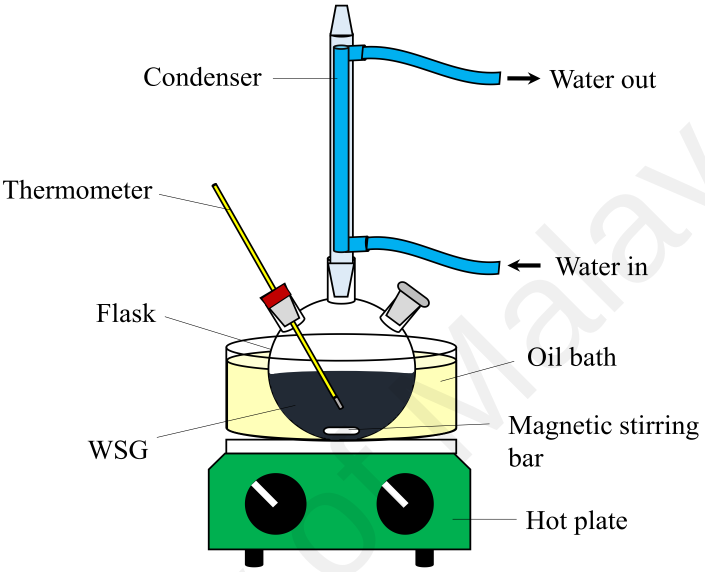

Figure 3.2: Experimental setup of GO reduction.

3.3.3 Preparation of Water-Soluble Graphene-Incorporated Agar (WSG-AGAR) Gel Electrolyte

0.6 M NaCl solution (approximately 3.5 % w/v NaCl) was prepared. 20 mg (0.1% w/v) of WSG-4 was subsequently added to 20 ml of the as-prepared NaCl solution and the mixture was stirred and treated with ultrasonication bath until the solution became homogeneous. In sequence, the solution was heated to 95 °C prior to the addition of 3 % w/v agar powder. After the agar had completely dissolved, the solution was poured into a mould and allowed to form gel at the room temperature. Various WSG-AGAR gel electrolytes were prepared under the similar experimental conditions by manipulating the WSG sample incorporated, agar concentration, WSG concentration, and types of electrolyte in order to produce the optimum WSG-AGAR gel electrolyte for the Mg-air battery application. The constant and independent variables for the preparation of WSG-AGAR gel electrolyte are shown in Table 3.2. An overview of the research methodology is also shown in Figure 3.3.

Table 3.2: Parameters investigated to produce the optimum WSG-AGAR gel electrolyte and the parameters kept at constant.

Independent Variables	Constant Variables
Incorporation of different WSG synthesised: WSG-4, WSG-7, WSG-10, WSG-11	Agar concentration= 3% w/v; WSG concentration= 0.1% w/v; 0.6 M NaCl electrolyte
Agar concentration in weight/ volume percentage (% w/v): 1% w/v, 2% w/v, 3% w/v, 4% w/v, 5% w/v	WSG-7; WSG concentration= 0.1% w/v; 0.6 M NaCl electrolyte
WSG concentration in weight/ volume percentage (% w/v): 0.01% w/v, 0.10% w/v, 0.30% w/v, 0.50% w/v	WSG-7; Agar concentration= 3% w/v; 0.6 M NaCl electrolyte
Types of electrolyte: Sodium chloride (NaCl) Sodium sulphate (Na_2SO_4) Magnesium chloride hexahydrate ($MgCl_2 \cdot 6H_2O$) Hydrochloric acid (HCl) Potassium hydroxide (KOH) Ammonia solution (NH_3)	Gelation test: Agar concentration= 3% w/v; Concentration of electrolyte= 0.6 M Electrochemical performance: WSG-7; Agar concentration= 3% w/v; WSG concentration= 0.1% w/v; Concentration of electrolyte= 0.6 M

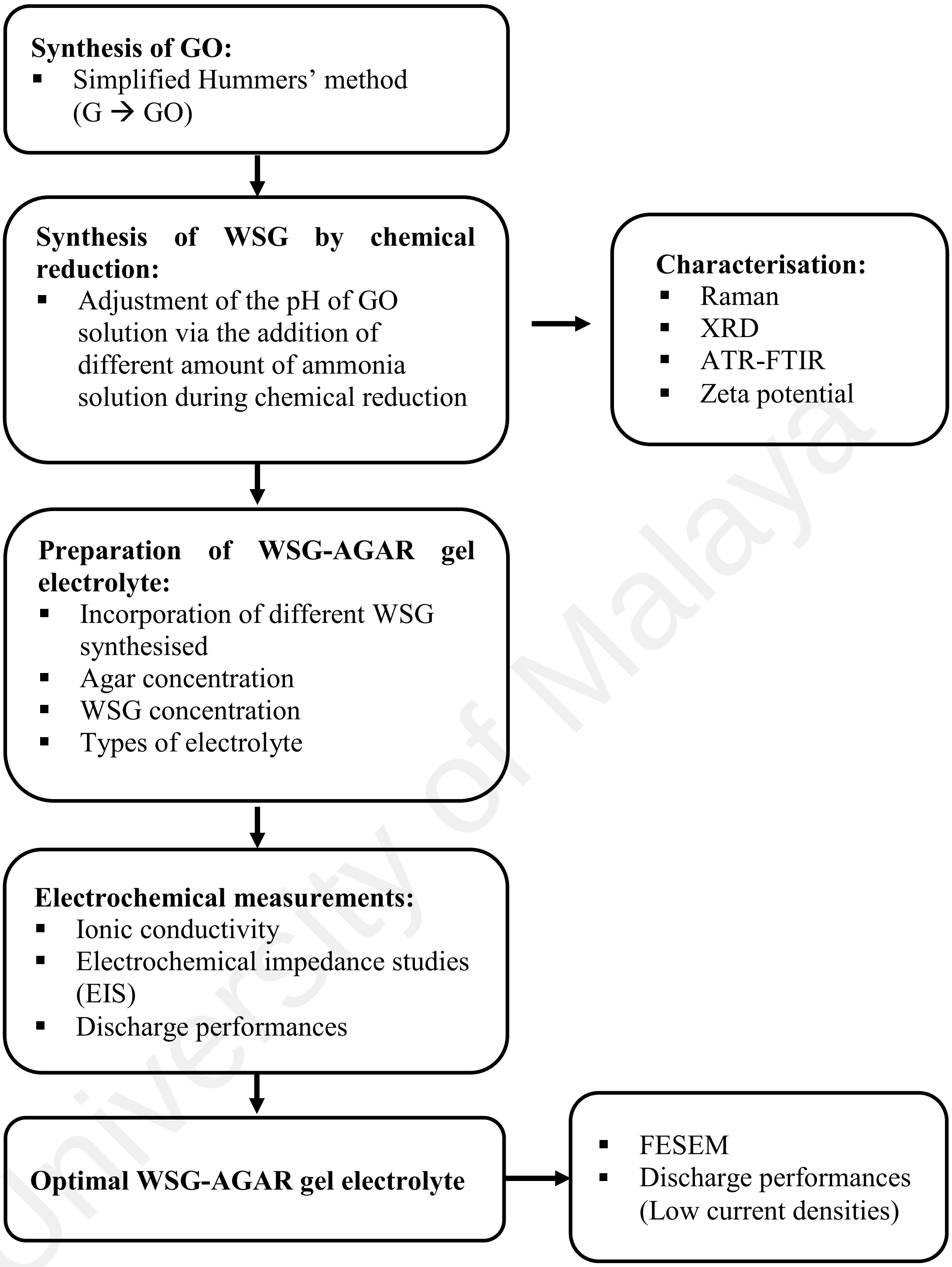

Figure 3.3: An overview of the research methodology.

3.4 Characterisation Techniques

3.4.1 Raman Spectroscopy

Raman spectroscopy is a rapid technique which is widely used to study the structure of carbon nanomaterials. In this study, a Raman spectrometer (inVia; Renishaw, United Kingdom) was used with an excitation source of Ar^+ laser at 514 nm. The sample was smeared uniformly onto the glass slide in order to perform the analysis. Raman scattering is produced by the inelastic scattering of monochromic light from the laser light source. The monochromic light interacts with the sample and results in a laser photon shift, which relates to the vibrational and rotational of the chemical bonds in the sample.

3.4.2 X-Ray Diffraction (XRD) Analysis

X-ray diffractometer is a rapid and non-destructive analytical technique commonly used for the study of crystal structures and atomic spacing. It consists of three basic components, which are the X-ray tube, sample holder, and X-ray detector. The X-rays are generated by the cathode ray tube, filtered to form monochromic radiation, and directed towards the sample. The incident rays interact with the sample, producing diffracted rays which are detected, processed, and counted, producing XRD spectrum.

In this study, an X-ray diffractometer (D8 Advance; Bruker AXS, Germany) was utilised. The sample was placed on the sample holder and ensured a flat upper surface was achieved. The sample was examined through a CuK_α radiation source at a wavelength of 1.5406 Å. A counter current of 30 mA and voltage rating of 40 kV were used for scanning the sample, and the rate of scanning was 0.05 min^{-1}. The sample was scanned at the angles ranging from 5° to 80°.

3.4.3 Attenuated Total Reflection Fourier Transform Infrared (ATR-FTIR) Spectroscopy

Attenuated total reflection Fourier transform infrared spectroscopy is a reliable fingerprinting method to characterise, identify, and quantify a substance. When an infrared beam is directed onto an optically dense crystal with a high refractive index, the internal reflectance generates an evanescent wave that reaches into the sample placed on the crystal surface. The evanescent wave is attenuated in the region where the sample absorbs energy. Each attenuated energy exits at the opposite end of the crystal and is recorded by the detector, producing an infrared spectrum.

In this study, an attenuated total reflectance Fourier transform infrared spectrometer (Spectrum 400; Perkin Elmer, United States) was used to identify the functional groups present in the sample. The sample was placed on the ATR crystal, assuring direct contact with the crystal was achieved. The sample was irradiated with the infrared (IR) radiation in the frequency range of 450 cm^{-1} to 4000 cm^{-1} with a scan resolution of 4 cm^{-1} to get the ATR-FTIR spectrum based on the transmittance characteristics of the sample.

3.4.4 Zeta Potential

The particles in a colloidal suspension commonly carry an electric charge. During the zeta potential measurement, an electric field is applied to the dispersion of particles, in which the particles will move with a velocity that relates to their zeta potential. The velocity is recorded to calculate the electrophoretic mobility, which is used to obtain electrostatic potential on the particle surface (zeta potential). Zeta potential is vital for determining the colloidal dispersion stability. It gives a measure of the magnitude and sign of the effective surface charge associated with the double layer around the colloidal particle.

A Zetasizer (Nano Series ZS; Malvern Panalytical; United Kingdom) was utilised to study the zeta potential of the sample. 1 mg of sample was dispersed in 10 ml of deionised water, forming a suspension with a concentration of 100 ppm to ensure good dispersion of the sample in the solution while enabling the zeta potential of the prepared sample to be measured. The sample suspension prepared was filled into the zeta cell, and ensure the absence of bubbles in the zeta cell or on the electrode. The conductivity of the sample in aqueous solution was also determined.

3.4.5 Field Emission Scanning Electron Microscope (FESEM)

Field emission scanning electron microscope is recognised as a tool to observe the structural morphology of a sample. Primary electrons are liberated from the field emission source and accelerated in a high electrical field gradient. They are focused and deflected by electronic lenses within the high vacuum column to generate a narrow scan beam that bombards the sample, resulting in the liberation of secondary electrons from each spot on the sample. The velocity and angle of the secondary electrons correspond to the sample's surface structure. The electronic signal generated by the detector is amplified and transformed into a video-scan image on a monitor or to a digital image that can be saved for further processing.

In this study, an environmental field emission scanning electron microscope (Quanta 200F; FEI, United States) was utilised to observe the morphology of the optimal WSG and WSG-AGAR gel electrolyte. For the WSG sample, the sample was scattered with a spatula and lightly pressed to ensure good mounting on the carbon tape. Generally, it is sprayed with rubber bulb air blower to remove the loose sample, which prevents the sample detachment from the sample holder in the vacuum environment. For the gel sample, the sample was cut into a small piece, mounted on the sample holder, and sent for the freeze-drying process in order to remove the moisture inside the gel. The freeze-dried gel sample was then coated with an extremely thin layer (1.5 - 3.0 nm) of gold, and ready for the FESEM analysis. The FESEM images of the samples were captured at the appropriate magnification and focal length.

3.5 Mg-air Battery Fabrication

The Mg-air battery was constructed by using a thin Mg strip as the anode and a commercial air cathode. The Mg anode was cut into a rectangular strip (50 × 3 mm) and cleaned prior to the utilisation. The low thickness of Mg strip allowed better monitoring of the corrosion rate of the magnesium as compared to a bulk rod electrode. Approximately 30 mm of the strip was in contact with the electrolyte during discharge measurement, with a total effective electrode surface area of 0.9 cm^2. The air cathode utilised for oxygen reduction was a commercially available, carbon-based air cathode sheet. The active side of the air cathode was a manganese based catalysed carbon layer supported by the nickel mesh (current collector) whereas the air side of the air cathode was a hydrophobic, gas-permeable laminated porous Teflon film. The air cathode sheet was cut into a rectangular sheet (50 × 10 mm). The WSG-AGAR gel electrolyte was cut and separated into a small cuboid (30 mm × 10 mm) (Figure 3.4(a) and 3.4(b)). The electrolyte was sandwiched between an Mg anode strip and an air cathode sheet, as shown in Figure 3.4(c), which functioned as both electrolyte and separator. The laminar structure enables simple fabrication of the cell. The schematic representation of the customised Mg-air battery which shows the energy generated by an electrochemical reaction is illustrated in Figure 3.4(d). Figure 3.4(e) depicts the side view of the customised Mg-air battery.

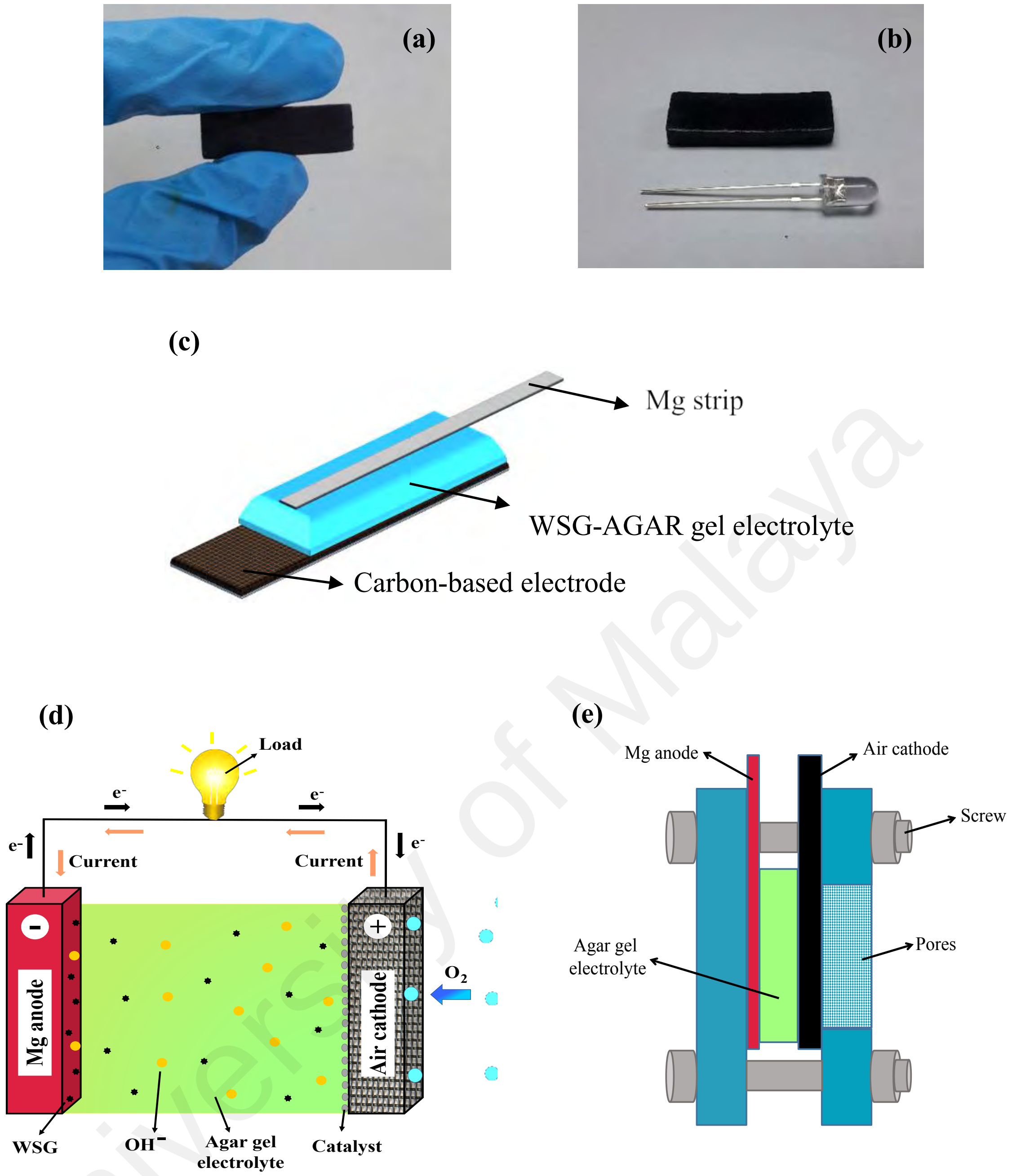

Figure 3.4: (a) Digital image of WSG-AGAR gel electrolyte cuboid; (b) the relatively small size of the gel electrolyte used for battery assembling as compared to a light emitting diode (LED); (c) schematic all-solid-state Mg-air battery with a laminar structure; (d) schematic representation of customised Mg-air battery, showing the energy generated by an electrochemical reaction; and (e) side view of the customised Mg-air battery.

3.6 Electrochemical Measurements

3.6.1 Ionic Conductivity

Ionic conductivity is the electrical conductivity due to the motion of ionic charge. It is an important aspect of electrolyte which greatly affects battery performance. The ionic conductivity of the gel sample was tested with an AC impedance using an electrochemical work station (PGSTAT302N; Metrohm Autolab, the Netherlands) in the frequency range of 100 kHz to 0.1 Hz. The gel sample was placed between two stainless steel plates with a testing area of 3.14 cm^2. The ionic conductivity (S cm^{-1}) was calculated based on Equation 3.1.

$$\sigma = \frac{d}{RA} \qquad \text{(Equation 3.1)}$$

where d is the thickness of the agar gel (cm), R is the bulk resistance (Ω) taken from the first intercept on the x-axis of the impedance data in the complex plane and A is the contact area (cm^{-2}).

3.6.2 Electrochemical Impedance Studies (EIS)

Electrochemical impedance studies is a technique in which the impedance data is obtained by applying a small amplitude of alternating potential over a wide range of frequency. In this study, EIS was studied by using the electrochemical work station (PGSTAT302N; Metrohm Autolab, the Netherlands), with the frequency range from 100 kHz to 0.1 Hz at open circuit potential. The Mg anode was immersed in the gel sample by using the three-electrode cell structure which consisted of Mg strip working electrode, platinum counter electrode, and Ag/AgCl reference electrode. The three-electrode configuration EIS was performed in order to test the corrosion inhibition property of the gel sample. The electrochemical impedance data collected was presented as the Nyquist plot. The plot was fitted and interpreted by Autolab Electrochemical EIS fitting software for its equivalent circuit.

3.6.3 Discharge Performances

In this study, the discharge performance of the Mg-air battery was studied by using a NEWARE BTS-5V10mA battery testing system. It is a technique utilised to investigate the electrochemical performance of the Mg-air batteries fabricated with different agar gel electrolyte prepared. In this technique, a constant discharge current is applied and the responding potential at the varied time is measured. The discharge process was conducted at a constant current density of 11.11 mA cm^{-2} for each of the fabricated Mg-air batteries, and the respective discharging curve was recorded. The discharge current data until the battery reached 0 V was used to determine the battery performance in terms of the discharge capacity. The discharge capacity was calculated based on Equation 3.2:

$$\text{Discharge capacity (mAh g}^{-1}\text{)} = \frac{\mathrm{i} \times \mathrm{A} \times \mathrm{t}}{\mathrm{W_i} - \mathrm{W_f}} \qquad \text{(Equation 3.2)}$$

where i is the current density (A cm^{-2}), t is the discharge time (h), A is the surface area (cm^2), W_i is the weight of Mg before the discharge test, and W_f is the weight of Mg after the discharge test. The weight of Mg anode after the discharge test was measured after removing the discharge products.

The Mg-air battery assembled with the optimal WSG-AGAR gel electrolyte was further discharged at constant current densities of 1.11 and 5.56 mA cm^{-2} in order to investigate its discharge performance at low current densities.

CHAPTER 4: RESULTS AND DISCUSSION

4.1 Introduction

In this chapter, the results obtained in the present study followed by the explanation and discussion of the analyses are presented. There are five main sections in this chapter. The first section presented in Chapter 4 is dealing with the information regarding the formation of WSG. The influence of the reduction condition on the formation of WSG is evaluated in detail. In addition, the influence of the respective WSG on the electrochemical performance of WSG-AGAR gel electrolyte is being investigated. The second section in this chapter illustrates the effect of the agar concentration on the electrochemical performance of WSG-AGAR gel electrolyte. The third section in this chapter is associated with the electrochemical performance of the WSG-AGAR gel electrolyte with respect to the WSG concentration. The fourth section demonstrates the influence of the types of electrolyte on the formation of WSG-AGAR gel electrolyte and their respective electrochemical performance. The last section in this chapter presents the further characterisation on the optimal WSG-AGAR gel electrolyte, in which the morphology and practical usability of the optimal gel are being investigated.

4.2 Effect of Different Amount of NH_3 on WSG

4.2.1 Characterisation on WSG Synthesised

Raman spectroscopy is commonly used to characterise graphene-based materials in term of their defects, disorders, and crystal structure (Sobon et al., 2012). D and G bands are the two characteristic peaks found in the graphene-based materials. D band indicates the presence of defects in the graphitic lattice with A_{1g} symmetry, whereas G band indicates the in-plane E_{2g} mode of single crystalline graphitic carbon atoms in the honeycomb lattice (M. P. Kumar et al., 2014). The changes in the relative intensity of the two main peaks (D band and G band) can be used to verify the reduction process. Generally, the I_D/I_G ratio is obtained to measure the degree of disorder and the average size of sp^2 domain in graphene materials (M. P. Kumar et al., 2014).

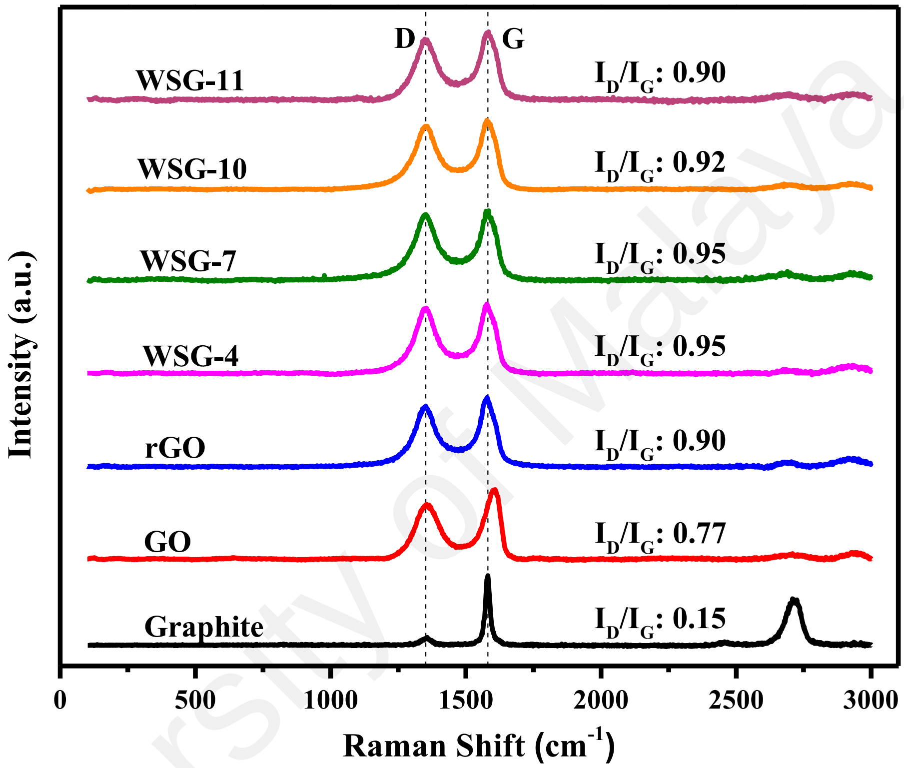

Figure 4.1: Raman spectra of graphite, GO, rGO, and WSG synthesised under the addition of different amount of ammonia solution (to selected pH) during chemical reduction.

Figure 4.1 shows the Raman spectra of graphite, GO, rGO, WSG-4, WSG-7, WSG-10, and WSG-11. For pristine graphite, the D and G peaks were centred at 1352 and 1581 cm^{-1} respectively. After the oxidation, the D band of GO increased in intensity (at 1354 cm^{-1}) and the G band was broadened and shifted to 1604 cm^{-1}. The higher I_D/I_G ratio of GO (0.77) as compared to graphite (0.15) indicates the oxidation of graphite due to the insertion of oxygen functional groups into the graphitic chain, thus increasing the D band.

The increase of the D band intensity in GO also shows the decrease in size of the in-plane sp^2 domains, which is caused by the extensive oxidation process (Stankovich et al., 2007).

After the reduction, the G bands of WSG were shifted to 1577 cm^{-1} for WSG-4 and WSG-10, and 1584 cm^{-1} for WSG-7 and WSG-11. The Raman shift of G band from a higher frequency of 1604 cm^{-1} (GO) to lower frequency of nearly 1581 cm^{-1} (towards the value of pristine graphite) indicates the restoration of the graphitic structure of WSG samples (Rao & Sood, 2013), which illustrates the successful reduction of GO. As shown in Figure 4.1, the significant increase in D band of WSG denotes the defected and disordered structure of WSG. The increase in the I_D/I_G ratio from 0.77 to 0.95, 0.95, 0.92, and 0.90 respectively for WSG-4, WSG-7, WSG-10, and WSG-11 in the Raman spectra shows the increase in defects with the reduction process. The removal of the oxygen-containing functional groups from GO results in the remaining unrecovered defects in WSG, thus increases the I_D/I_G ratio (Willemse, Tlhomelang, Jahed, Baker, & Iwuoha, 2011). In addition, the increment in the I_D/I_G ratio of WSG also proposes the decrease in the average size of the sp^2 domains in WSG after the reduction process. The smaller graphitic domains in WSG than those in GO give rise to large quantities of structural defects (Bo et al., 2014; Stankovich et al., 2007). It is well reported in the literature that the introduction of nitrogen atom into graphene can increase the formation of a large number of defects due to the development of smaller nanocrystalline graphene domain by heteroatom doping, which leads to a high intensity D band (Pimenta et al., 2007; Vinayan, Nagar, & Ramaprabhu, 2012). When comparing the I_D/I_G ratio of various WSG, it can be observed that there are not many changes in the ratio, which could be due to the merely similar defects produced for different amounts of N doping.

XRD was conducted in order to investigate the atomic structures and interlayer spacings of graphite, GO and WSG. Figure 4.2 shows the XRD pattern of graphite, GO, rGO, and WSG.

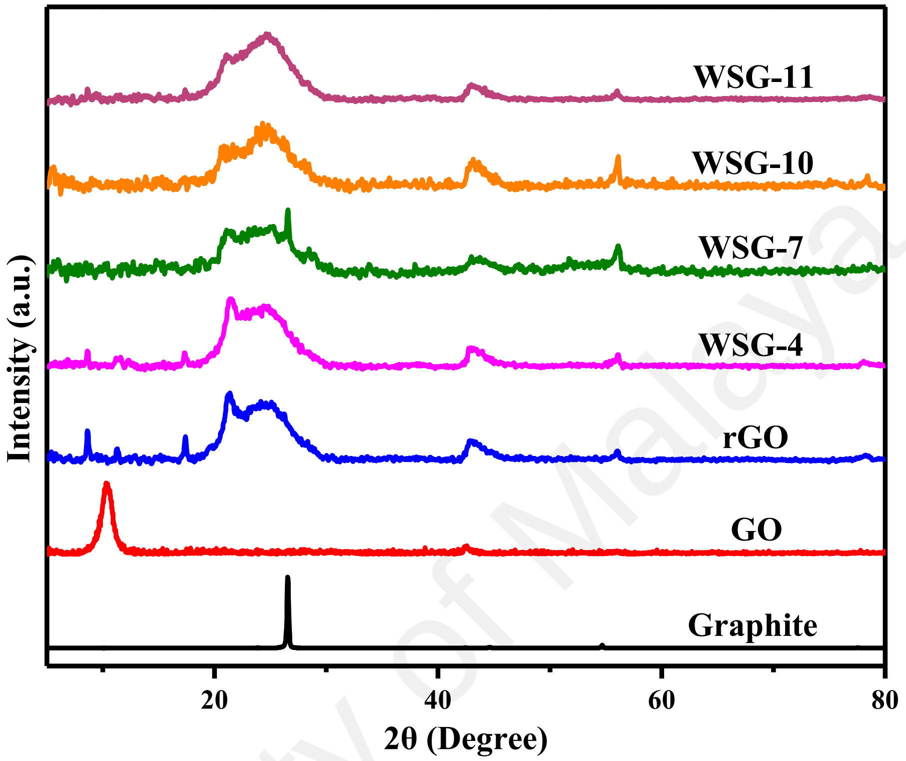

Figure 4.2: XRD pattern of graphite, GO, rGO, and WSG.

Graphite had a basal reflection (002) with a strong peak at 26.6° (d-spacing of 0.335 nm). After the oxidation process, the diffraction peak of GO shifted to 10.3° (d-spacing of 0.859 nm). One of the vital parameter to access the structural information of the carbon materials is the distance between the two layers (Gurunathan, Han, Dayem, Eppakayala, & Kim, 2012). The increase in d-spacing of GO as compared to that of graphite is owing to the intercalation of the water molecules and also the presence of oxygen-containing functional groups like hydroxyl, epoxy and carboxyl groups between the layers of graphite (Bo et al., 2014). The interlayer spacing of rGO and WSG were larger than that of graphite. rGO had a broad peak centred at 24.3° with a corresponding d-spacing of 0.366 nm. However, WSG synthesised with different amount of NH_3 solution (through pH adjustment of GO solution to pH 4, pH 7, pH 10, and pH 11 prior to the addition of hydrazine hydrate) exhibited pronounced peaks at 24.5°, 24.5°, 24.6°, and 24.6°, with corresponding interlayer spacing of 0.364 nm, 0.363 nm, 0.361, and 0.361, respectively. The d-spacings of rGO and WSG were significantly reduced after the reduction process, which denote the removal of oxygen-containing functional groups. These demonstrate that the conjugated sp^2 carbon network is restored during the reduction process. Nevertheless, the d-spacings of rGO and WSG were slightly higher than graphite, indicating the presence of some residual oxygen-containing functional groups after the reduction process (Gurunathan et al., 2012). The broad peaks of rGO and WSG indicate that the sheets produced have smaller crystalline size as compared to graphite (Singhbabu, Kumari, Parida, & Sahu, 2014), which is also deduced from the higher I_D/I_G ratio of rGO and WSG as compared to pristine graphite in the RAMAN data (Figure 4.1). Furthermore, the increasing amount of NH_3 solution slightly broadened the graphitic peak corresponding to the (002) plane, implying the slight reduction in the crystallinity (M. P. Kumar et al., 2014).

ATR-FTIR analysis for both GO and WSG was conducted. The corresponding ATR-FTIR spectra are demonstrated in Figure 4.3. For GO, the peak at 3408 cm^{-1} is attributed to O-H stretching vibration of the C-OH groups and the presence of water in GO. The carbonyl groups are shown at 1715 cm^{-1} as C=O stretching. The peak at 1059 cm^{-1} is attributed as C-O stretching vibration. The presence of characteristic peaks in GO spectra related to all these oxygen-containing groups indicates the successful oxidation of graphite.

The reduction of GO to form WSG is also observed from the ATR-FTIR spectra. The reduction of the WSG is confirmed by the reduction in the peaks' intensity and the removal of the peaks, as shown in Figure 4.3. The disappearance of peaks at 3408 cm^{-1} and 1059 cm^{-1} indicates the removal of the oxygen-containing groups in GO. The peaks at 2852 cm^{-1} and

2923 cm^{-1} is corresponding to the asymmetric and symmetric H-C-H stretching. The peak of WSG around 1741 cm^{-1} indicates the C=O bonding in carboxyl (D. Li et al., 2008). All of these WSG spectra demonstrate that most of the oxygen-containing functional groups in WSG are eliminated, with some remaining oxygen functional groups.

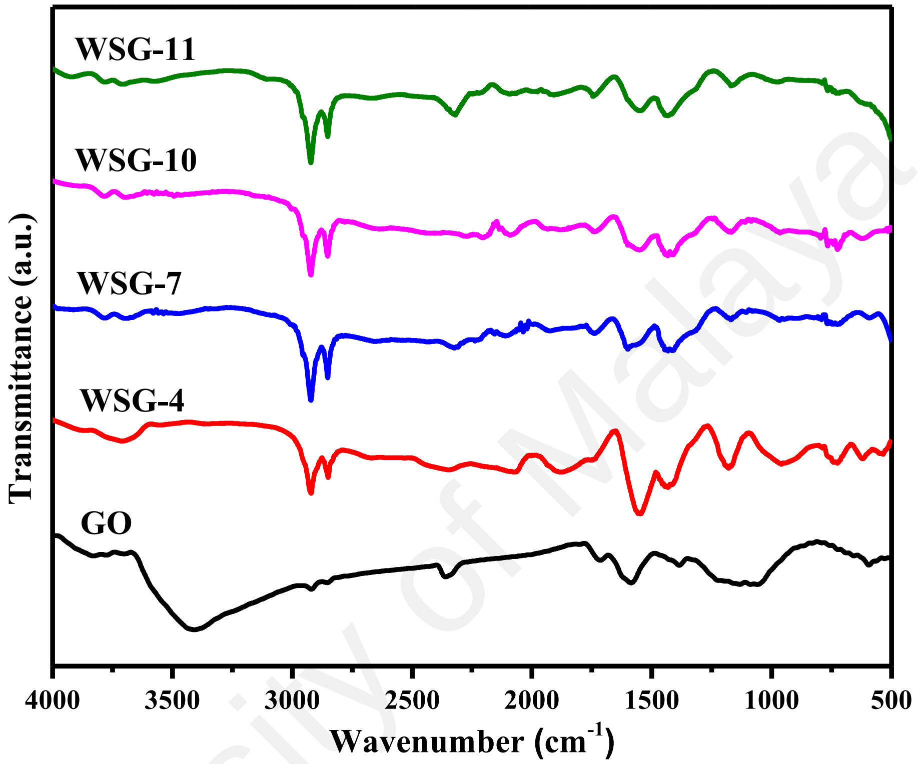

Figure 4.3: ATR-FTIR spectra of GO and WSG.

Besides that, the presence of peaks at 1601 cm^{-1} and 1433 cm^{-1} are attributed to the C-C=C symmetric stretch of alkenes and also the C-C=C symmetric and asymmetric stretching of the aromatic rings. This proposes the recovery of the sp^2 lattice through the reduction process. In all WSG, there are presence of nitrogen atoms which replace the oxygen atoms. The peaks around 1170 cm^{-1} in WSG samples indicates the medium peak of C-N stretching bond (M. P. Kumar et al., 2014).

From the ATR-FTIR spectra, it can be observed that the carboxyl group is present in all the WSG samples. The presence of carboxyl group around 1741 cm^{-1} implies that WSG sheets should have a charged surface in aqueous solution (D. Li et al., 2008). The intensity of the carboxyl peaks in WSG-7, WSG-10, and WSG-11 are higher than WSG-4 (increases in the order of WSG-4 < WSG-7 ≈ WSG-11 < WSG-10), which agreed with the zeta potential value of WSG samples.

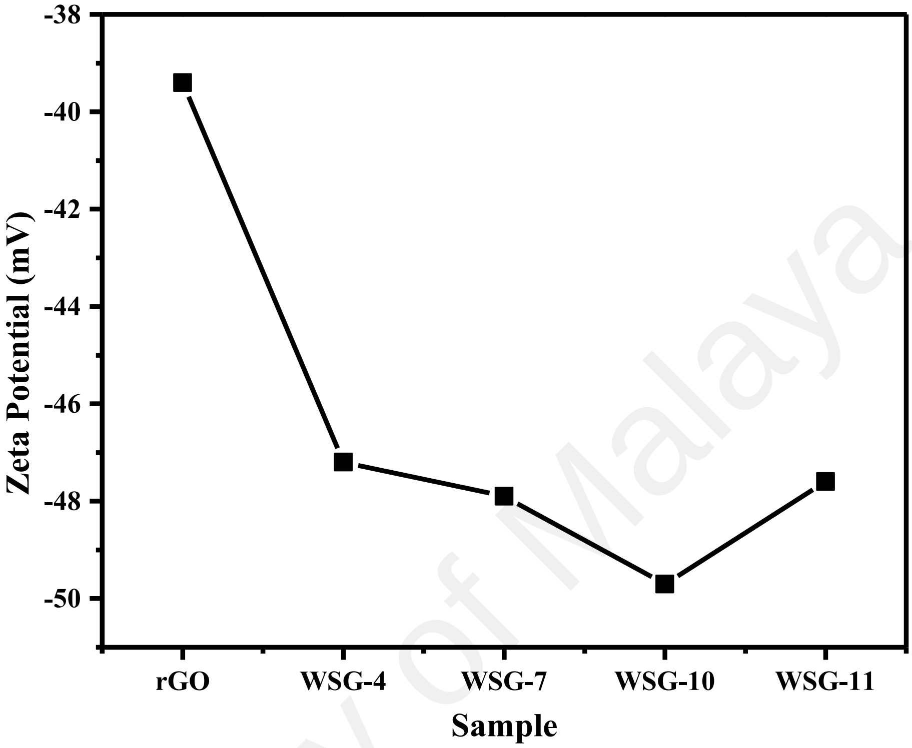

Figure 4.4: Zeta potential of rGO and WSG.

The dispersibility of the synthesised WSG is an important aspect as an electrolyte additive. WSG has to disperse efficiently in the polymer matrix without aggregation in order to enhance its functional performance in the electrolyte, thus ensuring the smooth functioning in the battery application. Figure 4.4 shows the zeta potential of rGO, WSG-4, WSG-7, WSG-10, and WSG-11 in aqueous dispersion. Zeta potential is important for determining the colloidal dispersion stability by measuring the effective surface charge associated with the double layer around the colloidal particle (Konkena & Vasudevan, 2012). Commonly, particles with the zeta potentials greater than +30 mV or lower than -30mV are considered to produce stable dispersions as a result of the high interparticle electrostatic repulsion (Konkena & Vasudevan, 2012). From Figure 4.4, it can be seen that the zeta potential of rGO and WSG were more negative than -30 mV, indicating the stable dispersion of the sample. In addition, all WSG had a more negative zeta potential than rGO, which shows that all WSG produce dispersions with greater dispersion stability as compared to rGO. The zeta potential of WSG became more negative when the amount of the ammonia solution added to GO solution during reduction increased (by adjusting the GO solution to pH 4, pH 7, pH 10, and pH 11). The stability of rGO and WSG dispersions are affected by the negative charge on rGO and WSG sheets that are produced due to the ionisation of different functionalities present (Konkena & Vasudevan, 2012). The addition of ammonia solution increases the basicity of GO solution, produces a greater charge density of GO, thus forming WSG with greater stability (D. Li et al., 2008). The electrostatic repulsion of WSG in the solution obstructs the π-π stacking between the WSG sheets and hinders the formation of aggregations, producing a stable WSG suspension (Jiali Zhang et al., 2010). However, the zeta potential of WSG-11 produced was lower as compared to WSG-10. This can be due to the compression of the double layer at high ionic strengths (Konkena & Vasudevan, 2012).

The conductivity of the water-dispersed rGO, WSG-4, WSG-7, WSG-10, and WSG-11 were 0.0247, 0.0332, 0.0465, 0.0306, and 0.0154 mS cm^{-1} respectively. It is observed that the addition of ammonia to GO solution during the reduction process can improve the conductivity of WSG synthesised. WSG produced from the adjustment of GO solution to pH 7 with ammonia prior to reduction gives the highest conductivity among all the doped samples. This can be due to the controlled defects' creation induced by the addition of ammonia during the reduction process, which provides greater conductivity of WSG-7 (Agrawal, Raghuveer, Li, & Ramanath, 2007).

4.2.2 Electrochemical Characterisation on WSG-AGAR Gel Electrolyte

Different agar gel electrolytes had been prepared by incorporating each WSG into a separate gel. The agar and WSG concentration added to form each electrolyte were kept at a constant of 3% w/v and 0.1% w/v, respectively. 0.6 M NaCl solution was used as the electrolyte solution.

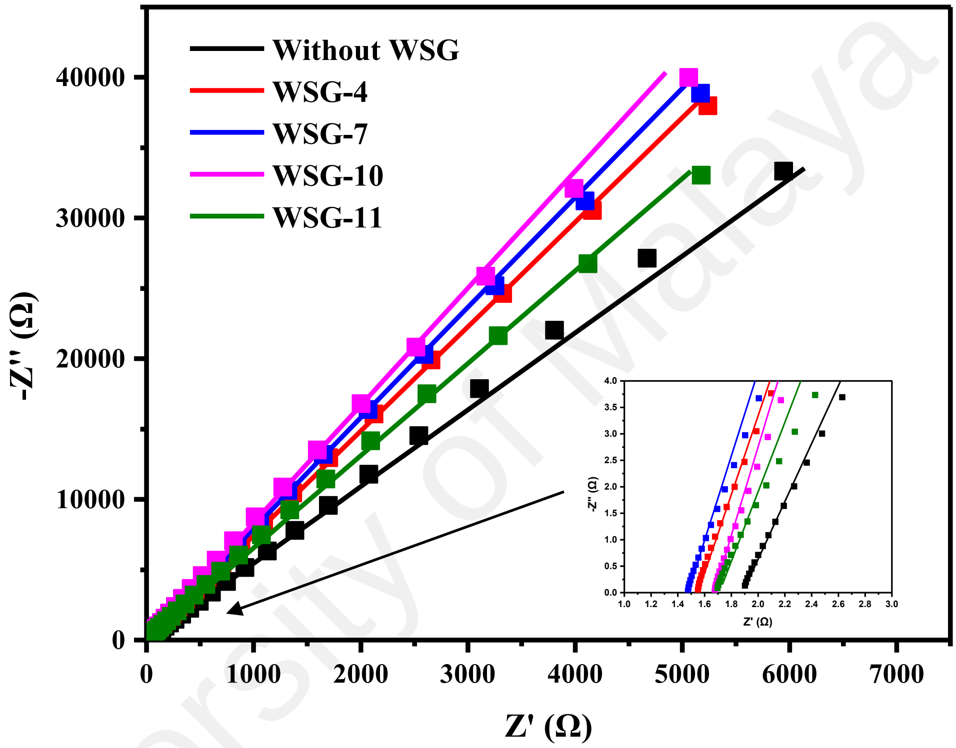

Figure 4.5: The AC impedance spectra of agar gel electrolytes containing different WSG (inset: expanded view at the high-frequency region).

Table 4.1: Solution resistance and ionic conductivity of individual agar gel electrolyte with and without incorporation of different WSG.

Agar Gel Electrolyte	Solution Resistance, R_s (Ω)	Ionic Conductivity ($S\ cm^{-1}$)
Without WSG	1.88	$(7.07 \pm 0.02) \times 10^{-2}$
WSG-4	1.55	$(8.74 \pm 0.03) \times 10^{-2}$
WSG-7	1.48	$(9.40 \pm 0.03) \times 10^{-2}$
WSG-10	1.67	$(8.05 \pm 0.01) \times 10^{-2}$
WSG-11	1.71	$(8.02 \pm 0.01) \times 10^{-2}$

Figure 4.5 and Table 4.1 show the R_s and ionic conductivities of the agar gel electrolytes incorporated with and without different WSG. From the data, it is observed that the agar gel electrolytes incorporated with different WSG had a higher ionic conductivity than agar gel electrolyte without WSG. The results agreed with the study conducted by Suganya, Hari Hara Priya, and Jaisankar (2015). This can be due to the increase in the electrical conductivity with the addition of WSG, which promotes the charge flow in the gel electrolyte.

Among the agar gel electrolytes prepared, it is observed that the agar gel electrolyte incorporated with WSG-7 had the greatest ionic conductivity. The ionic conductivity of the different agar gel electrolytes prepared is in line with the conductivity of the respective water-dispersed WSG, as shown in the previous section. The high ionic conductivity of the agar gel electrolyte incorporated with WSG-7 can be linked to the highest conductivity of WSG-7 when dispersed in water. This is as expected since ionic conductivity is a measure of the electrical conductivity induced by the motion of ionic charge (Allen & Bevington, 1989). The high conductivity of the WSG-7 when dispersed in the water illustrates that the motion of the ionic charge in the solution is high. Consequently, the incorporation of WSG-7 in the agar gel electrolyte enables the mobile movement of the ionic charge and contributes to a greater ionic conductivity. Incorporation of WSG-7 had contributed to the increase in ionic conductivity by 32.96% as compared to the agar gel electrolyte without the electrolyte additive.

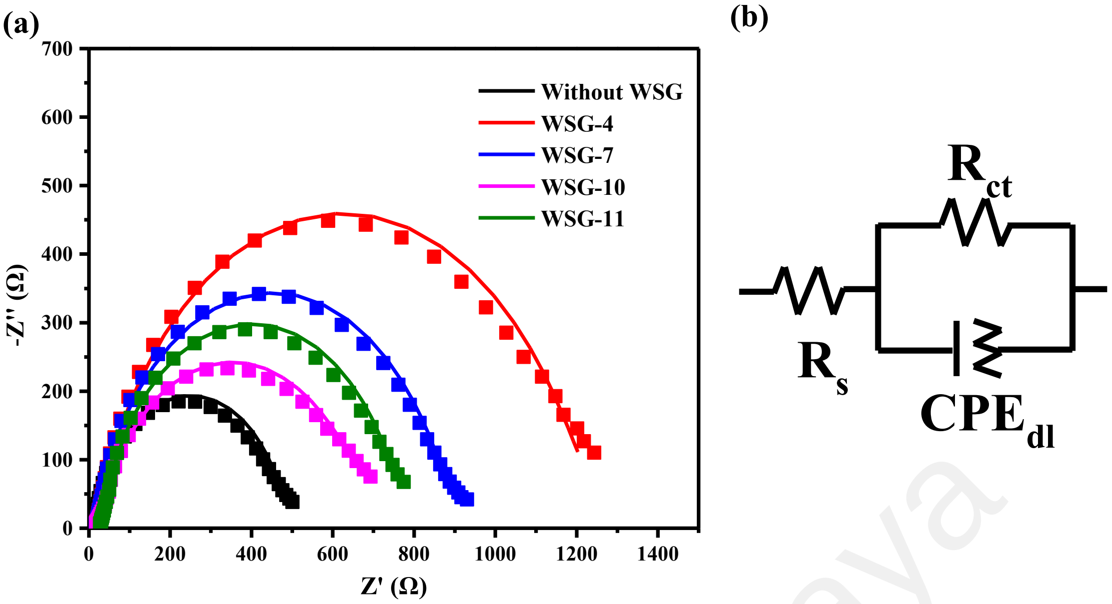

Figure 4.6: (a) EIS spectra and (b) equivalent circuit used to fit the EIS spectra of Mg strips immersed in agar gel electrolytes with and without different WSG.

Table 4.2: R_{ct} of Mg strips in different agar gel electrolytes (with and without different WSG).

WSG Sample Incorporated in Agar Gel Electrolyte	Charge Transfer Resistance, R_{ct} (Ω)
Without WSG	473.53
WSG-4	1200.30
WSG-7	867.80
WSG-10	643.15
WSG-11	736.90

As mentioned earlier, Mg corrosion is one of the vital problems in Mg-air battery application. In order to study the corrosive effect of Mg in the different agar gel electrolytes, corrosion study was conducted by the immersion of Mg strips via three-electrode EIS analysis. The data is shown and tabulated in the form of Nyquist diagram (Figure 4.6(a), Table 4.2). The equivalent circuit used to fit the data is shown in Figure 4.6(b) where R_s is the solution resistance, R_{ct} is the charge transfer resistance and CPE_{dl}

is the constant phase element. The impedance spectra displayed a single imperfect semicircle, in which the diameter of the semicircle extrapolated depicts the charge transfer resistance (R_{ct}) happening at the interface of Mg electrode/electrolyte.

From the diagram, it can be seen that R_{ct} had increased due to the incorporation of different WSG in the agar gel electrolytes. WSG forms a protective coating over the Mg anode surface, which restricts the liberal discharge of electrons from the anode (Mayilvel Dinesh et al., 2015). The controlled electron discharge from Mg results in the decrease in the charge flow, which in turn increases the resistance offered during charge transfer. Hence, the increase in R_{ct} implies the protection from the anode corrosion due to the addition of WSG.

When comparing R_{ct} in the agar gel electrolytes incorporated with different WSG, the resistance for charge transfer decreased in the order of WSG-4, WSG-7, and WSG-10, after which increased for WSG-11. This depicts that the agar gel incorporated with WSG-4 provides the greatest Mg corrosion protection, whereas that of WSG-10 has the lowest Mg corrosion protection. The trend of R_{ct} value is in line with the zeta potential of WSG in Figure 4.4, which measures the effective surface charge associated with the double layer around the colloidal WSG particle (Konkena & Vasudevan, 2012). This proposes that the effective surface charge on WSG influences the formation of the protective layer over the Mg anode surface. When the zeta potential of WSG is more negative, the interparticle electrostatic repulsion is greater, which affects the transformation of OH^- along with WSG particle in the electrolyte. As a result, less graphene-rich OH^- is deposited over Mg anode, thus minimises the anode protection layer and lowers the R_{ct}.

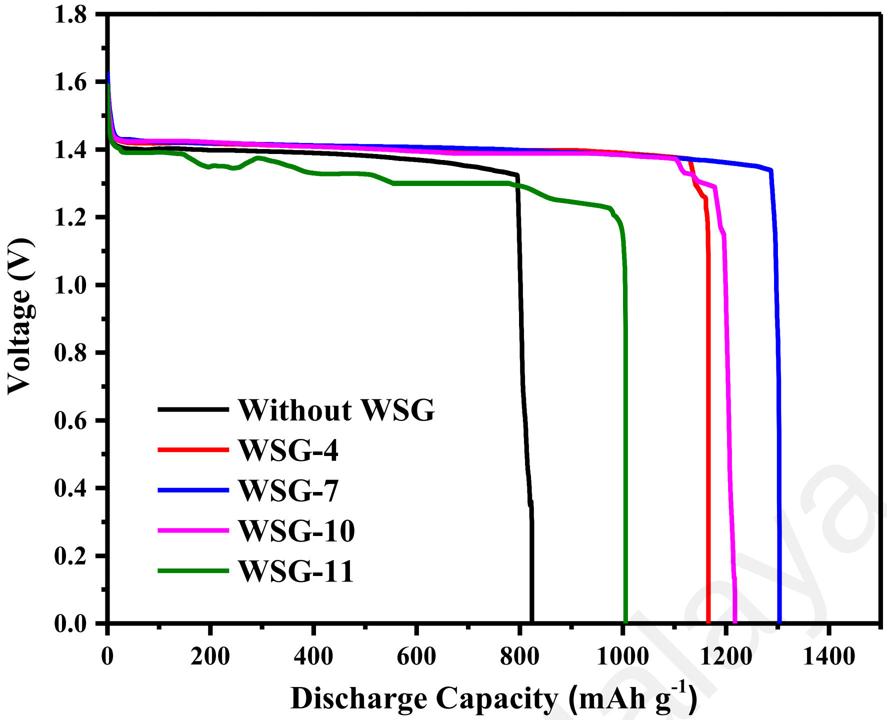

Figure 4.7: Discharge performance of Mg-air battery assembled with agar gel electrolytes with and without incorporation of different WSG at the current density of 11.11 mA cm^{-2}.

The influence of the as-synthesised WSG on the performance of the custom-designed Mg-air battery was investigated through the constant current discharge test (Figure 4.7). Agar gel electrolytes with and without the incorporation of different WSG (WSG-4, WSG-7, WSG-10, and WSG-11 respectively) were utilised as the electrolyte for the custom-designed Mg-air battery. The open circuit voltages for the assembled Mg-air batteries were around 1.6 V just after the cell was assembled. The cell voltage decreased promptly and reached a flat and stable discharge plateau around 1.4 V after the discharge current (current density of 11.11 mA cm^{-2}) was applied. At the end of the discharge process, the amount of Mg anode is exhausted whereas the amount of electrolyte is in excess (Z. Zhang et al., 2014), which is shown by the sharp decline.

The discharge curve for the WSG-based Mg-air battery had lengthened discharge plateau as compared to the Mg-air battery without WSG. This proposes that the mixture of WSG, NaCl, and agar exist in the electrolyte maintaining a nearly uniform conductivity. In addition, the anodic corrosion is reduced as a result of oxide layer partially produced over Mg anode due to WSG. As an electrolyte additive, WSG improves the electrical conductivity of electrolyte by transforming OH^- along with WSG particle in the electrolyte, which leads to the enhancement of the discharge performance. The graphene-rich OH^- supposes to be deposited over the Mg anode, protecting it and lessen its corrosion (Mayilvel Dinesh et al., 2015).

The highest performance was given by the Mg-air battery with WSG-7-incorporated agar gel electrolyte, which had the discharge capacity of 1303.94 mAh g^{-1} with respect to the mass of Mg anode consumed during discharging. In addition, it is 11.82%, 7.09%, and 29.73% greater than agar gel electrolytes incorporated with WSG-4, WSG-10, and WSG-11 respectively. The performance of Mg-air battery is greatly influenced by the ionic conductivity of the electrolyte and also the protection of Mg anode from self-corrosion. Therefore, the greater battery performance of Mg-air battery with WSG-7-AGAR gel electrolyte could be due to the optimisation between ionic conductivity and anodic protection. From Figure 4.5, it has been discussed that WSG-7-AGAR gel electrolyte gave the highest ionic conductivity. In terms of the anodic protection, WSG-4-AGAR gel electrolyte provides the greatest protection for Mg anode from corrosion (as shown in Figure 4.6). However, the greater protective oxide layer formed can also result in the passivation of Mg surface, causing premature end of discharge and lower the discharge capacity (Fotouhi, Auger, O'Neill, Cleaver, & Walus, 2017). Consequently, WSG-7 was the best candidate to be incorporated into the agar gel electrolyte in order to achieve the best Mg-air battery performance. The incorporation of WSG-7 in agar gel electrolyte had shown improvement in discharge capacity by 58.34% as compared to the Mg-air battery without the electrolyte additive.

4.3 Effect of Agar Concentration on WSG-AGAR Gel Electrolyte

4.3.1 ATR-FTIR of Agar Gel Electrolytes

A neutral (pH 7) polymeric-gelled electrolyte was formed with the addition of agar powder at a different concentration to the WSG-NaCl solution electrolyte. When the agar concentration was low at 1% w/v, the electrolyte solution did not gel properly, and the gel formed was too soft and liquefied for the application. On the other hand, at a high agar concentration (> 5% w/v), the gels formed were firm and hard, without a homogeneous flat surface. Therefore, the agar concentration between 2 - 5% w/v were tested throughout the study. The WSG-AGAR gel electrolytes prepared were named as 2% Agar, 3% Agar, 4% Agar, and 5% Agar respectively with accordance to the agar concentration in the gel. WSG-7 which gave the best battery performance as described in the previous section was selected for the incorporation into agar gel electrolytes. The WSG concentration added to form each electrolyte was kept at a constant of 0.1% w/v. 0.6 M NaCl solution was used as the electrolyte solution.

The ATR-FTIR spectra of pure agar and WSG-AGAR gel electrolytes with different agar concentrations are shown in Figure 4.8. Pure agar gel was prepared by dissolving 3% w/v agar in deionised water.

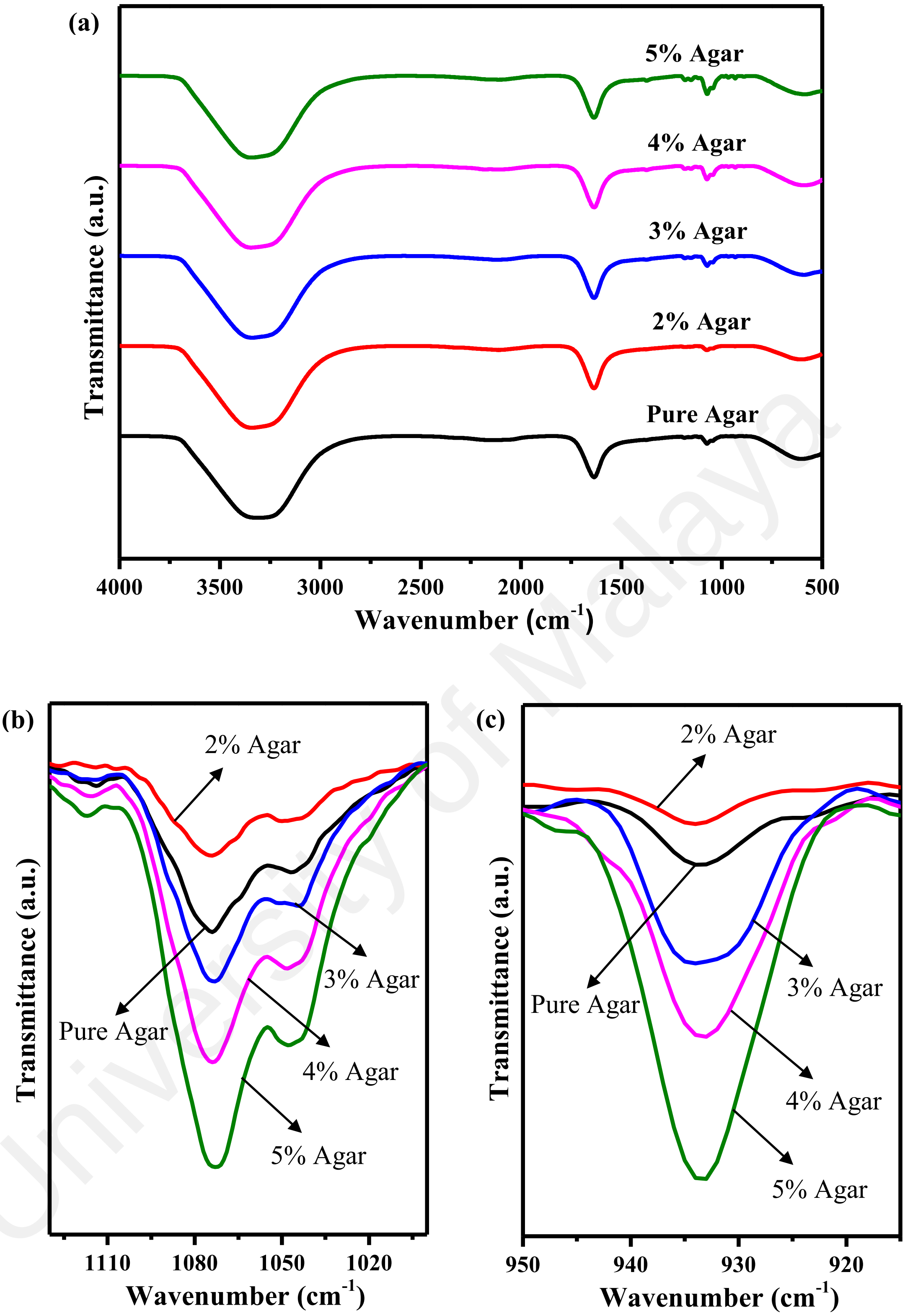

Figure 4.8: ATR-FTIR spectra of pure agar and WSG-AGAR gel electrolytes containing different amount of agar at (a) frequency range of 500-4000 cm^{-1}, (b) 1074 cm^{-1} peak, and (c) 934 cm^{-1} peak.

The broad band at 3328 cm^{-1} shown by pure agar corresponds to the hydroxyl (O-H) group stretching of agar that involves in the formation of intermolecular and intramolecular hydrogen bond (Selvalakshmi, Mathavan, Selvasekarapandian, & Premalatha, 2017; Shankar & Rhim, 2017). The characteristic band at 1636 cm^{-1} is associated with the C=O stretching (Selvalakshmi et al., 2017). The band at around 1376 cm^{-1} is assigned to the ester sulphate group of agar (Volery, Besson, & Schaffer-Lequart, 2004). The band at 1074 cm^{-1} corresponds to the coupling of the C-O or the C-C stretching modes with the C-O-H bending modes, apart from the C-O-C bridge of 3,6-anhydrogalactose bridges. The band at 934 cm^{-1} is due to C-O-C bridge of 3,6-anhydrogalactose (Selvalakshmi, Mathavan, Selvasekarapandian, & Premalatha, 2018; Shankar & Rhim, 2016; Shankar, Teng, & Rhim, 2014).

From the ATR-FTIR spectra in Figure 4.8(a), it is seen that the absorption peaks of WSG-AGAR gel electrolytes were almost similar to pure agar. However, the O-H stretching of WSG-AGAR gel electrolytes had shifted to 3342, 3341, 3348, and 3345 cm^{-1} in 2% w/v, 3% w/v, 4% w/v, and 5% w/v agar gel electrolytes, respectively. It is reported in the literature that O-H stretching appears between 3570 and 3200 cm^{-1} (Selvalakshmi et al., 2017). The shifting of the peak shows the interaction of agar segments with the remaining oxygen functional group of WSG through hydrogen bonding (Bora, Bharali, Baglari, Dolui, & Konwar, 2013). Therefore, it indicates that WSG has been successfully incorporated in the agar polymer matrix.

As shown in Figure 4.8(b) and 4.8(c), the intensity of the characteristic bands of agar were directly proportional to the agar concentration in the agar gel electrolyte. The intensities of 1074 and 934 cm^{-1} increased in the order of 2% w/v, 3% w/v, 4% w/v, and 5% w/v agar gel electrolyte, which indicate the increase of C-O-C group of 3,6-anhydrogalactose bridge present in the agar gel electrolyte with greater amount of agar

(Shankar & Rhim, 2016). This is anticipated since the 3,6-anhydrogalactose bridge is the polymer backbone of agar. The above results confirm the formation of agar gel electrolyte with different agar concentration.

When comparing the peaks of pure agar and WSG-incorporated 3% w/v agar gel electrolyte (both of them contained the same agar concentration) at 1074 cm^{-1} and 934 cm^{-1} (Figure 4.8(b) and 4.8(c)), WSG-incorporated 3% w/v agar showed a higher intensity at both peaks as compared to pure agar. This increase in intensity further indicates that WSG has been successfully incorporated into the agar polymer matrix, which results in the increase of C-O stretching in agar due to the interaction with WSG (Belay, Nagarale, & Verma, 2017; Wojtoniszak, Zielinska, Kalenczuk, & Mijowska, 2012).

A summary of vibrational frequencies observed in the pure agar and WSG-AGAR gel electrolytes with different agar concentrations is presented in Table 4.3.

Table 4.3: Absorption peaks for pure agar and WSG-AGAR gel electrolytes with different agar concentrations.

Wavenumber (cm^{-1})					**Assignment**
Pure Agar	**2% w/v Agar**	**3% w/v Agar**	**4% w/v Agar**	**5% w/v Agar**	
3328	3342	3341	3348	3345	O-H stretching
1636	1636	1636	1635	1638	C=O stretching
1376	1375	1376	1376	1375	Ester sulphate
1074	1074	1074	1074	1073	3,6-anhydrogalactose bridges
934	934	933	933	933	3,6-anhydrogalactose bridges

4.3.2 Electrochemical Characterisation on WSG-AGAR Gel Electrolyte

The AC impedance spectra of agar gel electrolytes with different agar concentrations (inset: expanded view at high-frequency region) are shown in Figure 4.9. The solution resistance and ionic conductivity of the individual agar gel electrolyte are shown in Table 4.4.

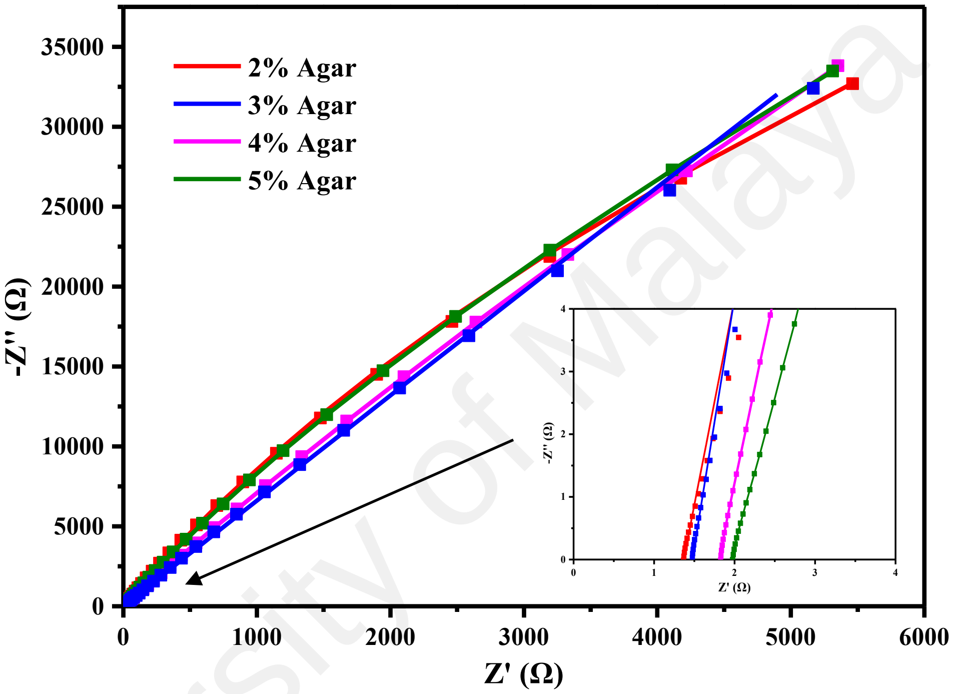

Figure 4.9: The AC impedance spectra of agar gel electrolytes containing different agar concentrations (inset: expanded view at high-frequency region).

Table 4.4. Solution resistance and ionic conductivity of individual agar gel electrolyte with different agar concentrations.

Agar Composition (% w/v)	Solution Resistance, R_s (Ω)	Ionic Conductivity (S cm^{-1})
2.00	1.37	$(9.71 \pm 0.04) \times 10^{-2}$
3.00	1.48	$(9.40 \pm 0.03) \times 10^{-2}$
4.00	1.83	$(7.68 \pm 0.01) \times 10^{-2}$
5.00	2.00	$(7.18 \pm 0.02) \times 10^{-2}$

From the above results, it is shown that R_s was directly proportional to the concentration of agar in the electrolyte; the higher the agar concentration in the electrolyte, the lower the ionic conductivity of the agar gel electrolyte. Agar gelation happens as a result of the helical conformation of the gelling fraction of agar polysaccharides (agarose) (Hernandez-Carmona, 2013; Moon et al., 2015). The aggregation of the double helices of agarose produces a 3D structure framework through the hydrogen-bonded cross-linking self-assembly, which holds the water molecules within the interstices of the framework (Hernandez-Carmona, 2013; Moon et al., 2015). Therefore, the WSG-AGAR gel electrolyte investigated in this study is formed from the entrapment of an electrolyte in an aqueous medium within a 3D channel network, which performs free ionic transportation. When the agar concentration increases, the chain entanglement within the polymer also increases, which in turn bounds the water molecules and hinders the transportation of ions. This explains the reduction in the ionic conductivity of the agar gel electrolyte with increasing agar concentration.

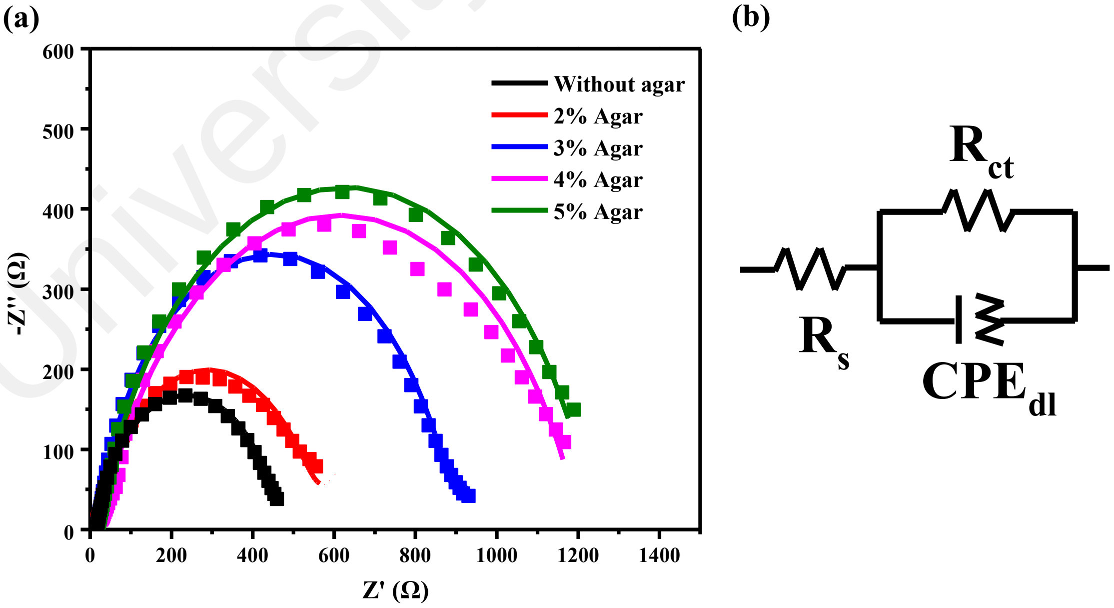

Figure 4.10: (a) EIS spectra and (b) equivalent circuit used to fit the EIS spectra of Mg strips immersed in WSG-AGAR gel electrolytes with different agar concentrations.

Table 4.5: R_{ct} of Mg strips in WSG-AGAR gel electrolytes containing different agar concentrations.

Agar Composition (% w/v)	Charge Transfer Resistance, R_{ct} (Ω)
Without agar	413.04
2.00	530.00
3.00	867.80
4.00	1097.60
5.00	1138.40

Figure 4.10 shows the EIS spectra and equivalent circuit used to fit the EIS spectra of Mg strips immersed in WSG-AGAR gel electrolytes with different agar concentrations. Table 4.5 reveals that R_{ct} values increased with the increasing concentration of agar in the WSG-AGAR gel electrolytes. As R_{ct} is related to the rate of corrosion of the Mg electrode, the larger diameter of the semicircle indicates the lower rate of Mg corrosion (Lebrini et al., 2007). In the neutral or acidic environment, Mg undergoes corrosion spontaneously, as represented by Equation 2.7.

$$Mg + 2H_2O \rightarrow Mg(OH)_2 + H_2 \qquad \text{(Equation 2.7)}$$

From Equation 2.7, it is noticeable that water is a major component in Mg corrosion. With the increasing agar concentration, more water molecules are bounded in the polymer matrix and less likely to attack Mg electrode. Therefore, the electrode/electrolyte interface is more stabilised and Mg corrosion decreases.

The performance of WSG-AGAR gel electrolytes with different agar concentrations for the custom-designed Mg-air battery was investigated through the constant current discharge test (Figure 4.11).

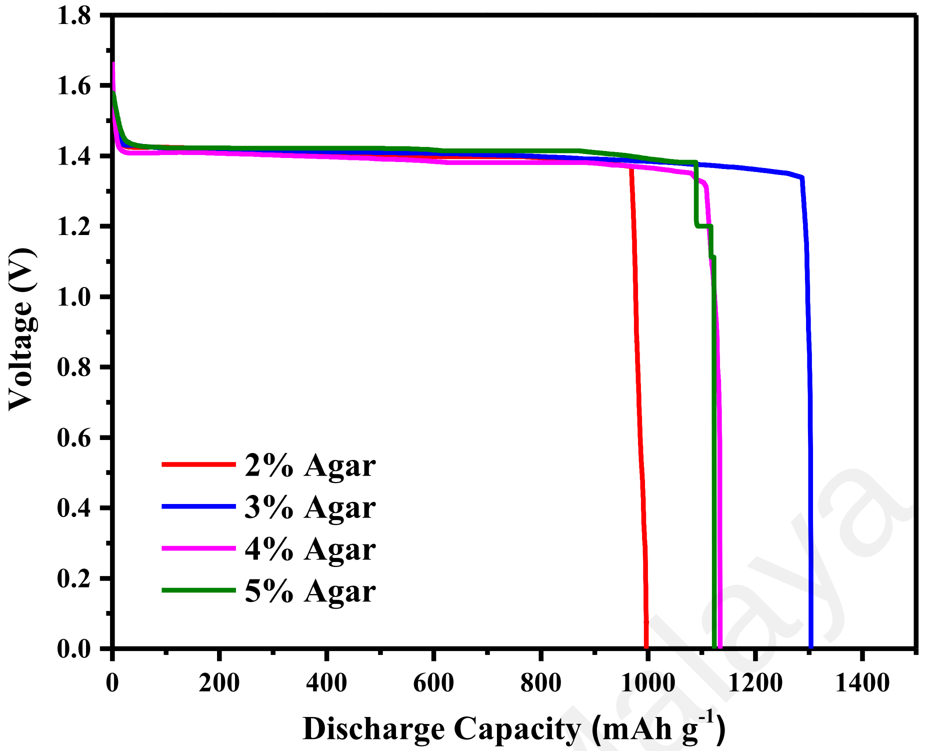

Figure 4.11: Discharge performance of Mg-air battery with WSG-AGAR gel electrolytes containing different agar concentrations at the current density of 11.11 mA cm^{-2}.

The open circuit voltages for the assembled Mg-air batteries were in the range of 1.7 V to 1.6 V just after the cells were assembled. The cell voltage for all the samples decreased rapidly and reached a flat and stable discharge plateau at approximately 1.4 V after the discharge current (current density of 11.11 mA cm^{-2}) was applied. At the end of the discharge process, the amount of Mg anode is exhausted whereas the amount of electrolyte is in excess (Z. Zhang et al., 2014), which is shown by the sharp decline. The highest performance was given by the Mg-air battery with the agar concentration of 3% w/v, which had the discharge capacity of 1303.94 mAh g^{-1} with respect to the mass of Mg anode consumed during discharging. It is 30.86%, 14.97% and 16.11% greater than 2%, 4%, and 5% w/v agar, respectively. Since the ionic conductivity and Mg corrosion are the important aspects in the operation of Mg-air battery, therefore the greater performance of Mg-air battery with WSG-incorporated 3% w/v agar gel electrolyte can be explained in terms of both of these aspects. With the increase in the agar concentration, both of the ionic conductivity and Mg corrosion decrease. However, in order to increase the performance of Mg-air battery, the electrolyte utilised should provide a high ionic conductivity while protecting Mg from corrosion. Therefore, the WSG-incorporated 3% w/v agar gel electrolyte which achieves the optimisation between high ionic conductivity and low Mg corrosion can obtain the greatest performance.

4.4 Effect of WSG Concentration on WSG-AGAR Gel Electrolyte

WSG-7 and 3% w/v agar were selected for the incorporation into agar gel electrolytes, owing to the best battery performance as described in the previous section. The effect of WSG concentration on WSG-AGAR was investigated through the incorporation of 0.01% w/v, 0.10% w/v, 0.30% w/v, and 0.50% w/v WSG-7 into the agar gel electrolyte. When the WSG concentration increased from 0.01% w/v to 0.50% w/v, the thickness of the respective WSG-AGAR gel electrolyte formed also increased from 0.41 cm to 0.46 cm. The increase in the thickness of WSG-AGAR gel electrolyte proves that a different amount of WSG-7 has been incorporated into the agar gel electrolyte.

Figure 4.12 illustrates the AC impedance spectra of agar gel electrolytes containing different WSG-7 concentrations (inset: expanded view at the high-frequency region). Table 4.6 shows the R_s and ionic conductivity of the agar gel electrolytes incorporated with different WSG-7 concentrations. From Table 4.6, it is shown that ionic conductivity increased with the addition of WSG-7 until the concentration of 0.10% w/v. The increase in the ionic conductivity is possibly due to the enhancement of charge flow in the agar gel electrolytes with the addition of WSG-7.

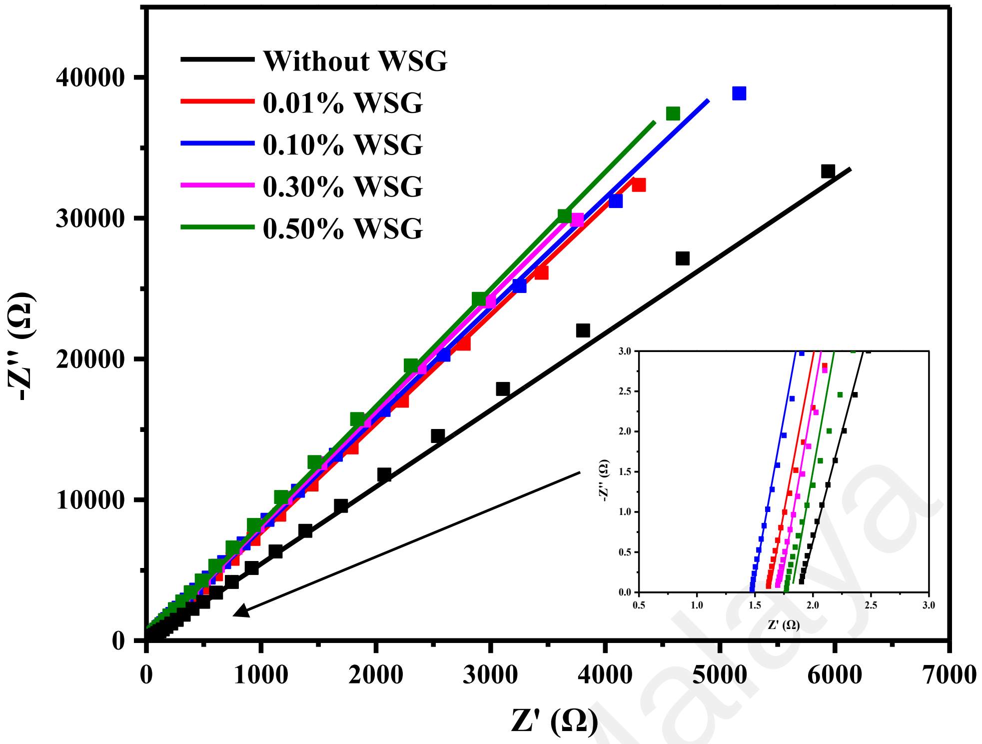

Figure 4.12: The AC impedance spectra of agar gel electrolytes containing different WSG-7 concentrations (inset: expanded view at the high-frequency region).

Table 4.6: Solution resistance and ionic conductivity of individual agar gel electrolyte containing different WSG-7 concentrations.

WSG-7 Composition (% w/v)	**Solution Resistance, R_s (Ω)**	**Ionic Conductivity (S cm^{-1})**
Without WSG	1.88	$(7.07 \pm 0.02) \times 10^{-2}$
0.01	1.62	$(7.98 \pm 0.01) \times 10^{-2}$
0.10	1.48	$(9.40 \pm 0.03) \times 10^{-2}$
0.30	1.71	$(8.19 \pm 0.04) \times 10^{-2}$
0.50	1.81	$(8.01 \pm 0.04) \times 10^{-2}$

However, when further increased the concentration of WSG-7 from 0.10% w/v to 0.50% w/v, the ionic conductivity of the WSG-AGAR gel electrolyte decreased. The WSG-AGAR gel electrolyte is produced from the entrapment of NaCl electrolyte and WSG in the solution within the 3D agar network. When the amount of WSG-7 inside the

WSG-AGAR gel electrolyte exceeds the optimum value, the excess WSG-7 is proposed to block the 3D channels within the agar structure which are used to perform free ionic transportation. Consequently, the transport of the ions in WSG-AGAR gel electrolyte through the 3D channels is hindered, which decreases the ionic conductivity.

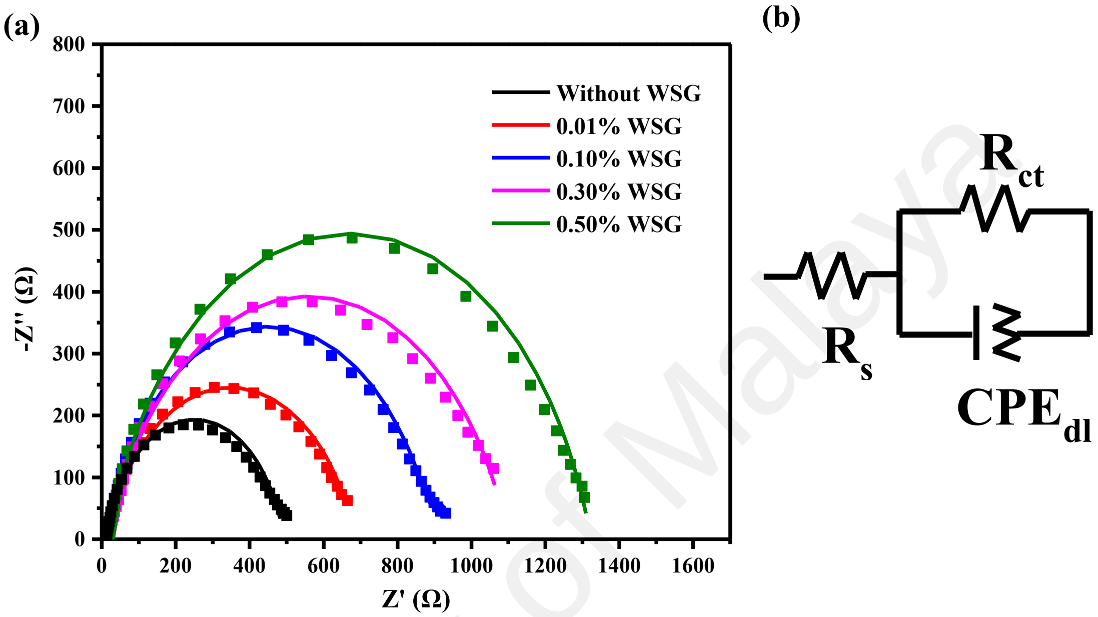

Figure 4.13: (a) EIS spectra and (b) equivalent circuit used to fit the EIS spectra of Mg strips immersed in WSG-AGAR gel electrolytes with different WSG-7 concentrations.

Table 4.7: R_{ct} of Mg strips in WSG-AGAR gel electrolytes containing different WSG-7 concentrations.

WSG Composition (% w/v)	**Charge Transfer Resistance, R_{ct} (Ω)**
Without WSG	473.53
0.01	673.27
0.10	867.80
0.30	1083.50
0.50	1305.20

Figure 4.13 illustrates the EIS spectra and equivalent circuit used to fit the EIS spectra of Mg strips immersed in WSG-AGAR gel electrolytes with different WSG-7

concentrations. Table 4.7 shows the R_{ct} of Mg strips in WSG-AGAR gel electrolytes with different WSG-7 concentrations. It reveals that R_{ct} value increased with the increasing WSG-7 concentration in the WSG-AGAR gel electrolytes. When the WSG-7 concentration in the WSG-AGAR gel electrolyte increases, the greater the protective coating over the Mg anode surface which restricts the liberal discharge of electron from Mg. Therefore, the charge flow at the electrode/electrolyte interface decreases and R_{ct} increases. This implies that the corrosion inhibition of the Mg anode increases with the increasing WSG-7 concentration.

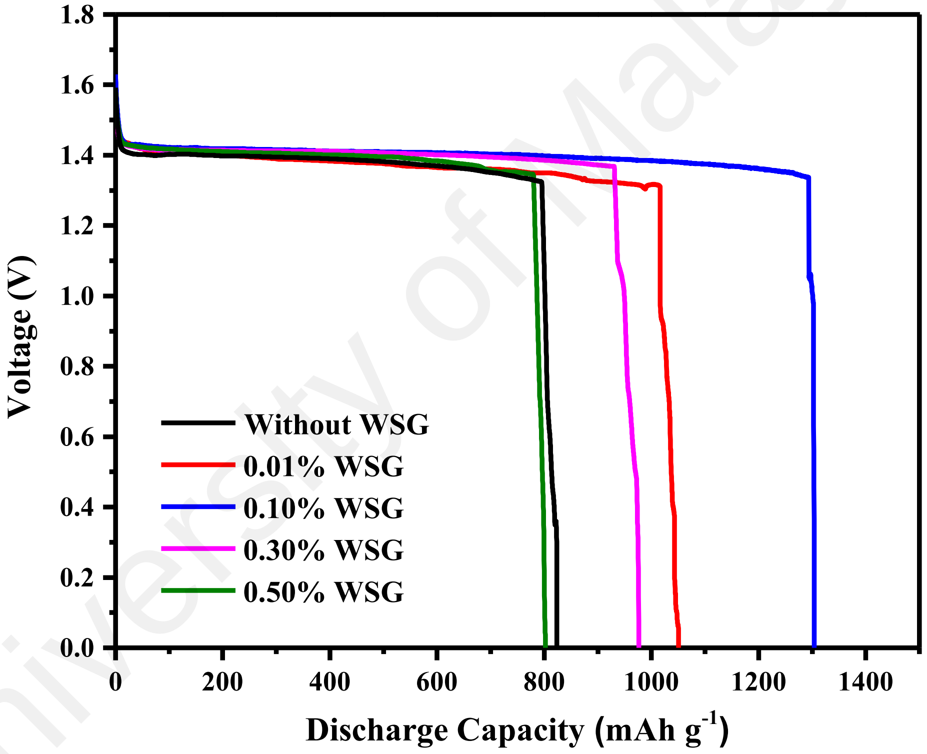

Figure 4.14: Discharge performance of Mg-air battery with WSG-AGAR gel electrolytes containing different WSG-7 concentrations at the current density of 11.11 mA cm^{-2}.

The performance of WSG-AGAR gel electrolytes with different WSG-7 concentrations for the custom-designed Mg-air battery was investigated by constant current discharge test at 11.11 mA cm^{-2} (Figure 4.14). It is observed that the incorporation of WSG-7 increased the battery performance. The best battery performance was given by the incorporation of 0.10% w/v WSG-7 into the agar gel electrolyte, with the discharge capacity of 1303.94 mAh g^{-1}, followed by 0.01% w/v (1050.38 mAh g^{-1}), 0.30% w/v (977.24 mAh g^{-1}), and 0.50% w/v (803.08 mAh g^{-1}). The incorporation of 0.10% w/v WSG-7 in the WSG-AGAR gel electrolyte provides the highest ionic conductivity while ensuring the Mg protection from corrosion. The lower battery performance given by 0.30% w/v and 0.50% w/v WSG-7 could be due to the interaction between ionic conductivity and Mg protection. Both of them produced WSG-AGAR gel electrolytes with lower ionic conductivity. Moreover, the stronger Mg protection film offered by 0.30% w/v and 0.50% w/v WSG-7 may suppress the further reaction of Mg anode, apart from protecting the Mg anode. This leads to the premature end of discharge and lowers the discharge capacity. Based on the above results, 0.10% w/v WSG-7 is found to be the optimum WSG concentration for the preparation of WSG-AGAR gel electrolyte.

4.5 Effect of Types of Electrolyte on WSG-AGAR Gel Electrolyte

The main electrolytes utilised in the investigation of Mg-air battery are the neutral saline electrolytes, especially NaCl. In this section, the use of other common electrolytes apart from NaCl is explored. When preparing the agar gel electrolyte for Mg-air battery, there are two main aspects for the selection of a suitable electrolyte, which are the ability of the agar to form a gel with the electrolyte and also the effect of the electrolyte on the performance of Mg-air battery. Both of the solidification of agar and the Mg-air battery performance are dependence on the acidity of electrolyte. Therefore, a few of the common electrolytes of different acidity were selected to test their compatibility for agar solidification and subsequently Mg-air battery performance.

The electrolytes selected were hydrochloric acid (HCl), sodium chloride (NaCl), magnesium chloride hexahydrate ($MgCl_2 \cdot 6H_2O$), sodium sulphate (Na_2SO_4), potassium hydroxide (KOH), and ammonia solution (NH_3). 0.6 M of each electrolyte was prepared, heated, and added with 3% w/v agar respectively for the gelation test. The gelation test was conducted without the incorporation of WSG-7. The results of the gelation test are shown in Table 4.8.

Table 4.8: Gelation test based on common electrolytes of different acidity.

Electrolyte	Gel	Description
HCl	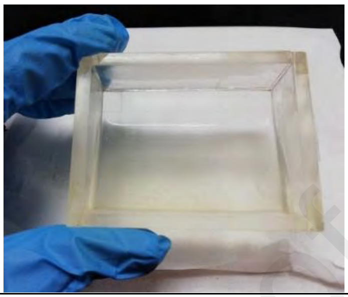	• Gelation did not occur after the addition of agar. • The agar powder was being hydrolysed, instead of soluble in the electrolyte.
NaCl	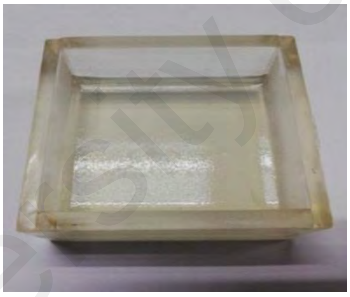	• Gelation occurred after the addition of agar. • The gel prepared was clear and transparent, with a good gel strength.
$MgCl_2 \cdot 6H_2O$	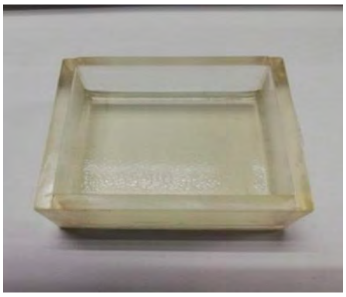	• Gelation occurred after the addition of agar. • The gel prepared was clear and transparent, with a good gel strength.

Table 4.8, continued: Gelation test based on common electrolytes of different acidity.

Electrolyte	Gel	Description
Na_2SO_4	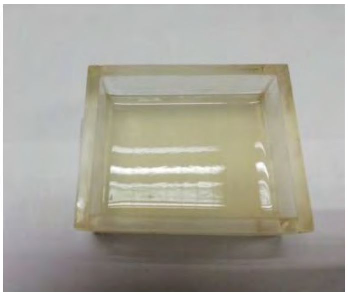 	• Gelation occurred after the addition of agar. • The gel has a clear and transparent appearance, but the gel strength is very weak. • Water was released from the gel. • The weak gel formed was too soft and liquefied for the application.
KOH	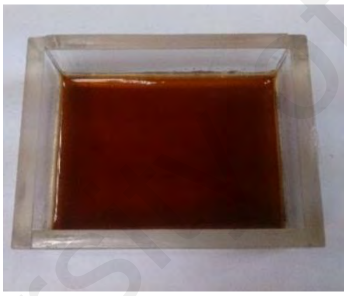 	• Gelation occurred after the addition of agar. • The gel has a dark brown colour, with a very weak gel strength. • The weak gel formed was too soft and liquefied for the application.
NH_3	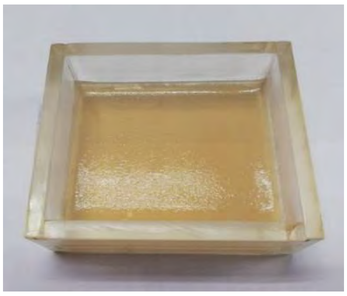	• Gelation occurred after the addition of agar. • The gel prepared was transparent with a light brown colour.

Based on the gelation test, NaCl, $MgCl_2•6H_2O$, and NH_3 can form stable agar gels, whereas HCl, Na_2SO_4, and KOH were unable to produce stable gels. The inability of the electrolytes to form stable gels with agar is most likely due to their interaction with the polysaccharides.

Agar consists of agarose (gelling component) and agaropectin (non-gelling component). The presence of sulphate group is the main difference between these two components, in which the sulphate group is present in the agaropectin (Venugopal, 2011). A little variation in the sulphate content of the agar molecule alters its gelling properties dramatically. The weak gel produced by the Na_2SO_4 could be due to the interaction of the sulphate ions with agar. Singh, Meena, and Kumar (2009) highlighted that Na_2SO_4 reduces the agarose-water interactions and eases the release of water from the gel network, thus weakens the gel structure. The water mediating the agar helices becomes lesser and the hydrogen bonding of water molecules in the gel also weakens with the addition of sodium sulphate (Singh et al., 2009).

Agar did not form a gel with HCl, but being hydrolysed by the acid. Armisén and Galatas (2009) mentioned that agar can suffer from hydrolysis which decreases its molecular weight, thus resulting in the loss of its gelling power. In agar, acid hydrolysis happens more easily as the pH is low and the time of the agar staying in high temperature dissolution is long (Armisén & Galatas, 2009).

For the alkaline electrolytes, it was observed that agar formed a stable gel with NH_3. On the other hand, a soft and weak gel was formed with KOH, which is not suitable for the application. Mesbah and Wiegel (2006) mentioned that pH value can affect the stability of the solidified agar gel produced. The soft and weak agar gel formed with KOH is most likely due to the instability of the agar gel at high pH, since KOH (pH 13) has a higher pH than NH_3 (pH 10) at the concentration of 0.6 M. The linkage of helices in agar during the gelation process occurs due to the presence of hydrogen bonding. The presence of any charged group affects the formation of intermolecular hydrogen bonding, which in turn interfere with the solidification of the agar gel (Azeem, Batool, Iqbal, & Haq, 2017). Strong base (KOH) produces more charged ions than the weak base (NH_3), which decreases the amount of intermolecular hydrogen bonding, forming a soft and weak gel.

Based on the gelation test, NaCl, $MgCl_2$•$6H_2O$, and NH_3 are suitable as the candidates for the preparation of agar gel electrolyte, whereas HCl, Na_2SO_4, and KOH are not compatible for the application. The agar gel electrolytes of NaCl, $MgCl_2$•$6H_2O$, and NH_3 were prepared by adding 0.1% w/v WSG-7 and 3% w/v agar into 0.6 M of each electrolyte solution produced.

The AC impedance spectra of agar gel electrolytes formed from different types of electrolyte (inset: expanded view at high-frequency region) are shown in Figure 4.15.

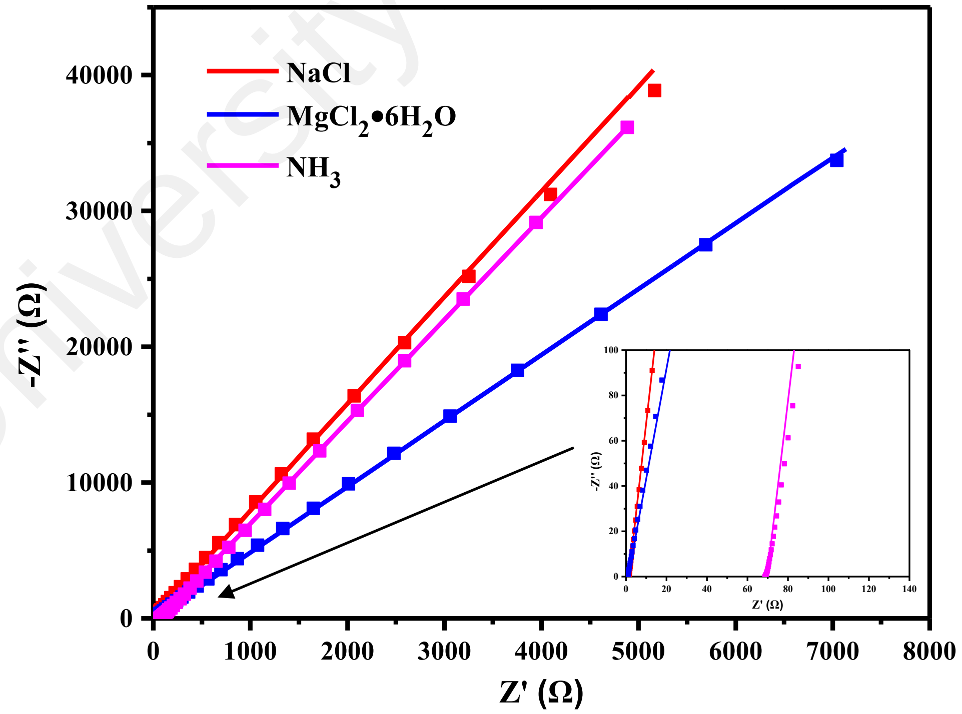

Figure 4.15: The AC impedance spectra of agar gel electrolytes containing different types of electrolyte (inset: expanded view at high-frequency region).

Table 4.9: Solution resistance and ionic conductivity of individual agar gel electrolyte containing different types of electrolyte.

Type of Electrolyte	Solution Resistance, R_s (Ω)	Ionic Conductivity (S cm^{-1})
NaCl	1.48	$(9.40 \pm 0.03) \times 10^{-2}$
$MgCl_2$•$6H_2O$	1.09	$(1.14 \pm 0.01) \times 10^{-1}$
NH_3	69.69	$(1.66 \pm 0.01) \times 10^{-3}$

The solution resistance and ionic conductivity of the individual agar gel electrolyte are shown in Table 4.9. From the above results, it is observed that the ionic conductivity of the agar gel electrolytes formed from different types of electrolyte increased in the order of NH_3 < NaCl < $MgCl_2$•$6H_2O$. NH_3 is commonly known as a weak electrolyte which partially dissociates in water, hence a weak conductor of electricity. Therefore, NH_3 has a much lower ionic conductivity than the other two electrolytes. Both NaCl and $MgCl_2$•$6H_2O$ are strong electrolytes which highly soluble and completely dissociate in water, producing ions for the high conductance of electricity. The ionic conductivity is proportional to the ion concentration in the electrolyte. When dissociates in water, $MgCl_2$•$6H_2O$ produces 3 moles of ions whereas NaCl only produces 2 moles of ions. Therefore, at the same molarity, the ionic conductivity of $MgCl_2$•$6H_2O$ is higher than NaCl. Consequently, the WSG-AGAR gel electrolyte formed from $MgCl_2$•$6H_2O$ also has a higher conductivity as compared to that formed from NaCl.

Figure 4.16(a) shows the EIS spectra of Mg strips immersed in WSG-AGAR gel electrolytes with different types of electrolyte solution. Figure 4.16(b) illustrates the equivalent circuit used to fit the EIS spectra of Mg immersed in WSG-AGAR gel electrolytes prepared from NaCl and $MgCl_2$•$6H_2O$, whereas Figure 4.16(c) shows the equivalent circuit used to fit the EIS spectra of Mg immersed in WSG-AGAR gel electrolyte prepared from NH_3.

From Figure 4.16(a), the EIS spectra of WSG-AGAR formed from NaCl and $MgCl_2•6H_2O$ had a capacitive semicircle in the whole frequency range. Nonetheless, the EIS spectrum of NH_3 was characterised by two capacitive semicircles in the whole frequency range.

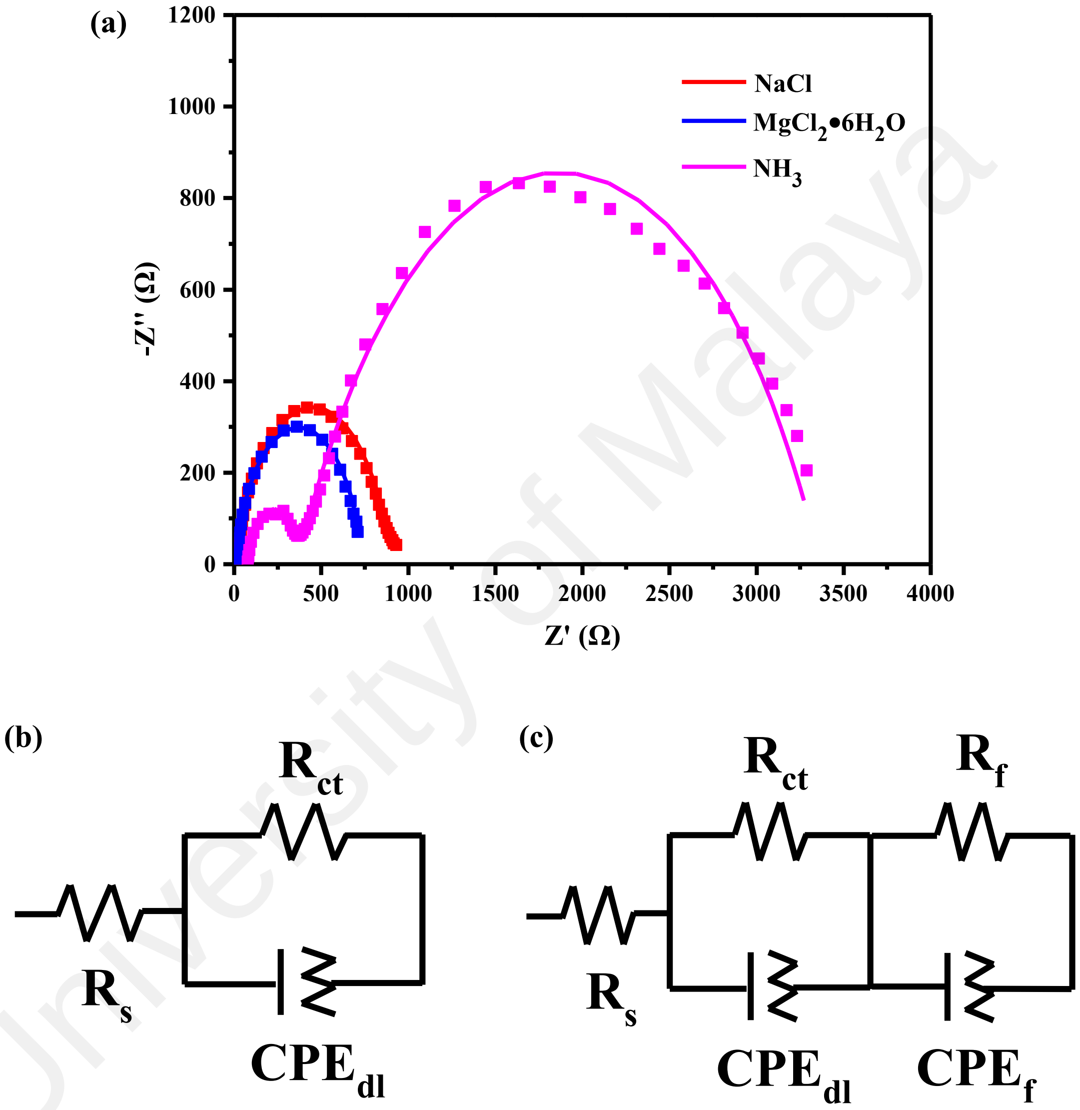

Figure 4.16: (a) EIS spectra; equivalent circuits used to fit the EIS spectra of Mg strips immersed in WSG-AGAR gel electrolytes prepared from (b) NaCl and $MgCl_2•6H_2O$, and (c) NH_3.

For NH_3, the semicircle at high frequencies corresponds to the charge transfer process and double layer at the electrode/electrolyte interface, whereas the semicircle at the low frequencies is due to the $Mg(OH)_2$ film attached to the surface of the Mg electrode (Feng et al., 2016). This phenomenon shows that $Mg(OH)_2$ is easily formed on the Mg anode surface immersed in the WSG-AGAR gel electrolyte prepared from NH_3. Moreover, WSG-AGAR gel electrolyte with NH_3 had an impedance which was notably greater than NaCl and $MgCl_2$•$6H_2O$, indicating the significantly improved corrosion resistance. The improved corrosion protection provided by NH_3 could be due to the higher resistance of Mg in the alkaline environment as compared to the neutral or acidic environment (T. Zhang et al., 2014). Mg^{2+} is the stable substance in the acidic, neutral, to the slightly alkaline electrolyte, whereas $Mg(OH)_2$ is the stable substance in the electrolyte with higher basicity (T. Zhang et al., 2014). Therefore, the alkaline NH_3 electrolyte enables the easy formation of $Mg(OH)_2$ film on Mg surface, thus higher corrosion resistance.

Apart from the influence of pH, the anions in the electrolyte also play an important role in Mg corrosion (T. Zhang et al., 2014). From the EIS spectra, the R_{ct} of WSG-AGAR gel electrolyte with $MgCl_2$•$6H_2O$ (729.46 Ω) was lower as compared to NaCl (867.80 Ω). Both of the electrolytes are categorised as the neutral electrolyte. However, $MgCl_2$•$6H_2O$ has a higher amount of Cl^- ions than NaCl at the same concentration, which is more likely to attack Mg and resulting in lower R_{ct}.

The different WSG-AGAR gel electrolytes prepared from NaCl, $MgCl_2$•$6H_2O$, and NH_3 were utilised to fabricate the Mg-air battery. Figure 4.17 shows the discharge performance of Mg-air battery with NaCl agar gel electrolyte and $MgCl_2$•$6H_2O$ agar gel electrolyte (both incorporated with WSG-7) at the current density of 11.11 mA cm^{-2}.

When NH_3 was used as the electrolyte for Mg-air battery, the discharge process was terminated after a few minutes, thereby the result was not included in Figure 4.17. NH_3 is a weak electrolyte which has a low ionic conductivity, as shown in Table 4.9. In addition, the use of the alkaline electrolyte promotes the formation of $Mg(OH)_2$ at the anode which protects Mg from corrosion, as illustrated by the large semicircle in Figure

4.16(a). Too much $Mg(OH)_2$ film can prevent further reaction of the anode, results in delayed response; thereby causing the premature end of the discharge process. All of these factors contributed to the poor discharge performance of WSG-AGAR gel electrolyte containing NH_3.

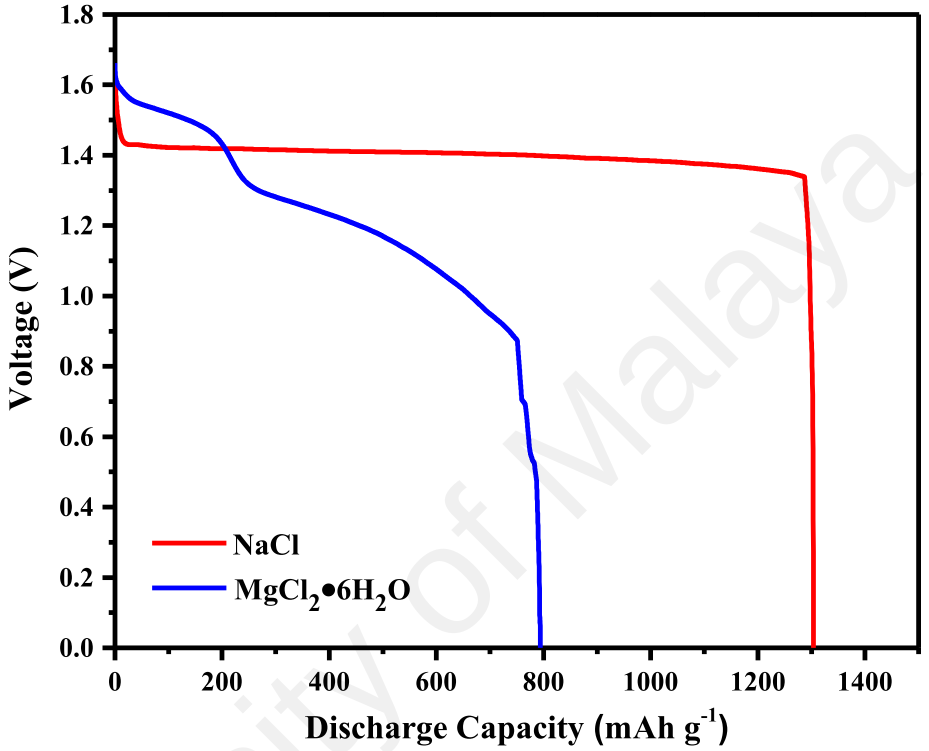

Figure 4.17: Discharge performance of Mg-air battery with NaCl agar gel electrolyte and $MgCl_2•6H_2O$ agar gel electrolyte incorporated with WSG-7 at the current density of 11.11 mA cm^{-2}.

From the discharge performance in Figure 4.17, NaCl provided a higher discharge capacity than $MgCl_2•6H_2O$ (793.71 mAh g^{-1}). In addition, NaCl also provided a flat discharge voltage of approximately 1.4 V. On the other hand, $MgCl_2•6H_2O$ had a relatively unstable discharge curve. Although $MgCl_2•6H_2O$ had a higher discharge voltage at the early stage of the discharge process, the discharge voltage gradually dropped until approximately 0.9 V.

The higher discharge voltage provided by $MgCl_2•6H_2O$ at the early discharge process as compared to NaCl is as expected since $MgCl_2•6H_2O$ had a higher ionic conductivity than NaCl (Table 4.9). However, as the discharge process proceeded, there was an interaction between the electrolyte and the discharged products, forming precipitation of by-products at the air diffusion cathode. This results in the clogging of electrode pores and blocking the electrolyte channels. The decrease in the contact between electrolyte and oxygen reduces the discharge voltage with time, which also lowers the discharge capacity of the Mg-air battery. Moreover, $MgCl_2•6H_2O$ agar gel electrolyte had a lower R_{ct} than NaCl, as shown in Figure 4.16(a). This suggests that Mg is more susceptible to corrosion in $MgCl_2•6H_2O$, thus contributing to a lower discharge capacity.

According to the above results, NaCl was the best electrolyte to be used for forming WSG-AGAR gel electrolyte. It provided the optimum ionic conductivity and Mg anode protection, thus giving a stable discharge current during the operation of Mg-air battery.

Based on the results for all the parameters, the optimal WSG-AGAR gel electrolyte was determined to contain 0.1% w/v WSG-7, 3% w/v agar, with NaCl electrolyte. The operation of Mg-air battery with this optimal electrolyte was terminated after about 6.95 h, when 1820.70 mWh g^{-1} of energy density had been discharged. It is noteworthy that the Mg-air battery customised in this study is small in area, size and thickness, which makes the discharge capacity and energy density obtained to be remarkable. The area densities between 77.22 mAh cm^{-2} and 107.83 mWh cm^{-2} were achieved.

Table 4.10 depicts the battery performance of Mg-air battery in recent literature. It is shown that the battery performance of Mg-air battery with the optimal WSG-AGAR gel electrolyte is comparatively higher than the other Mg-air battery. Apart from the higher discharge capacity and energy density, the operating voltage of the customised Mg-air battery in this study can reach up to 1.4 V, which surpass the performance of the recent literature (Ma et al., 2019; Mayilvel Dinesh et al., 2015), with the operating voltage between 0.6 V to 0.9 V at the same discharge current of 10mA.

All of these achievements support the utilisation of WSG-AGAR gel polymer electrolyte in Mg-air battery.

Table 4.10: Comparison of battery performance with other Mg-air battery in recent literature.

Battery Performance	Anode	Cathode	Electrolyte	Reference
Energy density: 1620 mWh g^{-1}	Mg-6 wt%Al-1 wt% In alloy	rGO/Mn_3O_4-based air cathode	3.5 wt% NaCl solution Electrolyte additive: PSS/rGO	Ma et al. (2019)
Discharge capacity: 1170 mAh g^{-1}.	AZ31B grade Mg	SS304 grade stainless steel mesh	$MgCl_2$ Electrolyte additive: Water dispersible nano MoS_2	Shyma et al. (2019)
Energy density: 1429 mWh g^{-1}	Mg-0.1 wt% Ca alloy	Carbon/MnO_2 -based air cathode	3.5 wt. % NaCl solution	Deng, Höche, Lamaka, Snihirova, and Zheludkevich (2018)
Discharge capacity: 1030.71 mAh g^{-1}	Mg ribbon	Stainless steel cathode	3.5 wt% NaCl solution Electrolyte additive: rGO	Mayilvel Dinesh et al. (2015)

4.6 Morphology and Practical Usability of Optimal WSG-AGAR Gel Electrolyte

The optimal WSG-AGAR gel electrolyte (with 0.1% w/v WSG-7, 3% w/v agar, and NaCl electrolyte) which had the best performance for Mg-air battery was further analysed to better understand its properties. The WSG-7 and WSG-7-AGAR gel electrolyte were characterised with FESEM to investigate their surface morphology. Figure 4.18 shows the FESEM images of WSG-7 and the surfaces of agar gel electrolyte (with and without WSG-7).

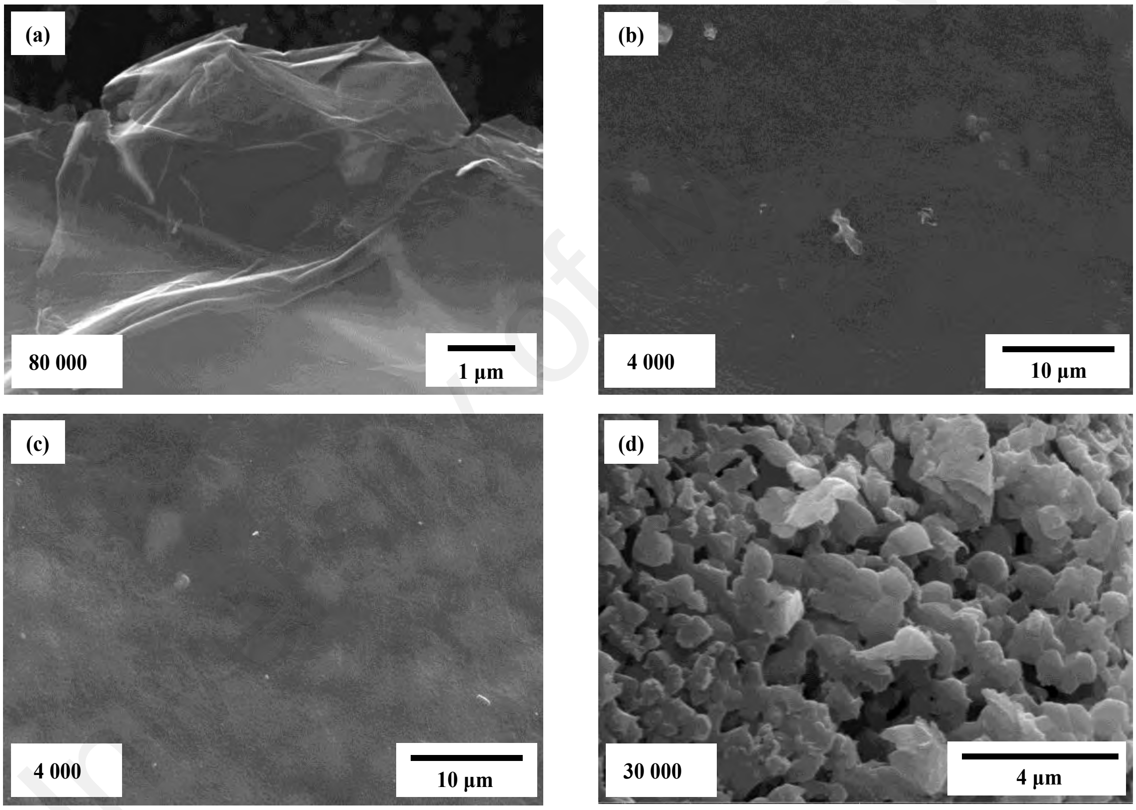

Figure 4.18: FESEM images of (a) WSG-7; (b) agar gel electrolyte containing WSG-7 and NaCl, (c) agar gel electrolyte containing only NaCl (at lower magnification), and (d) agar gel electrolyte containing only NaCl (at higher magnification).

Figure 4.18(a) shows the morphology of WSG-7, which existed as a thin and wrinkled paper-like structure. From Figure 4.18(b), WSG-7-AGAR gel electrolyte had a smooth and homogeneous surface with some tiny WSG-7 sheet attached on the gel surface. On the contrary, the agar gel electrolyte without incorporation of WSG-7 (Figure 4.18(c)) displayed a rougher and uneven surface. Figure 4.18(d) showed the surface of agar gel electrolyte without WSG-7 at a higher magnification. It proves that the gel is interconnected in a 3D manner, with the presence of an open porous structure. The greater smoothness of WSG-7-AGAR gel electrolyte proposes that WSG-7 disperses well in the aqueous medium and subsequently fills the pores within the 3D channel network, improving the uniformity and mechanical strength of the gel.

The discharging performance of the Mg-air battery assembled with the optimal WSG-7-AGAR gel electrolyte was further tested with constant current densities of 1.11 and 5.56 mA cm^{-2} (apart from the higher current density of 11.11 mA cm^{-2}) in order to evaluate their performance at low current densities. Figure 4.19 depicts the discharge performance of the optimal Mg-air battery in terms of time at the constant current densities of 1.11, 5.56, and 11.11 mA cm^{-2}.

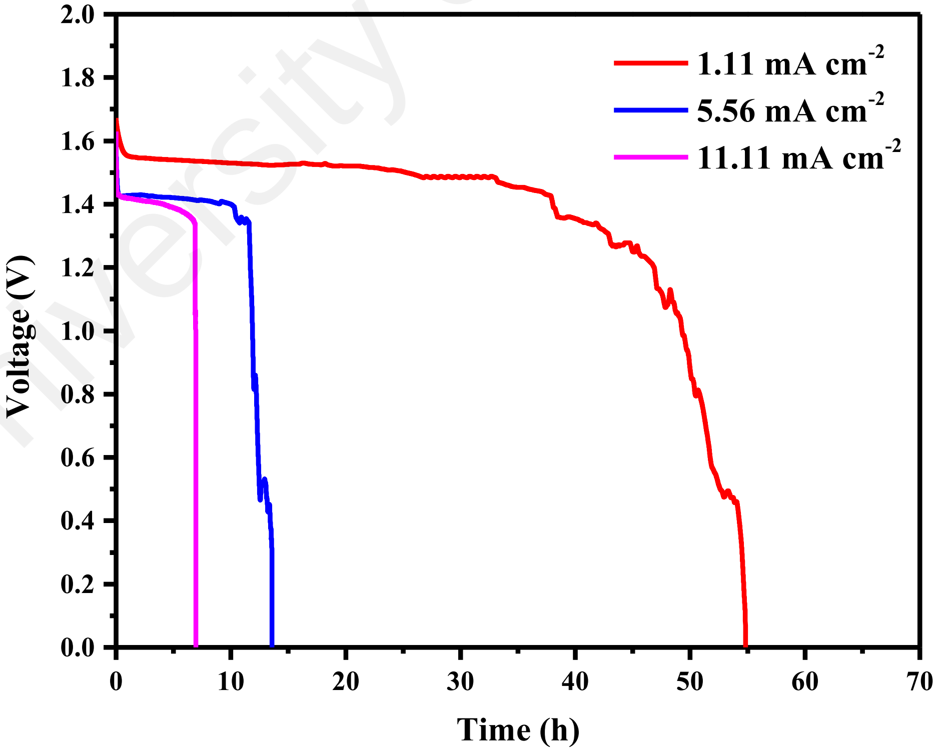

Figure 4.19: Discharge performance of Mg-air battery with the optimal WSG-7-AGAR gel electrolyte at the constant current densities of 1.11, 5.56, and 11.11 mA cm^{-2}.

From Figure 4.19, the discharging voltages remained stable for all of the current densities. The sharp decline at the end of the discharge process shows that the amount of Mg is exhausted whereas the electrolyte is in excess. When comparing the stable discharge voltages of the assembled Mg-air battery at different current densities, it is observed that the discharge voltage decreased with increasing current density. The voltage decline is possibly due to the increase in ohmic polarisation with the increase in discharge current (Z. Zhang et al., 2014). The battery life measured in hours obtained from the discharge plots were 54.81, 13.59, and 6.95 h at discharge current densities of 1.11, 5.56, and 11.11 mA cm^{-2}, respectively.

The discharge current density also influences the discharge capacity and energy density of the Mg-air battery, as demonstrated in Figure 4.20.

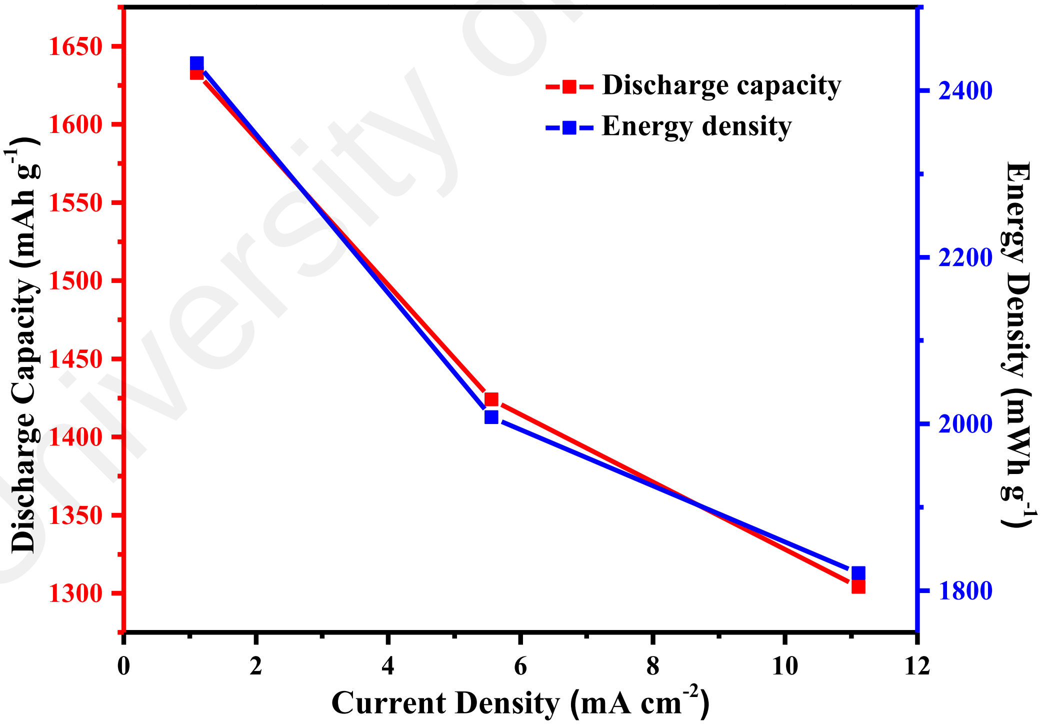

Figure 4.20: Discharge capacity and energy density of Mg-air battery with the optimal WSG-7-AGAR at the constant current densities of 1.11, 5.56, and 11.11 mA cm^{-2}.

The trend of the energy density profile is comparable to the discharge capacity profile owing to the relatively stable operating voltages. With respect to the mass of Mg anode consumed, the discharge capacity of the assembled Mg-air battery at the current densities of 1.11, 5.56, and 11.11 mAh g^{-1} were 1632.74, 1423.99, and 1303.94 mAh g^{-1}, respectively; whereas the energy density were 2432.78, 2007.82, and 1820.70 mWh g^{-1}, respectively.

It is shown that the discharge capacity and energy density of the Mg-air battery were inversely proportional to the discharge current density. The battery discharge capacity corresponds to the amount of electric charge which can be delivered during the discharging process (Kirchev, 2015). During the slow discharging process (low discharge current), the reactants have the sufficient time to be converted to their active form and transferred to their necessary positions, resulting in higher discharge capacity and energy density.

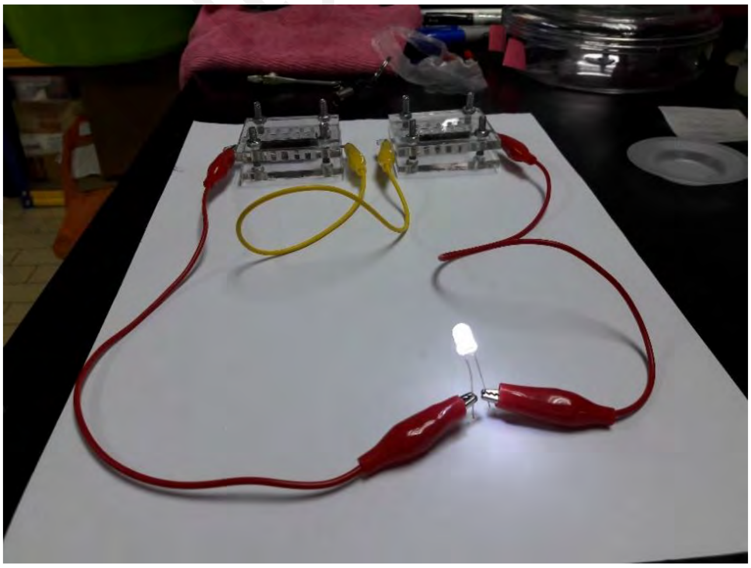

Figure 4.21: Digital image of a LED activated by the Mg-air batteries with the WSG-7-AGAR gel electrolyte.

In addition, the Mg-air battery assembled using the optimal WSG-AGAR gel electrolyte was used to activate a white LED in order to test the usability of the device fabricated (Figure 4.21). It was demonstrated that the assembled device can activate the white LED for hours.

CHAPTER 5: CONCLUSION

5.1 Conclusion

In summary, the objectives of this research study are well accomplished. An all-solid-state Mg-air battery with WSG-AGAR gel electrolyte achieved a high capacity and energy density without electrolyte leakage. The Mg-air battery is a laminar structure which consisted of a Mg anode, a WSG-AGAR gel electrolyte, and an air cathode. Firstly, GO was successfully synthesised via the simplified Hummers' method, and was reduced to form various WSG through the addition of the different amount of NH_3 to GO prior to chemical reduction. The amount of NH_3 affected the quality of WSG synthesised, which in turn altered the dispersion stability and conductivity of the aqueous solution formed. WSG synthesised was utilised as an additive in the electrolyte for Mg-air battery.

It was found that the adjustment of GO solution to pH 7 prior to the chemical reduction produced the best WSG for Mg-air battery application. The controlled defects in WSG-7 maintain the desired property of graphene, while at the same time has high dispersibility and conductivity in aqueous solution. Consequently, a WSG-AGAR gel electrolyte with good ionic conductivity and Mg anode protection was formed. The incorporation of WSG-7 in agar gel electrolyte had demonstrated the improvement in ionic conductivity by 32.96% and discharge capacity of Mg-air battery by 58.34% as compared to that without electrolyte additive.

In order to further improve the performance of Mg-air battery, considerable investigation had also been carried out on the role of agar concentration, WSG concentration, and types of electrolyte on WSG-AGAR gel electrolyte. An optimal composition of 0.1% w/v WSG-7 in 3.5% w/v sodium chloride (NaCl), entrapped in 3% w/v agar gel had demonstrated the balance between high ionic conductivity and sufficient anodic corrosion resistance. The ionic conductivity of this optimal gel electrolyte was

9.40×10^{-2} S cm^{-1}. At the current density of 11.11 mA cm^{-2}, the optimal gel electrolyte surpassed the other WSG-AGAR gel compositions with the discharge capacity and energy density of Mg-air battery at 1303.94 mAh g^{-1} and 1820.70 mWh g^{-1} (with respect to the mass of Mg anode consumed during discharging), respectively.

The further discharge of Mg-air battery with the optimal WSG-AGAR gel electrolyte at different current densities had demonstrated the increase in battery performance at lower current density. At the current density of 1.11 mA cm^{-2}, the peak discharge capacity and energy density (with respect to the mass of Mg anode consumed during discharging) were 1632.74 mAh g^{-1} and 2432.78 mWh g^{-1}, respectively. This achievement should be appraised with regard to the small area, size, and thickness of the Mg-air battery. The combination of NaCl and agar enables risk-free fabrication and applications. The successful development of this agar gel electrolyte enables a simple and effective way to produce an environmentally benign biopolymer electrolyte as a promising electrolyte for Mg-air batteries.

5.2 Recommendations for Future Research

Despite various exploitation on the WSG-AGAR electrolyte have been conducted, a number of challenges still remain and require attention in the future works. In order to enhance the electrochemical performance of Mg-air battery, further research and development are necessary. Several recommendations for future research were suggested as follows:

1. Investigation on a wide range of non-aqueous electrolyte in agar gel electrolyte is a possible direction for Mg-air battery. The use of ionic liquid (non-aqueous electrolyte) is one of the ways to improve the operating voltage of Mg-air battery and enhance the energy density. Ionic liquid has a wide and stable

electrochemical potential window, high ionic conductivity, ease of handling, low toxicity, non-volatility, and non-flammability. The compatibility between agar and ionic liquid can be tested and the influence of the ionic liquid on electrochemical performance of the agar gel electrolyte and Mg-air battery can be evaluated in further study.

2. Utilisation of Mg alloys as anode may improve the Mg-air battery performance. Pure Mg used in this study enables better monitoring of the Mg corrosion. However, it is more susceptible to corrosion as compared to Mg alloys. Alloying of Mg with other metals, for instance, Al, Zn, or Mn can hinder the hydrogen evolution reaction, thus decreases Mg self-corrosion and results in the improvement of discharge time and capacity. Therefore, the use of Mg alloys such as AZ31, AZ61, AM50, AM60, and MA8M06 as Mg anode will be a good suggestion for future study in order to produce Mg-air battery with higher performance.

REFERENCES

Achari, A., Datta, K., De, M., Dravid, V. P., & Eswaramoorthy, M. (2013). Amphiphilic aminoclay-rGO hybrids: A simple strategy to disperse a high concentration of rGO in water. *Nanoscale, 5*(12), 5316-5320.

Agrawal, S., Raghuveer, M., Li, H., & Ramanath, G. (2007). Defect-induced electrical conductivity increase in individual multiwalled carbon nanotubes. *Applied Physics Letters, 90*(19), 193104.

Al-Kahlout, A., Vieira, D., Avellaneda, C. O., Leite, E. R., Aegerter, M. A., & Pawlicka, A. (2010). Gelatin-based protonic electrolyte for electrochromic windows. *Ionics, 16*(1), 13-19.

Allen, G., & Bevington, J. C. (1989). *Comprehensive polymer science: Specialty polymers & polymer processing*. Ann Arbor, Michigan: Elsevier Science & Technology Books.

An, L., Zhao, T., & Zeng, L. (2013). Agar chemical hydrogel electrode binder for fuel-electrolyte-fed fuel cells. *Applied Energy, 109*, 67-71.

Armand, M., & Tarascon, J. M. (2008). Building better batteries. *Nature, 451*(7179), 652-657.

Armisén, R., & Galatas, F. (2009). Agar. In G. O. Philips & P. A. Williams (Eds.), *Handbook of hydrocolloids* (2nd ed., pp. 82-107). Cambridge: Woodhead Publishing Limited.

Arya, A., & Sharma, A. (2017). Polymer electrolytes for lithium ion batteries: A critical study. *Ionics, 23*(3), 497-540.

Aurbach, D., Lu, Z., Schechter, A., Gofer, Y., Gizbar, H., Turgeman, R., . . . Levi, E. (2000). Prototype systems for rechargeable magnesium batteries. *Nature, 407*(6805), 724-727.

Avellaneda, C. O., Vieira, D. F., Al-Kahlout, A., Leite, E. R., Pawlicka, A., & Aegerter, M. A. (2007). Solid-state electrochromic devices with Nb_2O_5: Mo thin film and gelatin-based electrolyte. *Electrochimica Acta, 53*(4), 1648-1654.

Azeem, M., Batool, F., Iqbal, N., & Haq, I. U. (2017). Algal-based biopolymers. In K. M. Zia, M. Zuber, & M. Ali (Eds.), *Algae based polymers, blends, and composites: Chemistry, biotechnology and materials science* (pp. 1-32). Amsterdam: Elsevier.

Aziz, M., Buraidah, M., Careem, M., & Arof, A. (2015). PVA based gel polymer electrolytes with mixed iodide salts ($K^+ I^-$ and $Bu_4 N^+ I^-$) for dye-sensitized solar cell application. *Electrochimica Acta, 182*, 217-223.

Bai, H., Xu, Y., Zhao, L., Li, C., & Shi, G. (2009). Non-covalent functionalization of graphene sheets by sulfonated polyaniline. *Chemical Communications, 2009*(13), 1667-1669.

Barat, B. R., & Cano, E. (2015). The use of agar gelled electrolyte for in situ electrochemical measurements on metallic cultural heritage. *Electrochimica Acta, 182*, 751-762.

Bayer, T., Cunning, B. V., Selyanchyn, R., Nishihara, M., Fujikawa, S., Sasaki, K., & Lyth, S. M. (2016). High temperature proton conduction in nanocellulose membranes: Paper fuel cells. *Chemistry of Materials, 28*(13), 4805-4814.

Begum, S., Pandian, R., Aswal, V. K., & Ramasamy, R. P. (2014). Chitosan-gold-lithium nanocomposites as solid polymer electrolyte. *Journal of Nanoscience and Nanotechnology, 14*(8), 5761-5773.

Belay, M., Nagarale, R. K., & Verma, V. (2017). Preparation and characterization of graphene-agar and graphene oxide-agar composites. *Journal of Applied Polymer Science, 134*(33), 45085.

Bella, F., Mobarak, N. N., Jumaah, F. N., & Ahmad, A. (2015). From seaweeds to biopolymeric electrolytes for third generation solar cells: An intriguing approach. *Electrochimica Acta, 151*, 306-311.

Bhattacharya, M. (2016). Polymer nanocomposites-a comparison between carbon nanotubes, graphene, and clay as nanofillers. *Materials, 9*(4), 262.

Bini, M., Capsoni, D., Ferrari, S., Quartarone, E., & Mustarelli, P. (2015). Rechargeable lithium batteries: Key scientific and technological challenges. In A. A. Franco (Ed.), *Rechargeable lithium batteries: From fundamentals to applications*. Sawston, Cambridge: Elsevier Science.

Bo, Z., Shuai, X., Mao, S., Yang, H., Qian, J., Chen, J., . . . Cen, K. (2014). Green preparation of reduced graphene oxide for sensing and energy storage applications. *Scientific Reports, 4*(4684), 1-8.

Boopathi, G., Pugalendhi, S., Selvasekarapandian, S., Premalatha, M., Monisha, S., & Aristatil, G. (2017). Development of proton conducting biopolymer membrane based on agar–agar for fuel cell. *Ionics, 23*(10), 2781-2790.

Bora, C., Bharali, P., Baglari, S., Dolui, S. K., & Konwar, B. K. (2013). Strong and conductive reduced graphene oxide/polyester resin composite films with improved mechanical strength, thermal stability and its antibacterial activity. *Composites Science and Technology, 87*, 1-7.

Cambaz, Z. G., Yushin, G., Osswald, S., Mochalin, V., & Gogotsi, Y. (2008). Noncatalytic synthesis of carbon nanotubes, graphene and graphite on SiC. *Carbon, 46*(6), 841-849.

Cano, E., Crespo, A., Lafuente, D., & Barat, B. R. (2014). A novel gel polymer electrolyte cell for in-situ application of corrosion electrochemical techniques. *Electrochemistry Communications, 41*, 16-19.

Cheng, F., & Chen, J. (2012). Metal-air batteries: From oxygen reduction electrochemistry to cathode catalysts. *Chemical Society Reviews, 41*(6), 2172-2192.

Chiappone, A., Bella, F., Nair, J. R., Meligrana, G., Bongiovanni, R., & Gerbaldi, C. (2014). Structure-performance correlation of nanocellulose-based polymer electrolytes for efficient quasi-solid DSSCs. *ChemElectroChem, 1*(8), 1350-1358.

Chong, S. W., Lai, C. W., & Abd Hamid, S. B. (2015). Green preparation of reduced graphene oxide using a natural reducing agent. *Ceramics International, 41*(8), 9505-9513.

Cohn, G., Starosvetsky, D., Hagiwara, R., Macdonald, D. D., & Ein-Eli, Y. (2009). Silicon-air batteries. *Electrochemistry Communications, 11*(10), 1916-1918.

Cui, Y., Chai, J., Du, H., Duan, Y., Xie, G., Liu, Z., & Cui, G. (2017). Facile and reliable in situ polymerization of poly(ethyl cyanoacrylate)-based polymer electrolytes toward flexible lithium batteries. *ACS Applied Materials & Interfaces, 9*(10), 8737-8741.

Das, S. K. (2016). *Mobile terminal receiver design: LTE and LTE-advanced*. Singapore: John Wiley & Sons.

Deng, M., Höche, D., Lamaka, S. V., Snihirova, D., & Zheludkevich, M. L. (2018). Mg-Ca binary alloys as anodes for primary Mg-air batteries. *Journal of Power Sources, 396*, 109-118.

Deyab, M. A. (2016). Decyl glucoside as a corrosion inhibitor for magnesium-air battery. *Journal of Power Sources, 325*, 98-103.

Di Noto, V., Lavina, S., Giffin, G. A., Negro, E., & Scrosati, B. (2011). Polymer electrolytes: Present, past and future. *Electrochimica Acta, 57*, 4-13.

Di Palma, T., Migliardini, F., Caputo, D., & Corbo, P. (2017). Xanthan and κ-carrageenan based alkaline hydrogels as electrolytes for Al/air batteries. *Carbohydrate Polymers, 157*, 122-127.

DJDC Battery. (2015). *World batteries (Industry study 3309).* Retrieved from https://www.freedoniagroup.com/industry-study/world-batteries-3309.htm.

Downing, B. W. (2016). Magnesium-air battery. In V. Neburchilov & J. Zhang (Eds.), *Metal-air and metal-sulfur batteries: Fundamentals and applications*. Boca Raton, Florida: CRC Press.

Du, J., Wang, Z., Niu, Y., Duan, W., & Wu, Z. (2014). Double liquid electrolyte for primary Mg batteries. *Journal of Power Sources, 247*, 840-844.

Enderlein, C. (2010). *Graphene and its interaction with different substrates studied by angular-resolved photoemission spectroscopy*. Berlin: Freie Universität Berlin.

Feng, Y., Xiong, W., Zhang, J., Wang, R., & Wang, N. (2016). Electrochemical discharge performance of the Mg-Al-Pb-Ce-Y alloy as the anode for Mg-air batteries. *Journal of Materials Chemistry A, 4*(22), 8658-8668.

Fotouhi, A., Auger, D. J., O'Neill, L., Cleaver, T., & Walus, S. (2017). Lithium-sulfur battery technology readiness and applications-a review. *Energies, 10*(12), 1937.

Gelman, D., Shvartsev, B., & Ein-Eli, Y. (2014). Aluminum-air battery based on an ionic liquid electrolyte. *Journal of Materials Chemistry A, 2*(47), 20237-20242.

Godard, H. P., Jepson, W. P., Bothwell, M. R., & Lane, R. L. (1967). *The corrosion of light metals*. New York: John Wiley & Sons.

Gray, F. M. (1991). *Solid polymer electrolytes: Fundamentals and technological applications*. New York: Verlag Chemie.

Gray, F. M. (1997). *Polymer electrolytes*. Cambridge: Royal Society of Chemistry.

Gurunathan, S., Han, J. W., Dayem, A. A., Eppakayala, V., & Kim, J.-H. (2012). Oxidative stress-mediated antibacterial activity of graphene oxide and reduced graphene oxide in Pseudomonas aeruginosa. *International Journal of Nanomedicine, 7*, 5901.

Hamlen, R. P. (1995). Metal/air batteries. In D. Linden (Ed.), *Handbook of batteries* (2nd ed., pp. 38.31-38.45). Bronson, Texas: McGraw-Hill Publishing Company.

Hernandez-Carmona, G., Freile-Pelegrin, Y., Garibay, E. H. (2013). Conventional and alternative technologies for the extraction of algal polysaccharides. In H. Dominguez (Ed.), *Functional ingredients from algae for foods and nutraceuticals* (pp. 475-509). La Vergne, Tennessee: Woodhead Publishing Limited.

Hernandez, Y., Nicolosi, V., Lotya, M., Blighe, F. M., Sun, Z., De, S., . . . Gun'Ko, Y. K. (2008). High-yield production of graphene by liquid-phase exfoliation of graphite. *Nature Nanotechnology, 3*(9), 563-568.

Huc, V., Bendiab, N., Rosman, N., Ebbesen, T., Delacour, C., & Bouchiat, V. (2008). Large and flat graphene flakes produced by epoxy bonding and reverse exfoliation of highly oriented pyrolytic graphite. *Nanotechnology, 19*(45), 455601.

Hummers Jr, W. S., & Offeman, R. E. (1958). Preparation of graphitic oxide. *Journal of the American Chemical Society, 80*(6), 1339-1339.

Inkwood Research. (2019). *Global battery market forecast 2019-2027*. Retrieved from https://www.inkwoodresearch.com/reports/global-battery-market/.

Jia, X., Wang, C., Ranganathan, V., Napier, B., Yu, C., Chao, Y., . . . Wallace, G. G. (2017). A biodegradable thin-film magnesium primary battery using silk fibroin-ionic liquid polymer electrolyte. *ACS Energy Letters, 2*(4), 831-836.

Jia, X., Wang, C., Zhao, C., Ge, Y., & Wallace, G. G. (2016). Toward biodegradable Mg-air bioelectric batteries composed of silk fibroin-polypyrrole film. *Advanced Functional Materials, 26*(9), 1454-1462.

Jia, X., Yang, Y., Wang, C., Zhao, C., Vijayaraghavan, R., MacFarlane, D. R., . . . Wallace, G. G. (2014). Biocompatible ionic liquid-biopolymer electrolyte-enabled thin and compact magnesium-air batteries. *ACS applied materials & interfaces, 6*(23), 21110-21117.

Jörissen, L. (2006). Bifunctional oxygen/air electrodes. *Journal of Power Sources, 155*(1), 23-32.

Kasem, K. K. (2005). Electrochemical behavior of some redox systems pendant in agar gel. *Journal of New Materials for Electrochemical Systems, 8*(3), 189.

Khoo, T., Howlett, P. C., Tsagouria, M., MacFarlane, D. R., & Forsyth, M. (2011). The potential for ionic liquid electrolytes to stabilise the magnesium interface for magnesium/air batteries. *Electrochimica Acta, 58*, 583-588.

Kim, H., Jeong, G., Kim, Y.-U., Kim, J.-H., Park, C.-M., & Sohn, H.-J. (2013). Metallic anodes for next generation secondary batteries. *Chemical Society Reviews, 42*(23), 9011-9034.

Kim, K. S., Zhao, Y., Jang, H., Lee, S. Y., Kim, J. M., Kim, K. S., . . . Hong, B. H. (2009). Large-scale pattern growth of graphene films for stretchable transparent electrodes. *Nature, 457*(7230), 706-710.

Kirchev, A. (2015). Chapter 20 - battery management and battery diagnostics. In P. T. Moseley & J. Garche (Eds.), *Electrochemical energy storage for renewable sources and grid balancing* (pp. 411-435). Amsterdam: Elsevier.

Konkena, B., & Vasudevan, S. (2012). Understanding aqueous dispersibility of graphene oxide and reduced graphene oxide through pK_a measurements. *The Journal of Physical Chemistry Letters, 3*(7), 867-872.

Koyikkal, S. (2013). Natural and bioprocess chemicals. *Chemical process technology and simulation* (pp. 15-75). Delhi: PHI Learning Private Limited.

Kumar, K. K., Brindha, R., Nandhini, M., Selvam, M., Saminathan, K., & Sakthipandi, K. (2019). Water-suspended graphene as electrolyte additive in zinc-air alkaline battery system. *Ionics*, 1-9.

Kumar, M. P., Kesavan, T., Kalita, G., Ragupathy, P., Narayanan, T. N., & Pattanayak, D. K. (2014). On the large capacitance of nitrogen doped graphene derived by a facile route. *RSC Advances, 4*(73), 38689-38697.

Kuo, C.-W., Li, W.-B., Chen, P.-R., Liao, J.-W., Tseng, C.-G., & Wu, T.-Y. (2013). Effect of plasticizer and lithium salt concentration in PMMA-based composite polymer electrolytes. *International Journal of Electrochemical Science*, 5007-5021.

Lai, C. W., Low, F. W., Chong, S. W., Wong, C. P. P., Mohamed Siddick, S. Z., Juan, J. C., & Abdul Hamid, S. B. (2015). An overview: Recent development of titanium dioxide loaded graphene nanocomposite film for solar application. *Current Organic Chemistry, 19*(19), 1882-1895.

Lebrini, M., Lagrenée, M., Traisnel, M., Gengembre, L., Vezin, H., & Bentiss, F. (2007). Enhanced corrosion resistance of mild steel in normal sulfuric acid medium by 2,5-bis(n-thienyl)-1,3,4-thiadiazoles: Electrochemical, X-ray photoelectron spectroscopy and theoretical studies. *Applied Surface Science, 253*(23), 9267-9276.

Lee, J. S., Kim, S. T., Cao, R., Choi, N. S., Liu, M., Lee, K. T., & Cho, J. (2011). Metal-air batteries with high energy density: Li-air versus Zn-air. *Advanced Energy Materials, 1*(1), 34-50.

Leones, R., Sentanin, F., Rodrigues, L., Marrucho, I., Esperança, J., Pawlicka, A., & Silva, M. (2012). Investigation of polymer electrolytes based on agar and ionic liquids. *eXPRESS Polymer Letters, 6*(12), 1007-1016.

Li, D., Müller, M. B., Gilje, S., Kaner, R. B., & Wallace, G. G. (2008). Processable aqueous dispersions of graphene nanosheets. *Nature Nanotechnology, 3*(2), 101-105.

Li, Y., Ma, J., Wang, G., Ren, F., Zhu, Y., & Song, Y. (2018). Investigation of sodium phosphate and sodium dodecylbenzenesulfonate as electrolyte additives for AZ91 magnesium-air battery. *Journal of The Electrochemical Society, 165*(9), A1713-A1717.

Li, Y., Zhang, X., Li, H.-B., Yoo, H. D., Chi, X., An, Q., . . . Yao, Y. (2016). Mixed-phase mullite electrocatalyst for pH-neutral oxygen reduction in magnesium-air batteries. *Nano Energy, 27*, 8-16.

Lih, E. T. Y., Ling, T. L., & Chong, K. F. (2012). Facile corrosion protection coating from graphene. *International Journal of Chemical Engineering and Applications, 3*(6), 453.

Lima, E., Raphael, E., Sentanin, F., Rodrigues, L., Ferreira, R., Carlos, L., . . . Pawlicka, A. (2012). Photoluminescent polymer electrolyte based on agar and containing europium picrate for electrochemical devices. *Materials Science and Engineering: B, 177*(6), 488-493.

Lin, Y., Li, J., Liu, K., Liu, Y., Liu, J., & Wang, X. (2016). Unique starch polymer electrolyte for high capacity all-solid-state lithium sulfur battery. *Green Chemistry, 18*(13), 3796-3803.

Linden, D., & Reddy, T. B. (2002). *Handbook of batteries* (3rd ed.). New York: McGraw-Hill Education.

Liu, Y., Sun, Q., Li, W., Adair, K. R., Li, J., & Sun, X. (2017). A comprehensive review on recent progress in aluminum-air batteries. *Green Energy & Environment, 2*(3), 246-277.

Lotya, M., King, P. J., Khan, U., De, S., & Coleman, J. N. (2010). High-concentration, surfactant-stabilized graphene dispersions. *ACS Nano, 4*(6), 3155-3162.

Luder, D., & Ein-Eli, Y. (2014). Electrochemical grignard reagent synthesis for ionic-liquid-based magnesium-air batteries. *ChemElectroChem, 1*(8), 1319-1326.

Ma, J., Qin, C., Li, Y., Ren, F., Liu, Y., & Wang, G. (2019). Properties of reduced graphene oxide for Mg-air battery. *Journal of Power Sources, 430*, 244-251.

Mainar, A. R., Iruin, E., Colmenares, L. C., Kvasha, A., de Meatza, I., Bengoechea, M., . . . Blazquez, J. A. (2018). An overview of progress in electrolytes for secondary zinc-air batteries and other storage systems based on zinc. *Journal of Energy Storage, 15*, 304-328.

Mantri, V. A., Reddy, C. R. K., & Jha, B. (2010). Cultivation of seaweeds in globally changing environments. In A. Israel, R. Einav, & J. Seckbach (Eds.), *Seaweeds and their role in globally changing environments* (pp. 251-356). Dordrecht, Heidelberg, London, New York: Springer.

Masri, M., Nazeri, M., & Mohamad, A. (2010). Sago gel polymer electrolyte for zinc-air battery. *Advances in Science and Technology, 72*, 305-308.

Matsuhashi, T. (1990). Agar. In P. Harris (Ed.), *Food gels* (pp. 1-52). London, New York: Elsevier Science Publishers Limited.

Mayilvel Dinesh, M., Saminathan, K., Selvam, M., Srither, S. R., Rajendran, V., & Kaler, K. V. I. S. (2015). Water soluble graphene as electrolyte additive in magnesium-air battery system. *Journal of Power Sources, 276*, 32-38.

McHugh, D. J. (1991). Worldwide distribution of commercial resources of seaweeds including *Gelidium*. *Hydrobiologia, 221*(1), 19-29.

Mesbah, N. M., & Wiegel, J. (2006). Isolation, cultivation and characterization of alkalithermophiles. In F. A. Rainey & A. Oren (Eds.), *Methods in microbiology* (Vol. 35, pp. 451-468). New Year: Elsevier Academic Press.

Monisha, S., Mathavan, T., Selvasekarapandian, S., Milton Franklin Benial, A., Aristatil, G., Mani, N., . . . Vinoth pandi, D. (2017). Investigation of bio polymer electrolyte based on cellulose acetate-ammonium nitrate for potential use in electrochemical devices. *Carbohydrate Polymers, 157*(Supplement C), 38-47.

Moon, W. G., Kim, G.-P., Lee, M., Song, H. D., & Yi, J. (2015). A biodegradable gel electrolyte for use in high-performance flexible supercapacitors. *ACS Applied Materials & Interfaces, 7*(6), 3503-3511.

Muldoon, J., Bucur, C. B., Oliver, A. G., Sugimoto, T., Matsui, M., Kim, H. S., . . . Kotani, Y. (2012). Electrolyte roadblocks to a magnesium rechargeable battery. *Energy & Environmental Science, 5*(3), 5941-5950.

Muthukrishnan, M., Shanthi, C., Selvasekarapandian, S., Manjuladevi, R., Perumal, P., & Chrishtopher Selvin, P. (2018). Synthesis and characterization of pectin-based biopolymer electrolyte for electrochemical applications. *Ionics*, 1-12.

Nagaraj, P., Sasidharan, A., David, V., & Sambandam, A. (2017). Effect of cross-linking on the performances of starch-based biopolymer as gel electrolyte for dye-sensitized solar cell applications. *Polymers, 9*(12), 667.

Nasir, S., Hussein, M., Zainal, Z., & Yusof, N. (2018). Carbon-based nanomaterials/allotropes: A glimpse of their synthesis, properties and some applications. *Materials, 11*(2), 295.

Neburchilov, V., Wang, H., Martin, J. J., & Qu, W. (2010). A review on air cathodes for zinc-air fuel cells. *Journal of Power Sources, 195*(5), 1271-1291.

Novoselov, K. S., Geim, A. K., Morozov, S. V., Jiang, D., Zhang, Y., Dubonos, S. V., . . . Firsov, A. A. (2004). Electric field effect in atomically thin carbon films. *Science, 306*(5696), 666-669.

Osada, I., de Vries, H., Scrosati, B., & Passerini, S. (2016). Ionic-liquid-based polymer electrolytes for battery applications. *Angewandte Chemie International Edition, 55*(2), 500-513.

Othman, R., & Saputra, H. (2013). Zinc-air battery-powering electric vehicles to smart active labels. *International Journal of Engineering Science and Technology Development, 1*(1), 1-5.

Parvez, K., Wu, Z.-S., Li, R., Liu, X., Graf, R., Feng, X., & Müllen, K. (2014). Exfoliation of graphite into graphene in aqueous solutions of inorganic salts. *Journal of the American Chemical Society, 136*(16), 6083-6091.

Pawlicka, A., Danczuk, M., Wieczorek, W., & Zygadło-Monikowska, E. (2008). Influence of plasticizer type on the properties of polymer electrolytes based on chitosan. *The Journal of Physical Chemistry A, 112*(38), 8888-8895.

Pei, S., & Cheng, H.-M. (2012). The reduction of graphene oxide. *Carbon, 50*(9), 3210-3228.

Peng, B., Liang, J., Tao, Z., & Chen, J. (2009). Magnesium nanostructures for energy storage and conversion. *Journal of Materials Chemistry, 19*(19), 2877-2883.

Perumal, P., Selvin, P. C., & Selvasekarapandian, S. (2018). Characterization of biopolymer pectin with lithium chloride and its applications to electrochemical devices. *Ionics*, 1-12.

Pimenta, M., Dresselhaus, G., Dresselhaus, M. S., Cancado, L., Jorio, A., & Saito, R. (2007). Studying disorder in graphite-based systems by Raman spectroscopy. *Physical Chemistry Chemical Physics, 9*(11), 1276-1290.

Purwanto, M., Atmaja, L., Mohamed, M. A., Salleh, M., Jaafar, J., Ismail, A., . . . Widiastuti, N. (2016). Biopolymer-based electrolyte membranes from chitosan incorporated with montmorillonite-crosslinked GPTMS for direct methanol fuel cells. *RSC Advances, 6*(3), 2314-2322.

Qiu, H., & Zou, F. (2012). Nanoporous PtCo surface alloy architecture with enhanced properties for methanol electrooxidation. *ACS applied materials & interfaces, 4*(3), 1404-1410.

Rahman, M. A., Wang, X., & Wen, C. (2013). High energy density metal-air batteries: A review. *Journal of The Electrochemical Society, 160*(10), A1759-A1771.

Ramesh, S., Liew, C.-W., & Ramesh, K. (2011). Evaluation and investigation on the effect of ionic liquid onto PMMA-PVC gel polymer blend electrolytes. *Journal of Non-Crystalline Solids, 357*(10), 2132-2138.

Rao, C. N. R., & Sood, A. K. (2013). *Graphene: Synthesis, properties, and phenomena*. Hoboken: Wiley-Verlag Chemie.

Raphael, E., Avellaneda, C. O., Manzolli, B., & Pawlicka, A. (2010). Agar-based films for application as polymer electrolytes. *Electrochimica Acta, 55*(4), 1455-1459.

Reddy, T. (2010). *Linden's handbook of batteries* (4th ed.). New York: McGraw-Hill Education.

Rhein-Knudsen, N., Ale, M. T., & Meyer, A. S. (2015). Seaweed hydrocolloid production: An update on enzyme assisted extraction and modification technologies. *Marine Drugs, 13*(6), 3340-3359.

Richey, F. W., McCloskey, B. D., & Luntz, A. C. (2016). Mg anode corrosion in aqueous electrolytes and implications for Mg-air batteries. *Journal of The Electrochemical Society, 163*(6), A958-A963.

Roche, I., & Scott, K. (2010). Effect of pH and temperature on carbon-supported manganese oxide oxygen reduction electrocatalysts. *Journal of Electroanalytical Chemistry, 638*(2), 280-286.

Saha, A., Basiruddin, S., Ray, S. C., Roy, S., & Jana, N. R. (2010). Functionalized graphene and graphene oxide solution via polyacrylate coating. *Nanoscale, 2*(12), 2777-2782.

Saxman, D. (2017). *Advanced materials for advanced batteries and fuel cells: Technologies and global markets*. Retrieved from https://www.bccresearch.com/market-research/fuel-cell-and-battery-technologies/advanced-batteries-fuel-cells-report.html.

Scherson, D. A., & Palencsár, A. (2006). Batteries and electrochemical capacitors. *Interface, 15*(1), 17-22.

Scrosati, B., & Vincent, C. A. (2011). Polymer electrolytes: The key to lithium polymer batteries. *Materials Research Society Bulletin, 25*(3), 28-30.

Sekhon, S. (2003). Conductivity behaviour of polymer gel electrolytes: Role of polymer. *Bulletin of Materials Science, 26*(3), 321-328.

Selvalakshmi, S., Mathavan, T., Selvasekarapandian, S., & Premalatha, M. (2017). Study on NH_4I composition effect in agar-agar-based biopolymer electrolyte. *Ionics, 23*(10), 2791-2797.

Selvalakshmi, S., Mathavan, T., Selvasekarapandian, S., & Premalatha, M. (2018). Effect of ethylene carbonate plasticizer on agar-agar: NH_4Br-based solid polymer electrolytes. *Ionics*, 1-9.

Selvalakshmi, S., Mathavan, T., Selvasekarapandian, S., & Premalatha, M. (2019). Characterization of biodegradable solid polymer electrolyte system based on agar-NH_4Br and its comparison with NH_4I. *Journal of Solid State Electrochemistry, 23*(6), 1727-1737.

Selvam, M., Sakthipandi, K., Suriyaprabha, R., Saminathan, K., & Rajendran, V. (2013). Synthesis and characterization of electrochemically-reduced graphene. *Bulletin of Materials Science, 36*(7), 1315-1321.

Selvin, P. C., Perumal, P., Selvasekarapandian, S., Monisha, S., Boopathi, G., & Chandra, M. L. (2018). Study of proton-conducting polymer electrolyte based on K-carrageenan and NH_4SCN for electrochemical devices. *Ionics*, 1-8.

Sen, R. K., Van Voorhees, S. L., & Ferrel, T. (1988). *Metal-air battery assessment*. Springfield, Virginia: United States Department of Energy.

Shan, C., Yang, H., Han, D., Zhang, Q., Ivaska, A., & Niu, L. (2009). Water-soluble graphene covalently functionalized by biocompatible poly-L-lysine. *Langmuir, 25*(20), 12030-12033.

Shankar, S., & Rhim, J.-W. (2016). Preparation of nanocellulose from micro-crystalline cellulose: The effect on the performance and properties of agar-based composite films. *Carbohydrate Polymers, 135*, 18-26.

Shankar, S., & Rhim, J.-W. (2017). Preparation and characterization of agar/lignin/silver nanoparticles composite films with ultraviolet light barrier and antibacterial properties. *Food Hydrocolloids, 71*, 76-84.

Shankar, S., Teng, X., & Rhim, J.-W. (2014). Properties and characterization of agar/CuNP bionanocomposite films prepared with different copper salts and reducing agents. *Carbohydrate Polymers, 114*, 484-492.

Shen, J., Hu, Y., Li, C., Qin, C., & Ye, M. (2009). Synthesis of amphiphilic graphene nanoplatelets. *Small, 5*(1), 82-85.

Shyma, A. P., Palanisamy, S., Rajendhran, N., & Venkatachalam, R. (2019). Enhanced discharge capacity of Mg-air battery with addition of water dispersible nano MoS_2 sheet in $MgCl_2$ electrolyte. *Ionics, 25*(2), 583-592.

Si, Y., & Samulski, E. T. (2008). Synthesis of water soluble graphene. *Nano Letters, 8*(6), 1679-1682.

Singh, T., Meena, R., & Kumar, A. (2009). Effect of sodium sulfate on the gelling behavior of agarose and water structure inside the gel networks. *The Journal of Physical Chemistry B, 113*(8), 2519-2525.

Singhbabu, Y., Kumari, P., Parida, S., & Sahu, R. K. (2014). Conversion of pyrazoline to pyrazole in hydrazine treated N-substituted reduced graphene oxide films obtained by ion bombardment and their electrical properties. *Carbon, 74*, 32-43.

Sivadevi, S., Selvalakshmi, S., Umamaheswari, A., & Bhuvaneswari. (2016). Investigation of a novel biodegradable blend polymer electrolyte based on PVA and agar. *International Journal of Scientific Research, 5*(6).

Sobon, G., Sotor, J., Jagiello, J., Kozinski, R., Zdrojek, M., Holdynski, M., . . . Abramski, K. M. (2012). Graphene oxide vs. reduced graphene oxide as saturable absorbers for Er-doped passively mode-locked fiber laser. *Optics Express, 20*(17), 19463-19473.

Stankovich, S., Dikin, D. A., Piner, R. D., Kohlhaas, K. A., Kleinhammes, A., Jia, Y., . . . Ruoff, R. S. (2007). Synthesis of graphene-based nanosheets via chemical reduction of exfoliated graphite oxide. *Carbon, 45*(7), 1558-1565.

Stankovich, S., Piner, R. D., Chen, X., Wu, N., Nguyen, S. T., & Ruoff, R. S. (2006). Stable aqueous dispersions of graphitic nanoplatelets via the reduction of exfoliated graphite oxide in the presence of poly (sodium 4-styrenesulfonate). *Journal of Materials Chemistry, 16*(2), 155-158.

Stephan, A. M. (2006). Review on gel polymer electrolytes for lithium batteries. *European Polymer Journal, 42*(1), 21-42.

Strudwick, A. J., Weber, N. E., Schwab, M. G., Kettner, M., Weitz, R. T., Wünsch, J. R., . . . Sachdev, H. (2014). Chemical vapor deposition of high quality graphene films from carbon dioxide atmospheres. *ACS Nano, 9*(1), 31-42.

Su, C.-Y., Lu, A.-Y., Wu, C.-Y., Li, Y.-T., Liu, K.-K., Zhang, W., . . . Chen, F.-R. (2011). Direct formation of wafer scale graphene thin layers on insulating substrates by chemical vapor deposition. *Nano Letters, 11*(9), 3612-3616.

Suganya, N., Hari Hara Priya, G., & Jaisankar, V. (2015). A study on ionic conductivity of certain polymer nanocomposite electrolyte on the addition of reduced graphene oxide for solar cell applications. *International Journal of Advanced Chemical Science and Applications, 3*(1), 73-79.

Vaghela, C., Kulkarni, M., Haram, S., Karve, M., & Aiyer, R. (2016). Biopolymer-polyaniline composite for a wide range ammonia gas sensor. *IEEE Sensors Journal, 16*(11), 4318-4325.

Venugopal, V. (2011). Polysaccharides from seaweed and microalgae. *Marine polysaccharides: Food applications* (pp. 89-134). Boca Raton, Florida: CRC Press.

Vieira, D. F., & Pawlicka, A. (2010). Optimization of performances of gelatin/$LiBF_4$-based polymer electrolytes by plasticizing effects. *Electrochimica Acta, 55*(4), 1489-1494.

Vinayan, B., Nagar, R., & Ramaprabhu, S. (2012). Synthesis and investigation of mechanism of platinum-graphene electrocatalysts by novel co-reduction techniques for proton exchange membrane fuel cell applications. *Journal of Materials Chemistry, 22*(48), 25325-25334.

Volery, P., Besson, R., & Schaffer-Lequart, C. (2004). Characterization of commercial carrageenans by Fourier transform infrared spectroscopy using single-reflection attenuated total reflection. *Journal of Agricultural and Food Chemistry, 52*(25), 7457-7463.

Wang, G., Shen, X., Wang, B., Yao, J., & Park, J. (2009). Synthesis and characterisation of hydrophilic and organophilic graphene nanosheets. *Carbon, 47*(5), 1359-1364.

Wang, N., Wang, R., Peng, C., Peng, B., Feng, Y., & Hu, C. (2014). Discharge behaviour of Mg-Al-Pb and Mg-Al-Pb-In alloys as anodes for Mg-air battery. *Electrochimica Acta, 149*, 193-205.

Wang, X., Hou, Y., Zhu, Y., Wu, Y., & Holze, R. (2013). An aqueous rechargeable lithium battery using coated Li metal as anode. *Scientific Reports, 3*, 1401.

Weng, W., Sun, Q., Zhang, Y., He, S., Wu, Q., Deng, J., . . . Peng, H. (2015). A gum-like lithium-ion battery based on a novel arched structure. *Advanced Materials, 27*(8), 1363-1369.

Willemse, C. M., Tlhomelang, K., Jahed, N., Baker, P. G., & Iwuoha, E. I. (2011). Metallo-graphene nanocomposite electrocatalytic platform for the determination of toxic metal ions. *Sensors, 11*(4), 3970-3987.

Wojtoniszak, M., Zielinska, B., Kalenczuk, R., & Mijowska, E. (2012). Photocatalytic performance of titania nanospheres deposited on graphene in coumarin oxidation reaction. *Materials Science-Poland, 30*(1), 32-38.

Yan, Y. (2016). *Ionic liquid electrolytes in Mg-air batteries.* (Doctoral thesis, Deakin University, Burwood, Australia). Retrieved from http://dro.deakin.edu.au/eserv/DU:30085503/yan-ionicliquid-2016A.pdf.

Yan, Y., Khoo, T., Pozo-Gonzalo, C., Hollenkamp, A. F., Howlett, P. C., MacFarlane, D. R., & Forsyth, M. (2014). Roles of additives in the trihexyl (tetradecyl) phosphonium chloride ionic liquid electrolyte for primary Mg-air cells. *Journal of The Electrochemical Society, 161*(6), A974-A980.

Yang, Q., Pan, X., Huang, F., & Li, K. (2010). Fabrication of high-concentration and stable aqueous suspensions of graphene nanosheets by noncovalent functionalization with lignin and cellulose derivatives. *The Journal of Physical Chemistry C, 114*(9), 3811-3816.

Yang, W., Chen, G., Shi, Z., Liu, C.-C., Zhang, L., Xie, G., . . . Shi, D. (2013). Epitaxial growth of single-domain graphene on hexagonal boron nitride. *Nature Materials, 12*(9), 792-797.

Yang, W. Q., Yang, S. H., Sun, G. G., & Xin, Q. (2005). Development and application of magnesium fuel cell. *Chinese Journal of Power Sources, 29*, 182-186.

Yang, Y., Cui, J., Yi, P., Zheng, X., Guo, X., & Wang, W. (2014). Effects of nanoparticle additives on the properties of agarose polymer electrolytes. *Journal of Power Sources, 248*, 988-993.

Yang, Y., Zhou, C.-h., Xu, S., Hu, H., Chen, B.-l., Zhang, J., . . . Zhao, X.-z. (2008). Improved stability of quasi-solid-state dye-sensitized solar cell based on poly (ethylene oxide)-poly (vinylidene fluoride) polymer-blend electrolytes. *Journal of Power Sources, 185*(2), 1492-1498.

Yoo, H. D., Shterenberg, I., Gofer, Y., Gershinsky, G., Pour, N., & Aurbach, D. (2013). Mg rechargeable batteries: An on-going challenge. *Energy & Environmental Science, 6*(8), 2265-2279.

Zhang, J.-G., Bruce, P. G., & Zhang, X. G. (2011). Metal-air batteries. In J. O. Besenhard (Ed.), *Handbook of battery materials* (pp. 757-795). Weinheim: Wiley-VCH Verlag GmbH & Co. KGaA.

Zhang, J., Sun, B., Huang, X., Chen, S., & Wang, G. (2014). Honeycomb-like porous gel polymer electrolyte membrane for lithium ion batteries with enhanced safety. *Scientific Reports, 4*, 6007.

Zhang, J., Yang, H., Shen, G., Cheng, P., Zhang, J., & Guo, S. (2010). Reduction of graphene oxide via L-ascorbic acid. *Chemical Communications, 46*(7), 1112-1114.

Zhang, Q., Liu, K., Ding, F., & Liu, X. (2017). Recent advances in solid polymer electrolytes for lithium batteries. *Nano Research*, 1-36.

Zhang, T., Tao, Z., & Chen, J. (2014). Magnesium-air batteries: From principle to application. *Materials Horizons, 1*(2), 196-206.

Zhang, Y., Zhao, Y., Cheng, X., Weng, W., Ren, J., Fang, X., . . . Wang, Y. (2015). Realizing both high energy and high power densities by twisting three carbon-nanotube-based hybrid fibers. *Angewandte Chemie International Edition, 54*(38), 11177-11182.

Zhang, Z., Zuo, C., Liu, Z., Yu, Y., Zuo, Y., & Song, Y. (2014). All-solid-state Al-air batteries with polymer alkaline gel electrolyte. *Journal of Power Sources, 251*, 470-475.

Zhao, Y.-C., Huang, G.-S., Gong, G.-l., Han, T.-Z., Xia, D.-B., & Pan, F.-S. (2016). Improving the intermittent discharge performance of Mg-air battery by using oxyanion corrosion inhibitor as electrolyte additive. *Acta Metallurgica Sinica (English Letters), 29*(11), 1019-1024.

Zhao, Y., Huang, G., Zhang, C., Peng, C., & Pan, F. (2018). Effect of phosphate and vanadate as electrolyte additives on the performance of Mg-air batteries. *Materials Chemistry and Physics, 218*, 256-261.

Zhu, Y., Murali, S., Cai, W., Li, X., Suk, J. W., Potts, J. R., & Ruoff, R. S. (2010). Graphene and graphene oxide: Synthesis, properties, and applications. *Advanced Materials, 22*(35), 3906-3924.

LIST OF PUBLICATIONS AND PAPERS PRESENTED

ISI-Cited Publication:

1. Liew, S. Y., Juan, J. C., Lai, C. W., Pan, G.-T., Yang, T. C.-K., & Lee, T. K. (2018). An eco-friendly water-soluble graphene-incorporated agar gel electrolyte for magnesium-air batteries. *Ionics*, 1-11.

Presentation in Conference:

1. Liew, S. Y., Juan, J. C., Lai, C. W., Pan, G.-T., & Yang, T. C.-K. A novel eco-friendly graphene-incorporated agar gel for metal-air batteries, presented at The 7th Asian Conference on Colloid & Interface Science (ACCIS), Berjaya Times Square Hotel Kuala Lumpur, 8-11 August 2017.